Aircraft HCl Sampling of the Titan IV K-23 Launch Effluent Cloud

15 September 1996

Prepared by

R. N. ABERNATHY, R. F. HEIDNER III, and K. L. FOSTER
Space and Environment Technology Center
Technology Operations
Engineering and Technology Group

Prepared for

SPACE AND MISSILE SYSTEMS CENTER
AIR FORCE MATERIEL COMMAND
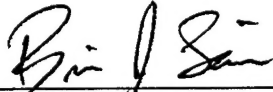2430 E. El Segundo Boulevard
Los Angeles Air Force Base, CA 90245

Space Systems Group

THE AEROSPACE CORPORATION
El Segundo, California

19961113 158

BRIAN LAINE, CAPT
Environmental Project Manager
Launch Programs

REPORT DOCUMENTATION PAGE

1. AGENCY USE ONLY (*Leave blank*)	2. REPORT DATE 15 September 1996	3. REPORT TYPE AND DATES COVERED

4. TITLE AND SUBTITLE

Aircraft HCl Sampling of the Titan IV K-23 Launch Effluent Cloud

5. FUNDING NUMBERS

F04701-93-C-0094

6. AUTHOR(S)

Abernathy, Robert N.; Heidner III, Raymond F.; and Foster, Karen L.

7. PERFORMING ORGANIZATION NAME(S) AND ADDRESS(ES)

The Aerospace Corporation
Technology Operations
El Segundo, CA 90245-4691

8. PERFORMING ORGANIZATION REPORT NUMBER

TR-96(1410)-2

9. SPONSORING/MONITORING AGENCY NAME(S) AND ADDRESS(ES)

Space and Missile Systems Center
Air Force Materiel Command
2430 E. El Segundo Blvd.
Los Angeles Air Force Base, CA 90245

10. SPONSORING/MONITORING AGENCY REPORT NUMBER

SMC-TR-96-22

11. SUPPLEMENTARY NOTES

12a. DISTRIBUTION/AVAILABILITY STATEMENT

Approved for public release; distribution unlimited

12b. DISTRIBUTION CODE

13. ABSTRACT (*Maximum 200 words*)

On 14 May 1995 at 09:45 EDT (13:45Z), the Titan IV K-23 mission was successfully launched from SLC-40 at CCAS. This report describes the reduction of data from an aircraft plume sampling campaign overseen by 45SPW that involved Air Force, NOAA and contractor organizations. A modified commercial total HCl (gaseous and aerosol) monitor (Geomet Model 401B), mounted in a Piper Seminole aircraft, performed post-launch sampling around SLC-40 for 100 minutes following the launch. The data consist of measured HCl concentration versus aircraft GPS location. Data are reported here in several alternative graphical formats to facilitate comparison with modeling and with plume imagery. After a brief overview of the sampling campaign, detailed information is provided for sequential 10 minute time windows. During the first 20 minutes following the launch, 3-D plume imaging documented the track and shape of the effluent ground cloud. Comparison of those imagery data to the aircraft sampling has been reported separately. The stabilized ground cloud (as defined by imagery) yielded aircraft sampling hits in the northeast quadrant referenced to SLC-40. Dispersal of the narrow launch column attached to the southern end of the ground cloud appears to be responsible for higher altitude aircraft hits in the southeast quadrant. The K-23 results are compared to previous aircraft sampling data from Titan III and STS launches from CCAS acquired by NASA Langley Research Center.

14. SUBJECT TERMS

Aircraft Plume Sampling	*In Situ* Sampling
HCl	K-23 Launch Cloud
Hydrochloric Acid	Titan IV

15. NUMBER OF PAGES
106

16. PRICE CODE

17. SECURITY CLASSIFICATION OF REPORT Unclassified	18. SECURITY CLASSIFICATION OF THIS PAGE Unclassified	19. SECURITY CLASSIFICATION OF ABSTRACT Unclassified	20. LIMITATION OF ABSTRACT

NSN 7540-01-280-5500

Standard Form 298 (Rev. 2-89)
Prescribed by ANSI Std. Z39-18
298-102

Preface

We wish to acknowledge the many participants in the K-23 sampling campaign who were responsible for acquiring the data presented in this report. In particular, thanks are due to personnel from the Florida Institute of Technology (FIT) and the NOAA Air Resources Laboratory Field Research Division. Mr. Dan Curran, of I-NET, Inc., who modified and calibrated the Geomet total HCl detector, and Ms. Jeanne Hawkins, of the 45th Space Wing AMDS/SGPB, who acquired the data during the flight campaign, deserve special recognition. From the beginning, this effort depended on the support of and technical interactions with Mr. Noble Dowling and Dr. Bart Lundblad of the Environmental Systems Department at The Aerospace Corporation.

Contents

Contents (continued)

Figures

Figures (continued)

Figures (continued)

Figures (continued)

Figures (continued)

Figures (continued)

Tables

1. Introduction

One of the key drivers for range safety at the Eastern and Western Test Ranges is the ability to map the fate of toxic or environmentally hazardous materials generated by space launch vehicles. The complex meteorology at both Cape Canaveral Air Station (CCAS) and Vandenberg Air Force Base (VAFB) makes this a very difficult task. Models describing various launch-related scenarios for release of toxic material have been developed since the 1960s. Currently, the Rocket Exhaust Effluent Diffusion Model (REEDM)[1,2] is employed at both ranges for that purpose.

By the 1970s, it was recognized that validation of the models describing launch vehicle effluents required data from a number of sources—ground sampling, remote sensing, and airborne *in situ* sampling. NASA's Langley Research Center (LaRC) played a central role in airborne sampling of the principal hazardous material emanating from Titan III and the Space Shuttle [space transportation system (STS)] solid rocket motors[3-6]—including HCl in both its gaseous and liquid aerosol form. During the late 1970s and early 1980s, aircraft fly-throughs of numerous Titan III and STS launches were conducted. Total HCl (gaseous and liquid aerosol) concentrations were measured with a Geomet chemiluminescent detector. In addition, gaseous HCl concentrations were measured with a nondispersive infrared (IR) instrument, thus permitting analysis of the partitioning of HCl between gaseous and liquid aerosol. In general, those partitioning results agreed well with theory.

The 14 May 1995 K-23 launch was the first in which *in situ* aircraft sampling was performed for a Titan IV vehicle. Once again, the Geomet total HCl detector was used to measure the profiles of HCl in the plume and to establish the peak concentrations as a function of time following launch. This sampling campaign was conducted by Aerospace's Environmental Systems Directorate and the Titan IV SPO at the Space and Missile Systems Center (SMC). It included the Florida Institute of Technology (FIT), which supplied the aircraft; the 45th Space Wing AMDS/SGPB, which supplied the Geomet and operated it in flight; I-NET, Inc., which modified and integrated the Geomet into the aircraft as well as calibrated it before and after flight; NOAA Air Resources Laboratory/Field Research Division (ARL/FRD), which provided the aircraft GPS system and data recording for both GPS and Geomet; and SRS, Inc., which managed the interface between FIT and I-NET. Aerospace received the GPS and the Geomet sampling data from ARL/FRD and was responsible for data analysis and for comparing the results to plume imagery data.[7,8]

This report serves as a repository for the entire 100 min of aircraft sampling. As noted, the data received consisted of measured HCl concentration versus aircraft GPS location. Data are reported in several alternative graphical formats to facilitate comparison with plume imagery and to aid in future model validation efforts. After a brief overview of the sampling campaign, detailed information is provided for sequential 10 min time windows. During the first 20 min following the launch, three-dimensional (3-D) plume imaging documented the track and shape of the effluent ground cloud. Detailed comparison of those imagery data to the aircraft sampling has been reported separately.[7,8] The stabilized ground cloud (as defined by imagery) yielded aircraft sampling hits in the northeast quadrant referenced to Space Launch Complex-40 (SLC-40). Dispersal of the narrow launch column attached to the

southern end of the ground cloud appears to be responsible for higher altitude aircraft hits in the southeast quadrant. The K-23 results are compared to previous aircraft sampling data from Titan III and STS launches at CCAS acquired by NASA LaRC.

Several concerns are raised in this report about the accuracy of the reported Geomet HCl concentrations. These concerns do not reflect on the implementation of the K-23 sampling campaign. Geomet detectors have many known advantages and several known limitations.[*][9] Their principal limitation for aircraft studies resides in their time dependent response to HCl exposure. The "fast" response time is inversely proportional to [HCl]. In addition, there is a second "slow" response time. Unimportant for most ground-based applications, these response times significantly impact data interpretation at the speeds of sampling aircraft (70 m/sec). Concentration data (parts per million [ppm]) in this report, however, reflect the *laboratory* calibration of the instrument's response by I-NET. This and other caveats related to aircraft sampling are given where appropriate.

---

[*]D. Curran, I-NET, Inc., private communication (1995).

2. Background

In previous reports on the K-23 launch,[7,8] 3-D plume imaging was compared to aircraft sampling for a 20 min period immediately following liftoff. Figure 1 reproduces the map from that report, with vectors indicating the imagery-derived track of the ground cloud (249°) and the rawinsonde wind vectors (centered on the balloon release facility) associated with the bottom, middle, and top of the imaged plume. The map also documents the locations of the three camera sites (Universal Camera Site-7 [UCS-7], Press Site, and SLC-34) that were used to view the Titan IV exhaust plume. The T-0.3 hr rawinsonde input data to REEDM and wind profiler data (T-9.5 min and T+5.5 min) taken at Mosquito Lagoon are presented in Appendix 1. A table comparing the plume track and stabilization height calculated by imagery and calculated by REEDM is presented in Appendix 2.
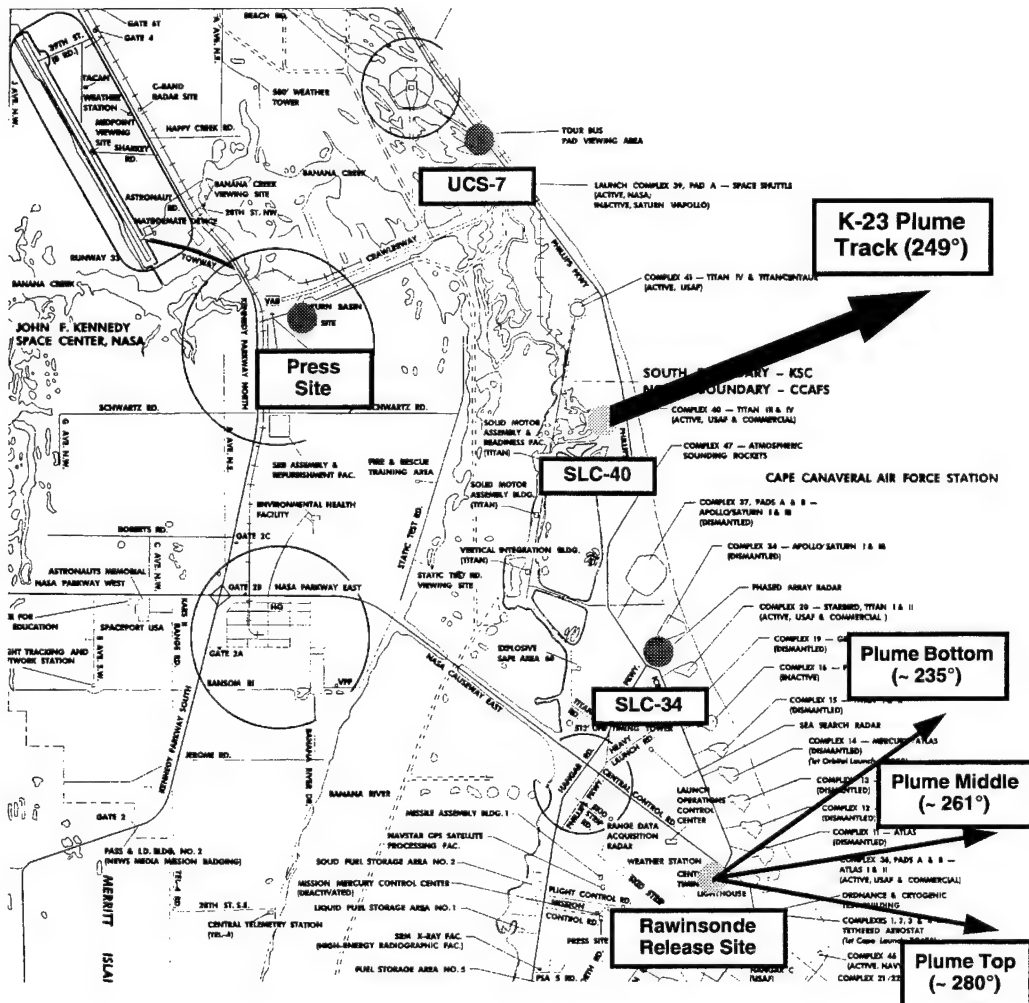
Figure 1: Map Documenting Camera Sites, Rawinsonde Release Point, Imagery Derived Plume Track, and Rawinsonde Derived Wind Vectors for the Titan IV K-23 Mission.

3

3. Results

3.1 Overview of Aircraft Sampling Campaign

I-NET, a NASA subcontractor, modified a commercial total HCl (gaseous and aerosol) monitor (Geomet 401B) for mounting in the nose of a Piper Seminole (PA-44-180) twin-engine, four-seat aircraft. This instrument sampled the air through a horizontally mounted 4-ft-long, 2-mm-i.d. ceramic inlet tube wetted with a bromate/bromide-containing reagent. Sampled HCl diffuses to the wetted walls of the ceramic tube and produces bromine vapor through reactions with this reagent. The bromine vapor is swept into a buffered hydrogen peroxide/luminol solution, resulting in photoluminescence detected by a filtered photometric detector. I-NET disabled the Geomet's autoranging electronics so that a single range produced a millivolt response that was proportional to the combined HCl vapor and aerosol concentration entering the inlet. (Note: Gregory and Moyer[9] determined that HCl vapor and acid aerosol give equivalent responses.) I-NET calibrated the Geomet before and after the K-23 mission.[*] The Geomet has a rather complicated time response upon exposure to HCl.[*, 9] That response is not characterized by a single time constant. Moreover, the "fast" response time to initial HCl exposure has been shown to be inversely proportional to [HCl] in the range 0.5–50 ppm.[9] The consequences of these instrumental artifacts, as well as artifacts associated with aircraft sampling, are discussed more fully in Appendix 3. The data reported here for [HCl] in ppm are the result of using the I-NET reported calibration constant for converting instrument signal to ppm under steady-state conditions in the laboratory. We will comment in the text and in Appendix 3 on systematic errors in the interpretation of the aircraft data.

SRS Technologies, Inc., an Air Force contractor, provided an interface between the I-NET laboratory and the FIT flight crew. NASA, NOAA ARL/FRD, I-NET, SRS, and FIT collaborated on the integration of the NOAA data handling systems, the FIT aircraft, and the Air Force Geomet into a complete airborne sampling and data logging system. FIT personnel piloted the aircraft during the K-23 mission, while the 45th Space Wing AMDS/SGPB personnel operated the NOAA data handling system and the Geomet detector. The NOAA data system logged GPS time and position as well as Geomet response every 0.25 sec during the flight. NOAA provided a comma-separated-variable (csv) raw data file to The Aerospace Corporation. Aerospace analysis of these data is presented in this report.

Table 1 presents a sample of the aircraft data delivered to The Aerospace Corporation with added headings. The headings are as follows: Log (mission log number assigned by NOAA); yr (year); d (Julian day of the year); hm (hour and minutes, two digits each); s (seconds); ppm (raw HCl concentration based upon single-point calibration and millivolt response from the Geomet); rng (range of the Geomet, disabled function); mV (Geomet response in millivolts); gps (GPS receiver time in hhmmss [documenting hours, minutes, and seconds as six digits without separation]); lat (latitude, ddmm.mmmm, in degrees and decimal minutes); N/S (label for latitude, North/South); lon (longitude, ddmm.mmmm, in degrees and decimal minutes);

---

[*]D. Curran, I-NET, Inc., private communication (1995).

Table 1: Portion of the Aircraft's Data File Provided to The Aerospace Corporation by NOAA. These Data Include the First Aircraft Pass Through the Titan IV K-23 Exhaust Cloud.

Log	yr	d	hm	s	ppm	mg	mV	gps	lat	N/S	lon	E/W	diff	# Sat	HDOP	alt	units
113	1995	134	1349	20.75	-0.040	1996	-0.997	134922	2833.7618	N	8034.0065	W	1	8	0.9	662	M
113	1995	134	1349	21	0.040	1996	0.997	134922	2833.7618	N	8034.0065	W	1	8	0.9	662	M
113	1995	134	1349	21.25	0.385	1996	9.630	134923	2833.7577	N	8033.9744	W	1	8	0.9	663	M
113	1995	134	1349	21.5	0.518	1996	12.960	134923	2833.7577	N	8033.9744	W	1	8	0.9	663	M
113	1995	134	1349	21.75	0.930	1996	23.250	134923	2833.7577	N	8033.9744	W	1	8	0.9	663	M
113	1995	134	1349	22	1.302	1996	32.550	134923	2833.7577	N	8033.9744	W	1	8	0.9	663	M
113	1995	134	1349	22.25	1.714	1996	42.850	134924	2833.7533	N	8033.9421	W	1	8	0.9	663	M
113	1995	134	1349	22.5	2.365	1996	59.130	134924	2833.7533	N	8033.9421	W	1	8	0.9	663	M
113	1995	134	1349	22.75	2.378	1996	59.460	134924	2833.7533	N	8033.9421	W	1	8	0.9	663	M
113	1995	134	1349	23	2.352	1996	58.800	134924	2833.7533	N	8033.9421	W	1	8	0.9	663	M
113	1995	134	1349	23.25	2.166	1996	54.150	134925	2833.7493	N	8033.9093	W	1	8	0.9	663	M
113	1995	134	1349	23.5	2.564	1996	64.110	134925	2833.7493	N	8033.9093	W	1	8	0.9	663	M
113	1995	134	1349	23.75	2.458	1996	61.450	134925	2833.7493	N	8033.9093	W	1	8	0.9	663	M
113	1995	134	1349	24	1.913	1996	47.830	134925	2833.7493	N	8033.9093	W	1	8	0.9	663	M
113	1995	134	1349	24.25	1.408	1996	35.210	134926	2833.7455	N	8033.8764	W	1	8	0.9	663	M
113	1995	134	1349	24.5	1.741	1996	43.520	134926	2833.7455	N	8033.8764	W	1	8	0.9	663	M
113	1995	134	1349	24.75	4.491	1996	112.300	134926	2833.7455	N	8033.8764	W	1	8	0.9	663	M
113	1995	134	1349	25	6.165	1997	154.100	134926	2833.7455	N	8033.8764	W	1	8	0.9	663	M
113	1995	134	1349	25.25	5.873	1997	146.800	134927	2833.7417	N	8033.8431	W	1	8	0.9	663	M
113	1995	134	1349	25.5	6.086	1997	152.100	134927	2833.7417	N	8033.8431	W	1	8	0.9	663	M
113	1995	134	1349	25.75	5.421	1996	135.500	134927	2833.7417	N	8033.8431	W	1	8	0.9	663	M
113	1995	134	1349	26	5.953	1997	148.800	134927	2833.7417	N	8033.8431	W	1	8	0.9	663	M
113	1995	134	1349	26.25	7.610	1997	190.300	134928	2833.7379	N	8033.8097	W	1	8	0.9	662	M
113	1995	134	1349	26.5	7.670	1997	191.700	134928	2833.7379	N	8033.8097	W	1	8	0.9	662	M
113	1995	134	1349	26.75	5.727	1997	143.200	134928	2833.7379	N	8033.8097	W	1	8	0.9	662	M
113	1995	134	1349	27	6.338	1997	158.500	134928	2833.7379	N	8033.8097	W	1	8	0.9	662	M
113	1995	134	1349	27.25	5.660	1996	141.500	134929	2833.7338	N	8033.7762	W	1	8	0.9	661	M
113	1995	134	1349	27.5	6.205	1997	155.100	134929	2833.7338	N	8033.7762	W	1	8	0.9	661	M
113	1995	134	1349	27.75	7.110	1997	177.700	134929	2833.7338	N	8033.7762	W	1	8	0.9	661	M
113	1995	134	1349	28	7.590	1997	189.700	134929	2833.7338	N	8033.7762	W	1	8	0.9	661	M
113	1995	134	1349	28.25	5.753	1997	143.800	134930	2833.7294	N	8033.7424	W	1	8	0.9	660	M

E/W (label for longitude, East/West); diff (differential, 2, or normal, 1, GPS mode); # Sat (number of GPS satellites); HDOP (horizontal dilution of precision [measure of GPS accuracy]); alt (altitude reported from GPS receiver); and units (M, meters for alt).

Personnel from The Aerospace Corporation have reviewed these data in 10 min increments and applied baseline corrections to eliminate apparently negative HCl concentrations. Personnel from The Aerospace Corporation have also performed the conversions necessary to report distance, polar angles, and Cartesian position in meters relative to SLC-40.

Figure 2 plots the spatial extent of aircraft sampling in the 100 min following the launch of K-23. It represents conversion of the latitude and longitude of the aircraft position to Cartesian coordinates centered on the SLC-40 launch complex. As shown in Figure 2, the aircraft flight pattern was largely confined to a 15 km x 15 km square occupying the northeast and southeast quadrants relative to the launch complex. Time (0–100 min) and altitude (0–3700 m) are variables in the flight tracks presented in other more detailed figures. Thus, the HCl concentration hits noted in Figure 2 must be interpreted in light of these other critical variables.

3.1.1 HCl Concentration Hits as a Function of Bearing from SLC-40

Figure 3 substantiates that the aircraft focused on a modest range of polar angles relative to the launch complex. In this report, the angles reported will conform to the convention of rawinsonde wind vectors (the angle from which the wind originates). Thus, the angles referenced are related by

$$\theta = 180 + \Phi \qquad\qquad (1)$$

where θ is the rawinsonde wind angle and Φ is the measured polar angle of the plume track with respect to true north. The nominal trajectory of the ground cloud was shown to be 249° in previous reports (see Figure 1).[7,8] The T-0.3 hr rawinsonde wind vectors of the bottom, middle, and top of the ground cloud were 235°, 261°, and 280°, respectively. Referring to Figure 3, it can be seen that there are two groups of HCl aircraft hits (0–50 min and 55–80 min). Subsequent data will show that hits within the first group (0–50 min) are at relatively low altitude (600–1500 m) along the nominal ground cloud track (250 +/- 20°). The second group (55–80 min) of hits occurs at higher altitude (2000–3500 m) and is located south (290 +/- 30°) of the nominal ground track. It is our preliminary conclusion that the second group of hits derives from the attached column of the vehicle exhaust that was deposited initially in this higher altitude range as documented by imagery during the first 20 min following launch.
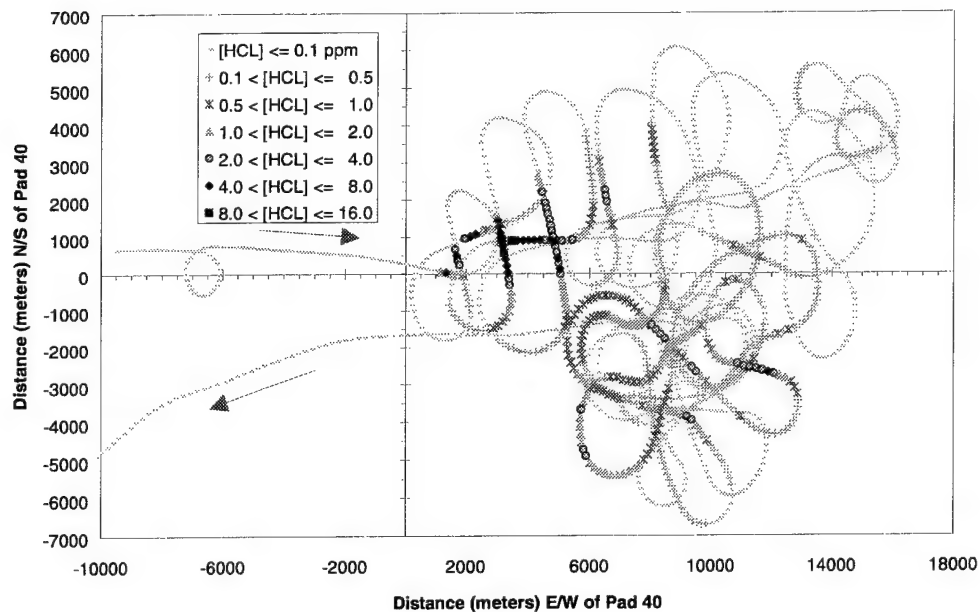
Figure 2.   Cartesian Plot Documenting the Aircraft's Position Relative to SLC-40 and the Measured HCl Concentration Throughout the 100 min K-23 Exhaust Cloud Sampling Mission.
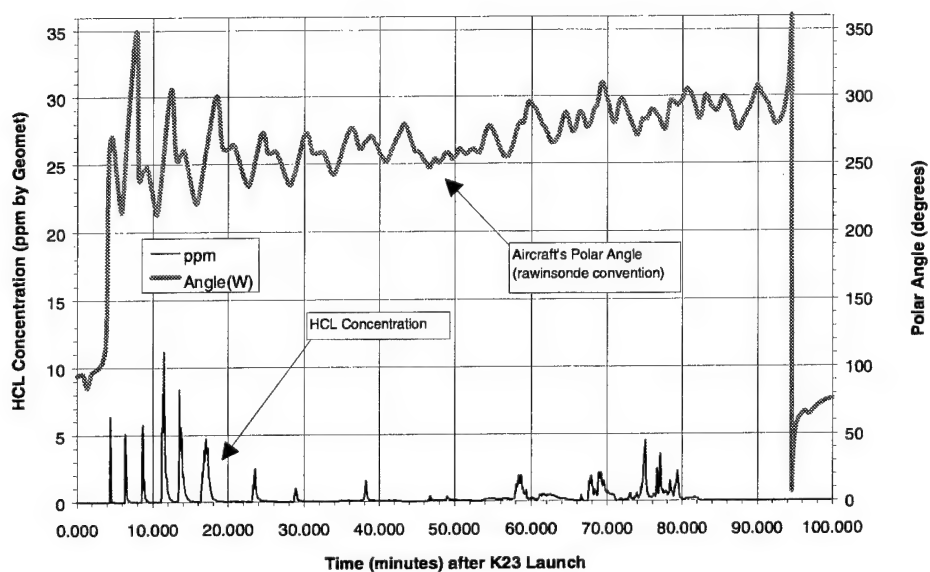
Figure 3.   Summary of the Aircraft's HCl Concentration Measurements and its Polar Angles (rawinsonde convention) Plotted Against Time (minutes) After the Titan IV K-23 Launch.

3.1.2 HCl Concentration Hits as a Function of Radial Distance from SLC-40

Figure 4 can be used to illustrate several logical conclusions regarding the sampling campaign. The highest HCl concentrations are encountered at early times and in close proximity (<7 km) to the launch complex. However, significant concentration hits (2–4 ppm) were observed at late times and at ranges of 10 +/- 2 km from SLC-40. As shown in Figure 5 and discussed below, these later hits were at high altitudes. All hits representative of the stabilized ground cloud, both initially and after downwind dispersion, were observed along the 250 +/- 20° track discussed in the previous paragraphs.
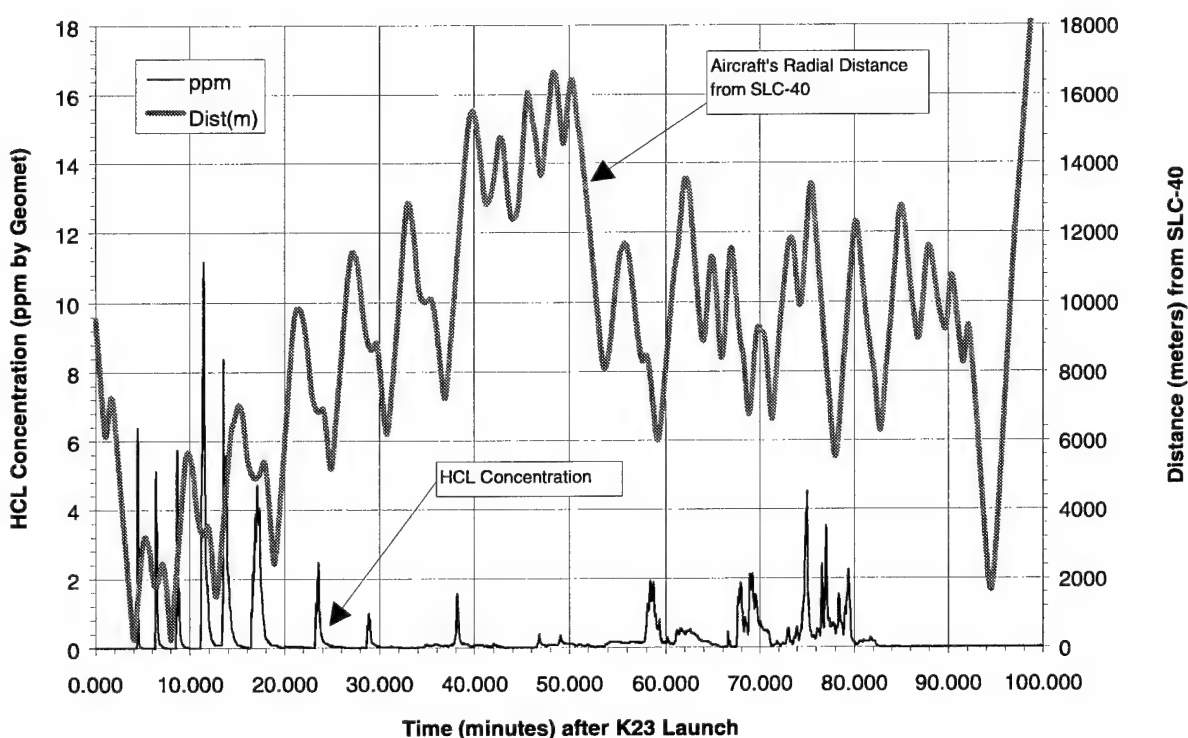
Figure 4. Summary of the Aircraft's HCl Concentration Measurements and Radial Distances (m) from SLC-40 Plotted Against Time (min) After the Titan IV K-23 Launch.

3.1.3 HCl Concentration Hits as a Function of Altitude

Figure 5 documents that the early time (0–50 min) HCl hits resulted from fly-throughs of the rising and stabilized ground cloud at altitudes below 1500 m. Three-dimensional imagery concluded that the top of the stabilized ground cloud initially reached altitudes of 2000 to 2200 m and later subsided to 1800 m (see Figure 13 in Section 3.2.1 of this report). Given the altitude range, radial distance range, and polar angle range covered in the time period of 30 to 60 min, it is perhaps surprising that so few HCl hits were observed. Examination of Figure 5 shows that the late time hits (60–80 min) all occurred at an altitude of roughly 2200 m and a bearing (Figure 3) of roughly 290 +/- 30°. The fact that no HCl hits were detected *below* that altitude as the plane decended (80–100 min) suggests that this material derives from the attached plume column. As noted, T-0.3 hr rawinsonde wind vectors at the highest altitude (2200 m) reached by the rising ground cloud (as revealed by imagery) were typically 280°– 290° (i.e., close to the bearing of the aircraft's high altitude HCl hits).
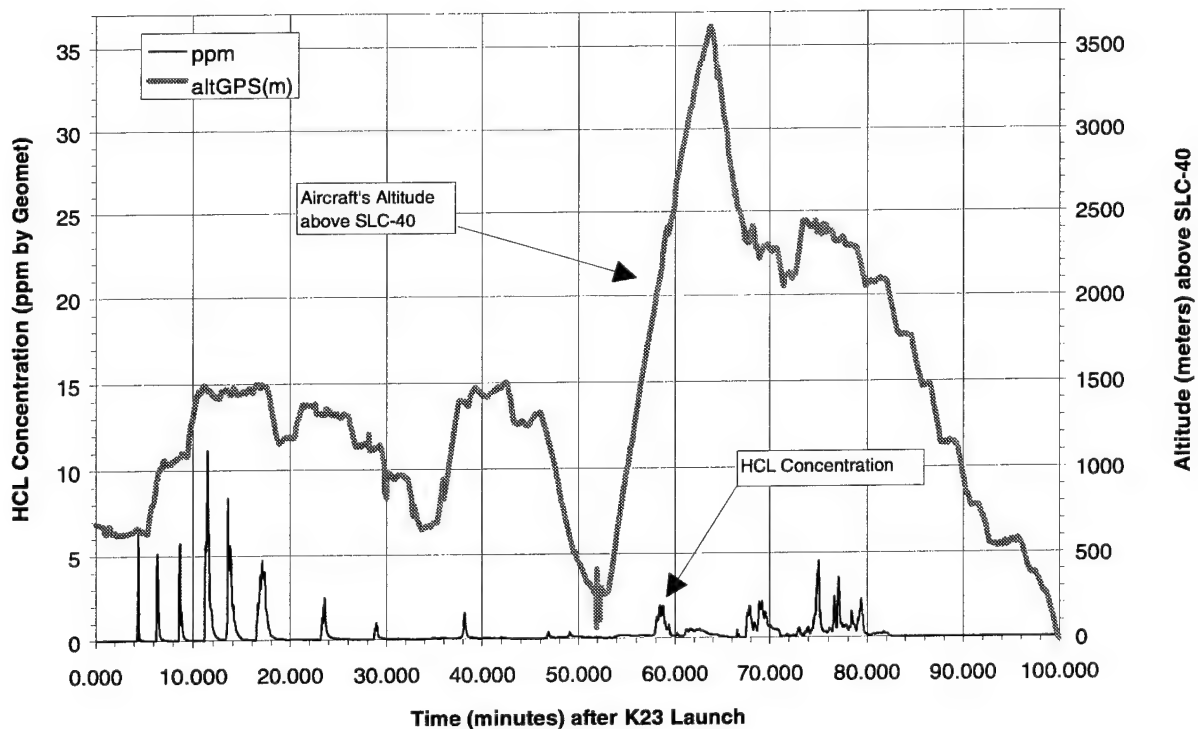
Figure 5. The Aircraft's HCl Concentration Measurements and Altitude (m) Plotted Against Time (min) After the Titan IV K-23 Launch.

3.1.4 HCl Concentration Hits as a Function of Altitude and Aircraft Position

This section will provide substantiation for observations made in previous portions of this overview of the aircraft sampling data. The figures referenced in this section are subsets of the data presented in the Cartesian plot in Figure 2.

3.1.4.1 HCl Hits at Altitudes Greater than 2000 m

Figure 6 depicts the high altitude sampling data. As previously noted, the observed HCl hits at high altitudes are in the southeast quadrant relative to SLC-40. They occur at late times (60–80 min) and in a fairly narrow altitude range centered around 2200 m. It is noteworthy that the imagery of the launch cloud documented extensive dispersed plume material above and to the south of the ground cloud (see Figure 2.5 of reference 8). Since no high altitude track was flown in the northeast quadrant (see Figure 5), it is not appropriate to conclude that no detectible high altitude HCl exists there.
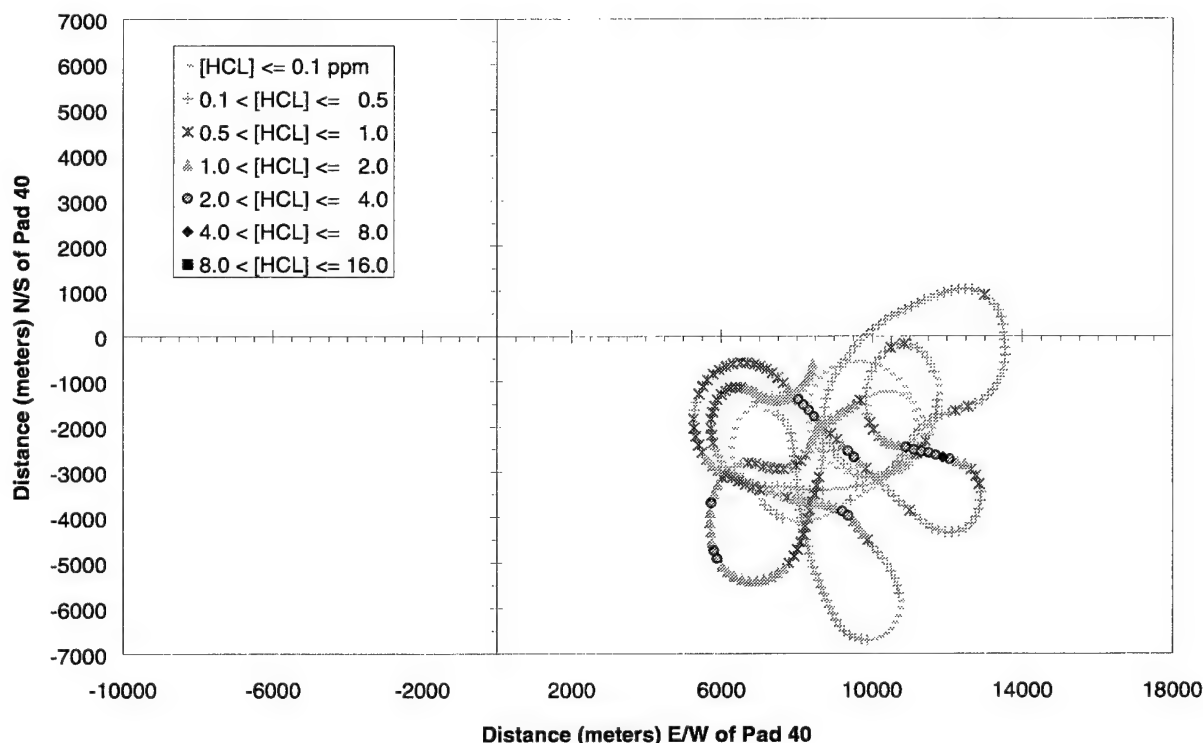
Figure 6. Summary Cartesian Plot Documenting the Aircraft's Position and Measured HCl Concentrations While Sampling at Altitudes Greater than 2000 m After the Titan IV K-23 Launch. The aircraft only sampled altitudes greater than 2000 m at times between 58 and 83 min after the K-23 launch.

11

3.1.4.2 HCl Hits at Altitudes Less than 2000 m

The majority of the stabilized K-23 ground cloud—as determined by 3-D plume imagery—lies below 2000 m and along a plume track centered on 250°. Examination of Figure 7 shows this observation is consistent with the position of the major HCl hits during aircraft plume transects at altitudes below 2000 m.
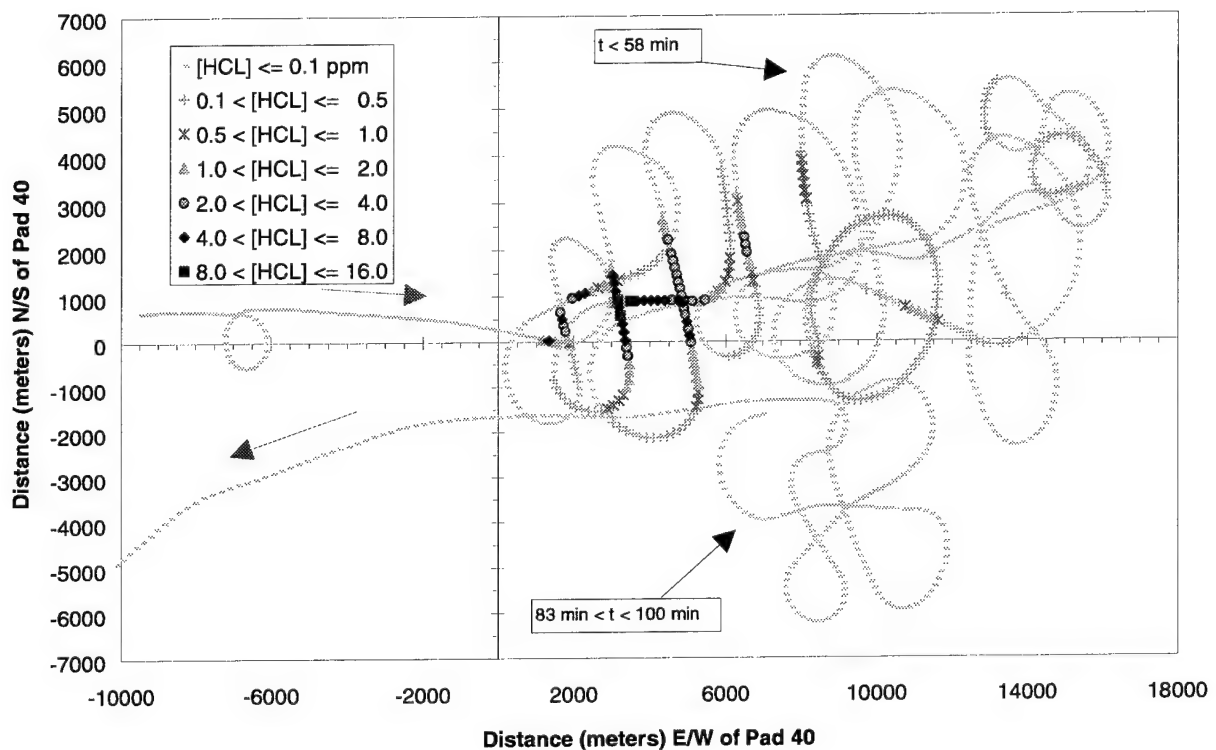
Figure 7. Summary Cartesian Plot Documenting the Aircraft's Position and Measured HCl Concentrations While Sampling at Altitudes Less than 2000 m After the Titan IV K-23 Launch. The aircraft only flew at altitudes less than 2000 m during two time periods: (1) 0–58 min while sampling the ground cloud as it moved into the northeast quadrant and (2) 83–100 min while spiraling to lower altitudes beneath the high altitude plume documented in Figure 6 in the southeast quadrant.

3.1.4.3 HCl Hits at Altitudes Less than 1000 m

A small fraction of the aircraft flight time was spent at altitudes below 1000 m. Figure 8 shows that the only major hits were at short times (< 8 min) at small distances (< 2.5 km) from the launch complex. There were, however, measurable levels of HCl at later times (40–55 min), altitudes between 400 and 700 m, ranges of 13 to 16 km, and angles of 245° to 260°. This is consistent with downward dispersion of lower portions of the stabilized ground cloud.
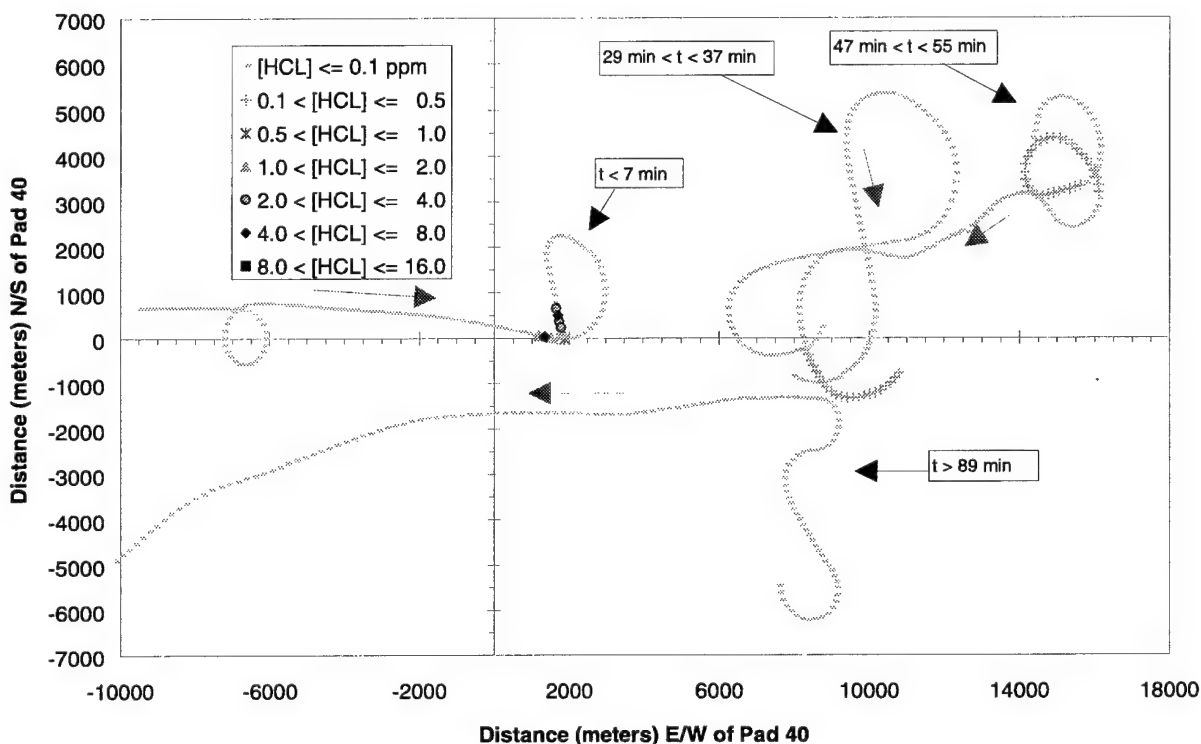
Figure 8. Summary Cartesian Plot Documenting the Aircraft's Position and Measured HCl Concentrations While Sampling at Altitudes Less than 1000 m after the Titan IV K-23 Launch. The aircraft flew at altitudes less than 1000 m during four time periods: (1) 0–7 min while sampling the ground cloud immediately adjacent to SLC-40; (2) 29–37 min while flying beneath the ground cloud in the northeast quadrant; (3) 47–55 min while flying through the bottom of the ground cloud in the northeast quadrant and climbing into the high altitude cloud in the southeast quadrant; and (4) 89–100 min while passing beneath the high altitude HCl cloud in the southeast quadrant (see Figure 6).

13

3.1.4.4 HCl Hits at Altitudes Less than 500 m

Only one brief period (49–54 min) was flown at altitudes below 500 m. The "plus" symbols in Figure 9 show a minor hit (0.1< HCl < 0.5 ppm) along the nominal ground cloud track at a distance of roughly 16 km from the complex.
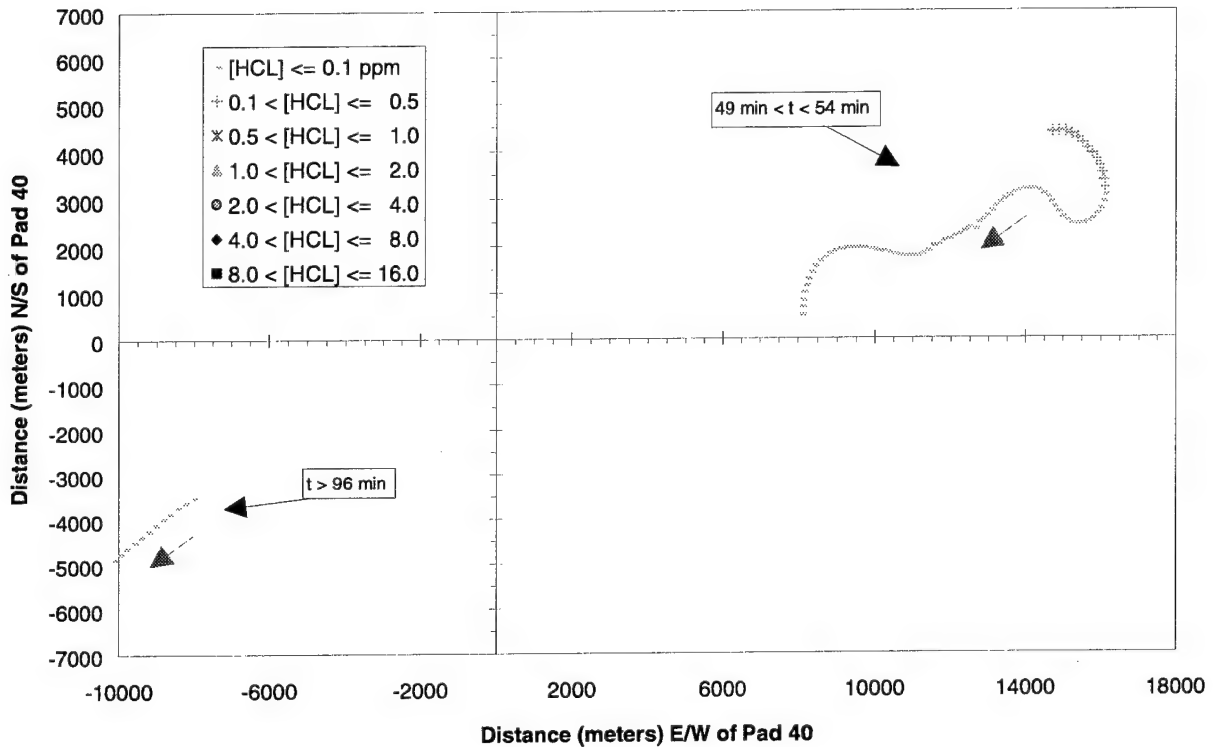
Figure 9. Summary Cartesian Plot Documenting the Aircraft's Position and Measured HCl Concentrations While Sampling at Altitudes Less than 500 m After the Titan IV K-23 Launch. The aircraft flew at altitudes less than 500 m during two time periods: (1) 49–54 min while flying through the bottom of the ground cloud in the northeast quadrant; and (2) 96–100 min while returning to the airport after sampling beneath the high altitude HCl cloud in the southeast quadrant (see Figure 6).

3.2 Details of Aircraft HCl Sampling Data for K-23: Observations in 10 Sequential 10 min Time Windows Following Launch

Seven types of plots will be presented for each of the 10 time windows of 10 min sampled by the aircraft subsequent to the launch of K-23. These plots are (1) Geomet HCl density traces; (2) latitude and longitude of the aircraft flight pattern; (3) Cartesian coordinates of the aircraft flight pattern; (4) HCl concentration, visible ground cloud dimensions, and aircraft altitude as a function of time (T = 0-Tw); (5) HCl concentration, visible ground cloud dimensions, and aircraft altitude as a function of time (T=Tw-10 to Tw min); (6) aircraft polar coordinate position during the T=Tw-10 to T=Tw min transects; and (7) aircraft altitude and angular position during the T=Tw-10 to Tw min transects. Note that Tw = 10, 20, ..., 100 in the 10 sets of plots. For the first two 10 min windows, a careful analysis of the HCl profiles is performed because the time dependence of the HCl can be directly compared to ground-based imagery of the plume geometry. In other words, by using the HCl time profile and converting it to a spatial profile using the relative aircraft and plume speed, we have described a chord through the volume of the ground cloud.

3.2.1 Aircraft Sampling from T=0 to T=10 min

Figure 10 (a)–(c) shows the baseline-corrected HCl concentration data for the three plume transects conducted by the aircraft in this time window. The sharp leading edge and the slow decay on the trailing edge are discussed in Appendix 3 and in previous reports on the K-23 launch.[7,8] The data in Figure 10 are consistent with the slow recovery time and fast rise time of the Geomet as configured for the aircraft. This complex response has been documented by I-NET,[*] as well as in previous literature.[9] According to Reference 9, the response time to 90% of peak using an HCl step function of 10 ppm is approximately 3 sec. Since the exposures in Figure 10 a-c are for roughly 3 sec (full-width at half-maximum [FWHM]), the peak concentrations reported in the figures will be relatively accurate but slightly low. The trailing edges are most likely to be experimental artifacts (Appendix 3).

---

[*] D. Curran, I-NET, Inc., private communication (1995).

Figure 10a. Baseline-Corrected [HCl] Data for Sampling Aircraft Pass 1: T = 13:45–13:55 Zulu window. Several "average" concentrations (ppm) are suggested, based on the fraction of total integrated HCl represented in two time windows defined by threshold criteria (see Appendix 3).
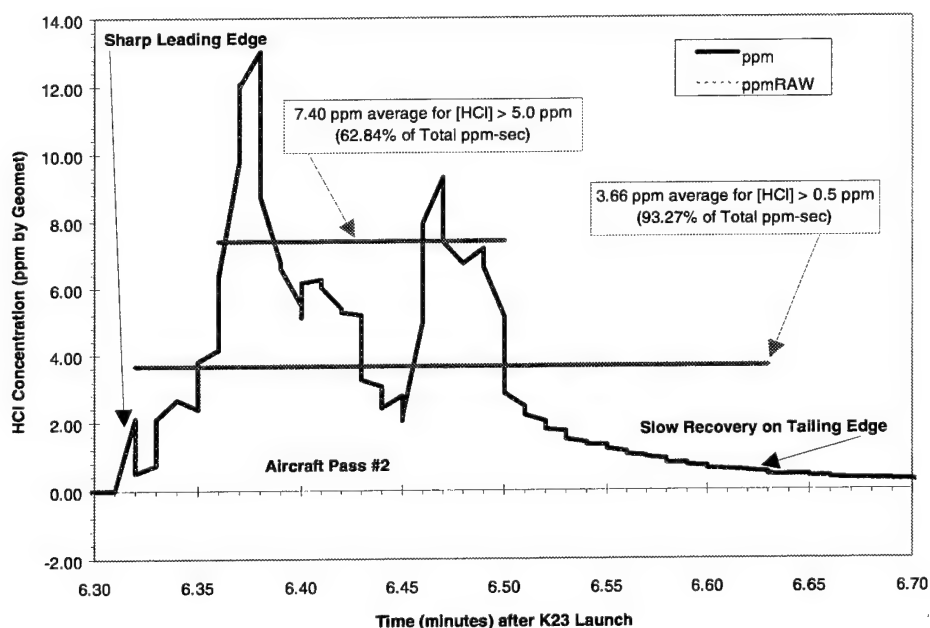
Figure 10b. Baseline-Corrected [HCl] Data for Sampling Aircraft Pass 2: T = 13:45–13:55 Zulu window. Several "average" concentrations (ppm) are suggested, based on the fraction of total integrated HCl represented in two time windows defined by threshold criteria (see Appendix 3).

16
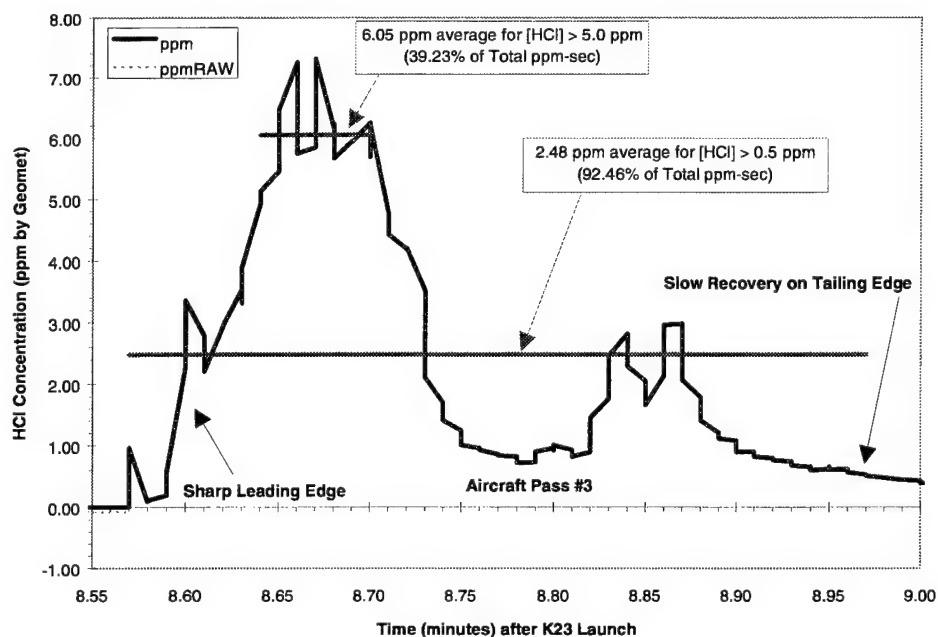
Figure 10c. Baseline-Corrected [HCl] Data for Sampling Aircraft Pass 3: T = 13:45–13:55 Zulu window. Several "average" concentrations (ppm) are suggested, based on the fraction of total integrated HCl represented in two time windows defined by threshold criteria (see Appendix 3).

Figure 11 presents the positional information from the aircraft GPS records (e.g., Table 1), together with the HCl concentration data from the three plume transects in this period (Figure 10 a-c). The flight direction of the aircraft is indicated by arrows. Figure 12 converts the data from Figure 11 to Cartesian coordinates centered on SLC-40.

17
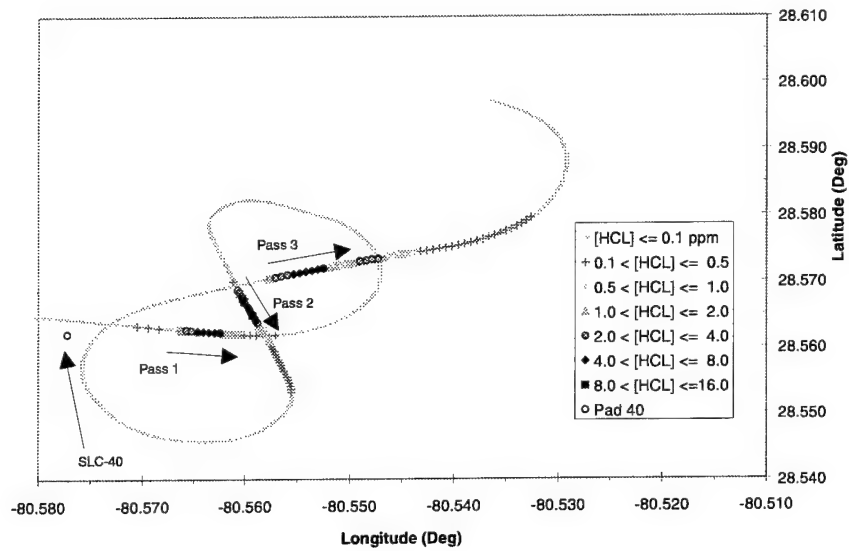
Figure 11. Aircraft GPS Latitude and Longitude: T = 13:45–13:55 Zulu.
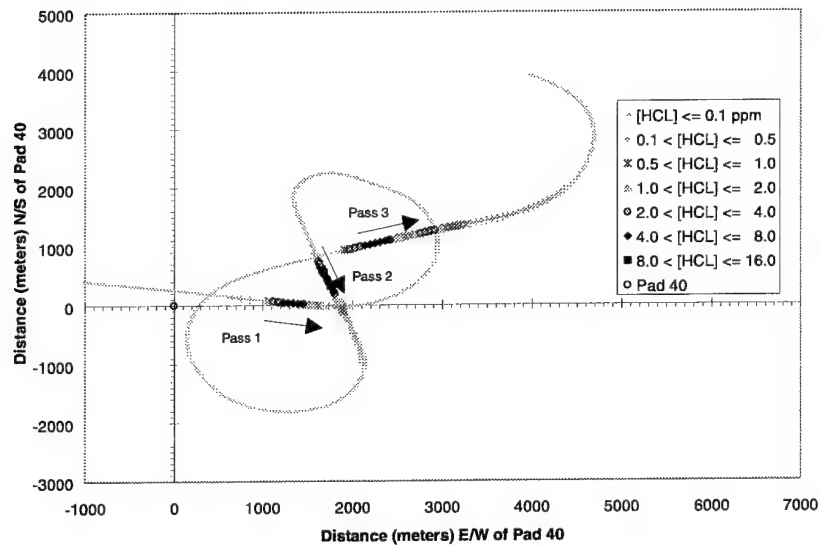
Figure 12. Cartesian Coordinates of the Aircraft Flight Pattern: T = 13:45–13:55 Zulu.

Figure 13 is a composite of aircraft sampling data (passes 1–3), aircraft altitude, and reduced plume imagery data showing the top and the bottom of the observed visible ground cloud, all as a function of time. The most salient feature of this plot is that when each of the three HCl hits is reported, the aircraft is located near the bottom edge of the ground cloud, as observed by visible imagery. Thus, the peak HCl concentrations observed may not reflect the highest HCl densities in the cloud center during this time window. Figure 14 shows a higher time resolution representation of the data in Figure 13 for the first 10 min of monitoring.

Figure 13. HCl Concentration , Visible Ground Cloud Dimensions, and Aircraft Altitude as a Function of Time (T=0–T=20 min).

Figure 14. HCl Concentration, Visible Ground Cloud Dimensions, and Aircraft Altitude as a Function of Time (T=0–T=10 min).

Figure 15 shows a polar coordinate plot of the direction of aircraft flight for the three transects occurring during this first 10 min window. Passes 1 and 3 varied range along roughly constant polar angles. Pass 2 varied polar angle at roughly constant range. Pass 2 is interesting in that it occurred roughly 6.5 min after launch. The rawinsonde wind speed is roughly 5 m/sec. Thus, the center of the plume should be 2 km downwind of the complex at the time of pass 2. Examination of Figure 15 shows that pass 2 was made 1.8 km downwind; therefore, it should be a reasonable measure of the early time angular spread of the plume (240°-270°) near the bottom of the visible cloud.

Pass 3 is relatively close (245°) to the center of the plume track (249°) and shows that 8.8 min after launch and 2.6 km downwind of SLC-40, the along-plume dimension is approximately 1.4 km near the bottom of the visible cloud. These observations are summarized in Section 4 of the report (Table 2).

20
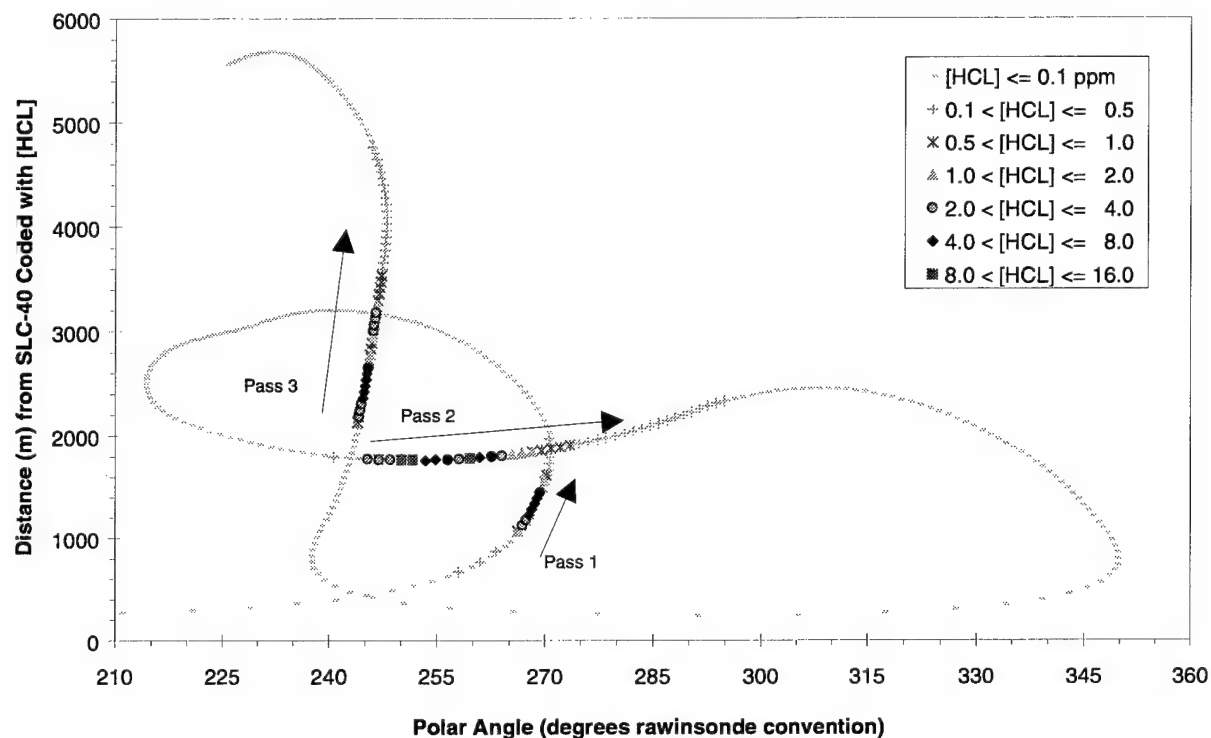
Figure 15. Aircraft Polar Coordinate Position During the T=0–T=10 min Transects.

Figure 16 provides supporting data to Figure 15, showing that the altitude of the aircraft during each of the three transects was roughly constant when HCl hits were experienced. As stated previously, all three passes occurred very close to the *bottom* of the plume as observed by 3-D visible imagery.

3.2.2 Aircraft Sampling from T=10 to T=20 min

Figures 17 (a)-(c) show the baseline-corrected HCl concentration data for the three plume transects conducted by the aircraft in this time window. The sharp leading edge and the slow decay on the trailing edge are discussed in Appendix 3 and in previous reports on the K-23 launch.[7,8]
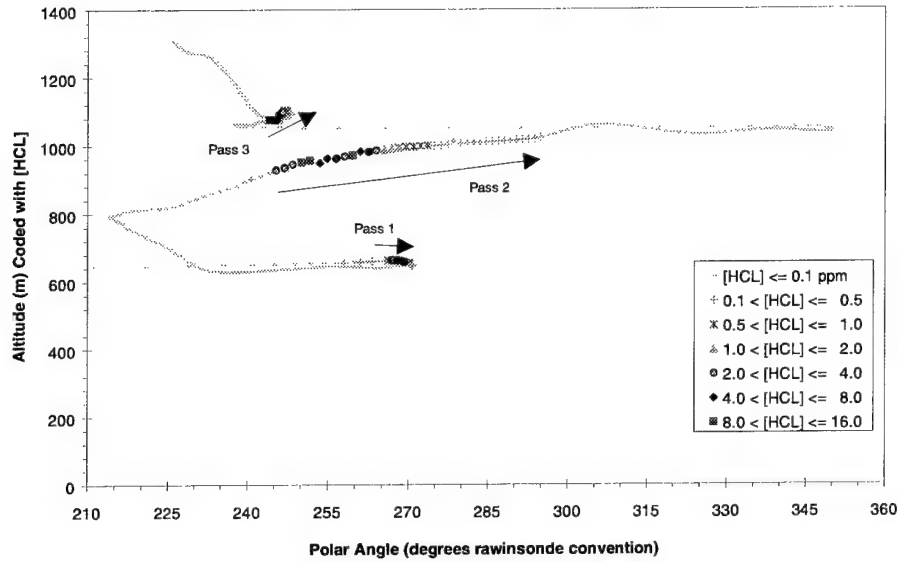
Figure 16. Aircraft Altitude and Angular Position During the T=0–T=10 min Transects.
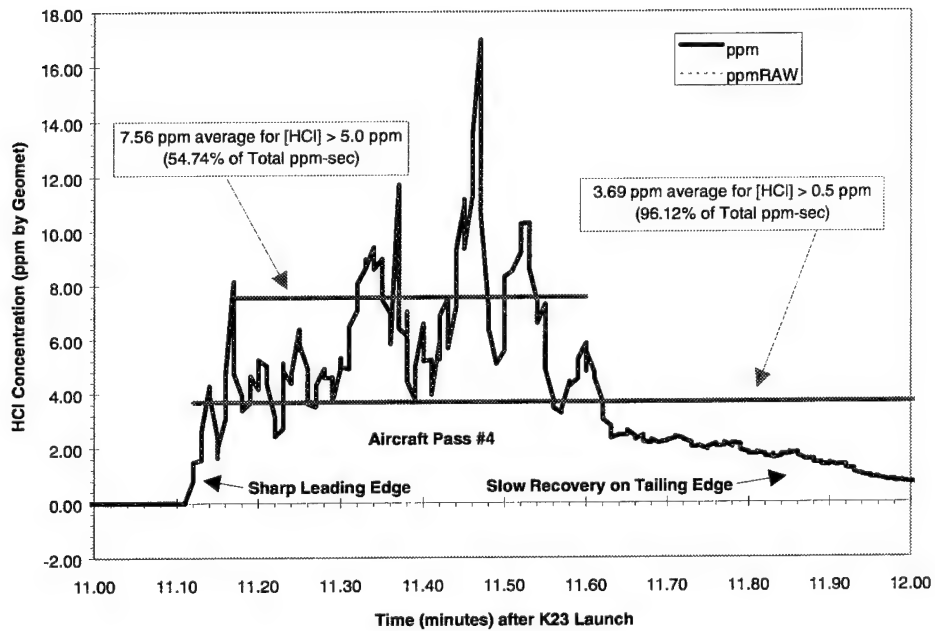
Figure 17a. Baseline-Corrected [HCl] Data for Sampling Aircraft Pass 4: T=13:55–14:05 Zulu window. Several "average" concentrations (ppm) are suggested, based on the fraction of total integrated HCl represented in two time windows defined by threshold criteria (see Appendix 3).
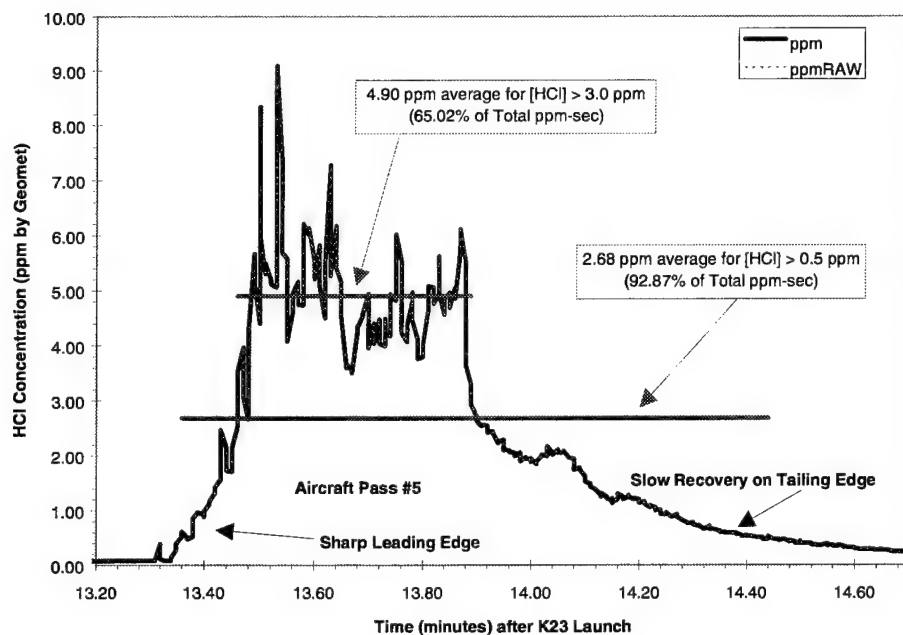
Figure 17b. Baseline-Corrected [HCl] Data for Sampling Aircraft Pass 5: T=13:55–14:05 Zulu window. Several "average" concentrations (ppm) are suggested, based on the fraction of total integrated HCl represented in two time windows defined by threshold criteria (see Appendix 3).
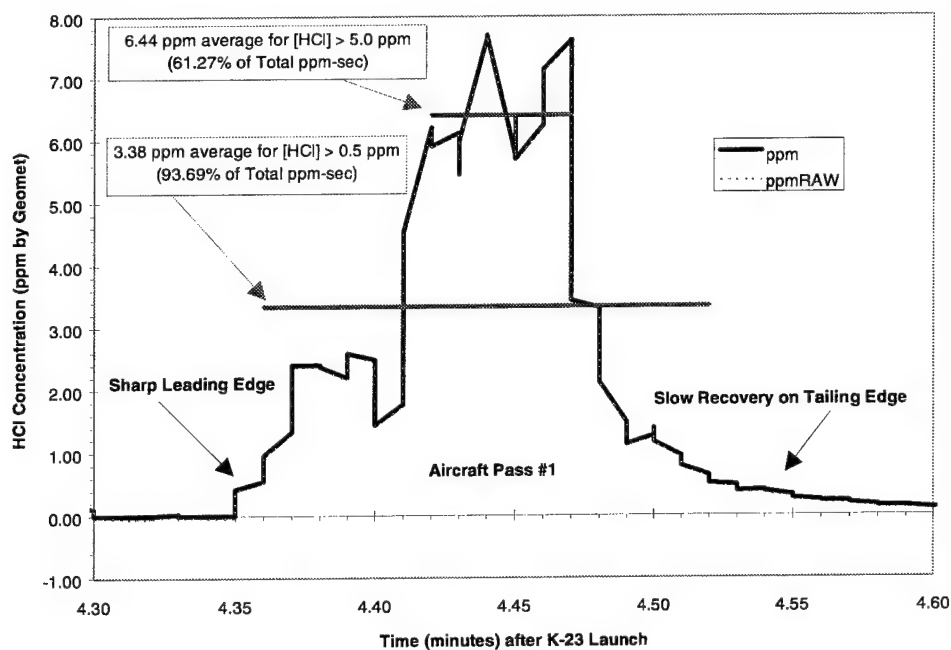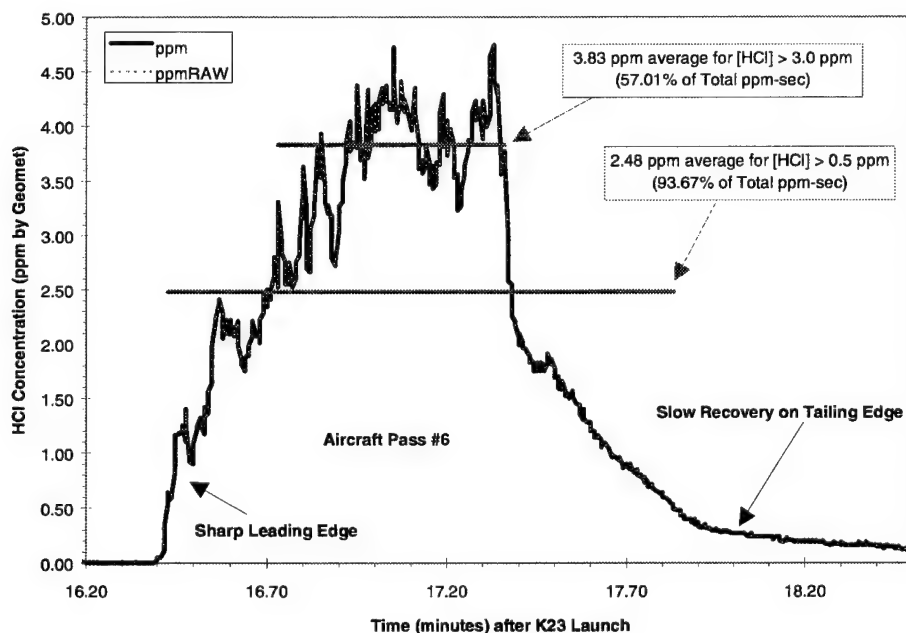

Figure 17c. Baseline-Corrected [HCl] Data for Sampling Aircraft Pass 6: T=13:55–14:05 Zulu window. Several "average" concentrations (ppm) are suggested, based on the fraction of total integrated HCl represented in two time windows defined by threshold criteria (see Appendix 3).

23

Figure 18 presents the positional information from the aircraft GPS records (e.g., Table 3) with the HCl concentration ranges of the three plume transects in this period (Figure 17 a–c). The flight direction of the aircraft is indicated by arrows.

Figure 19 converts the data in Figure 18 to Cartesian coordinates centered on SLC-40.
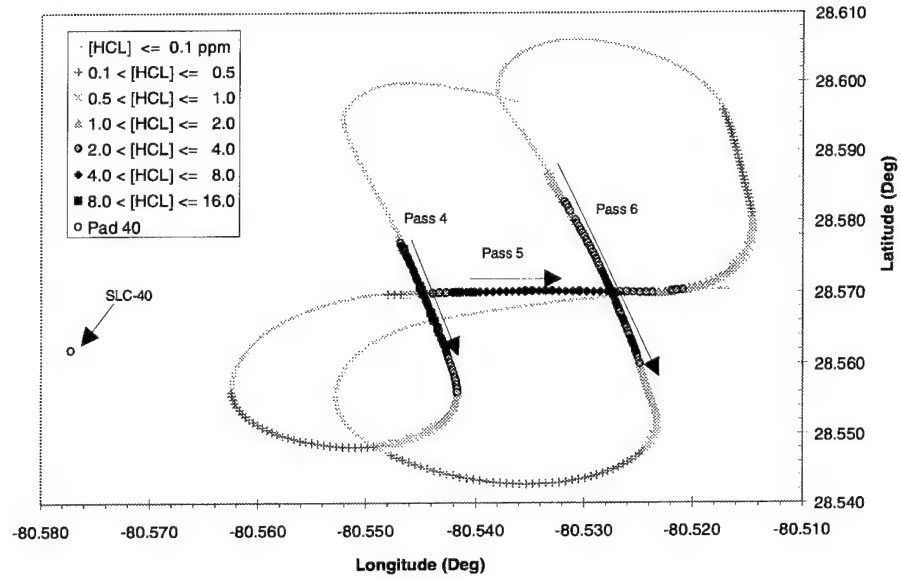
Figure 18. Aircraft GPS Latitude and Longitude: T=13:55–14:05 Zulu.
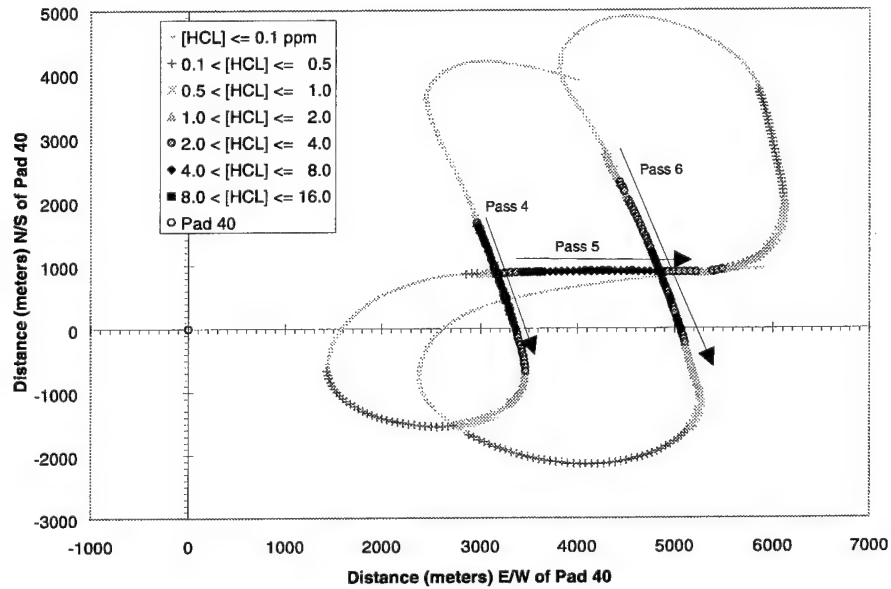
Figure 19. Cartesian Coordinates of the Aircraft Flight Pattern: T=13:55–14:05 Zulu.

24

Figure 20 is a composite of aircraft sampling data (passes 4–6) giving HCl concentrations, aircraft altitude, and reduced plume imagery data showing the top and the bottom of the observed visible ground cloud, all as a function of time. The most salient feature of this plot is that when each of the three HCl hits is reported, the aircraft is located near the middle of the ground cloud, as observed by imagery. Thus, the peak HCl concentrations observed are expected to represent the highest HCl densities in the cloud during this time window, assuming that the aircraft also flew near the center of the ground cloud in the x-y plane (see References 7 and 8).
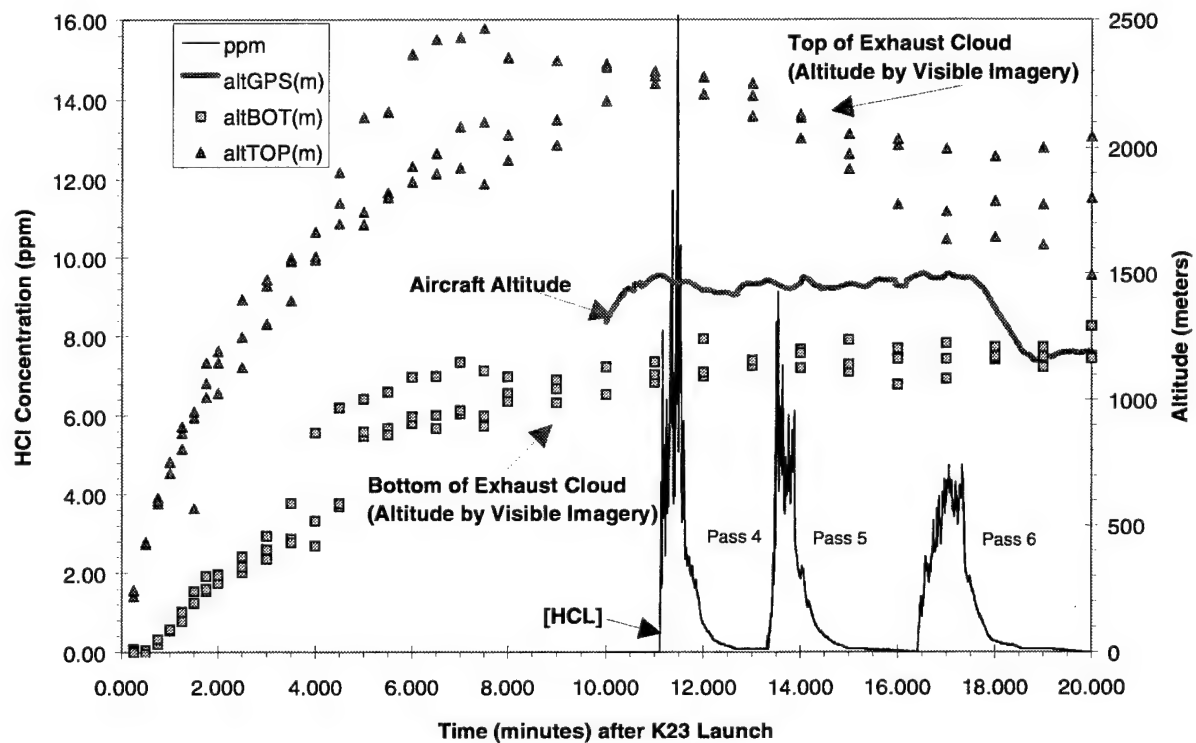
Figure 20. HCl Concentration, Visible Ground Cloud Dimensions, and Aircraft Altitude as a Function of Time (T=0–T=20 min).

25

Figure 21 shows a higher time resolution representation of the data in Figure 20 for the second 10 min of monitoring.

Figure 21. HCl Concentration, Visible Ground Cloud Dimensions, and Aircraft Altitude as a Function of Time (T=10–T=20 min).
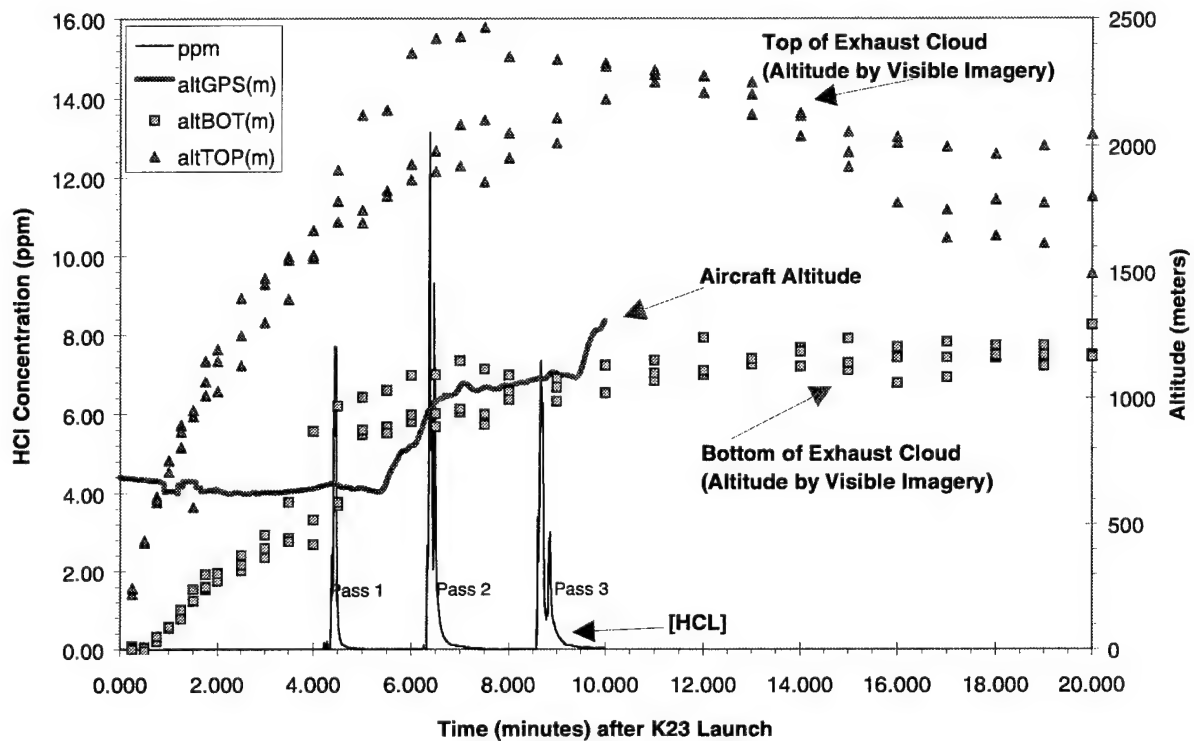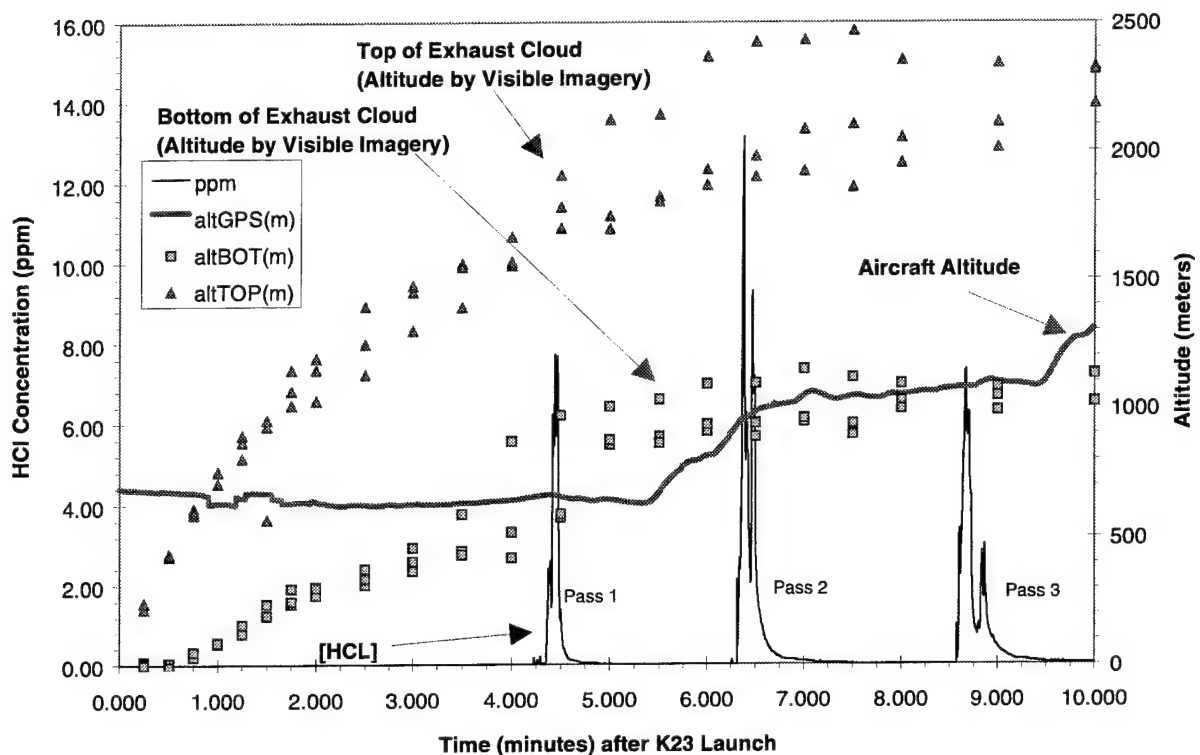
Figure 22 shows a polar coordinate plot of the direction of aircraft flight for the three transects occurring during this second 10 min window. Pass 5 varied range along roughly constant polar angles. Passes 4 and 6 varied polar angle at roughly constant range. Pass 4 (11.5 min) and pass 6 (17 min) show that the plume has similar angular spreads (235°–290°) at 3.5 and 5.2 km downwind, respectively. Geomet time response leads to the potential for overestimating the angular spreads (passes 4 and 6).

Pass 5 is relatively close (250°–260°) to the center of the plume track (249°) and shows that 14 min after launch and 4.1 km downwind of SLC-40, the along-plume dimension is approximately 3.5 km. Again, Geomet response time leads to the potential to overestimate this along-plume dispersion distance.

Figure 23 provides supporting data to Figure 22, showing that the altitudes of the three transects were roughly constant (1450–1500 m) when HCl hits were experienced. As stated previously, all three passes occurred near the *middle* of the plume, as observed by 3-D visible imagery.
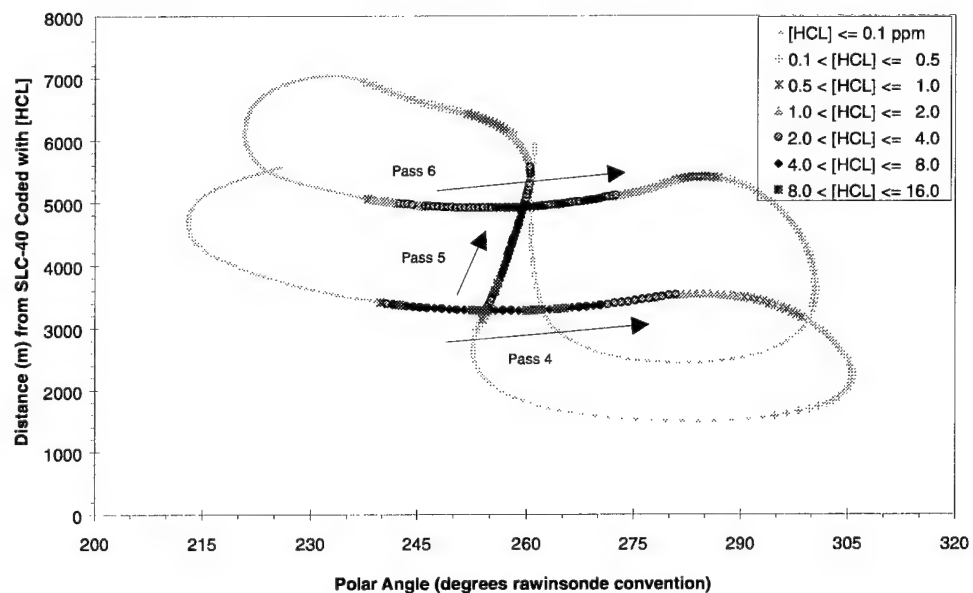
Figure 22. Aircraft Polar Coordinate Position During the T=10–T=20 min Transects.

Figure 23. Aircraft Altitude and Angular Position During the T=10–T=20 min Transects.

3.2.3 Aircraft Sampling from T=20 to T=30 min

Aircraft sampling data from 20 to 100 min are treated differently from the first 20 min of sampling because there are no corresponding imagery data. Thus, we do not have independent confirmation of the absolute location of the aircraft transect relative to the plume position and geometry. Figure 24 shows the raw and baseline-corrected HCl concentration data for the two plume transects conducted by the aircraft in this time window. The sharp leading edge and the slow decay on the trailing edge are discussed in Appendix 3 of this report.

Figure 24. Raw and Baseline-Corrected Aircraft Geomet Traces: T=14:05–14:15 Zulu.

Figure 25 presents the positional information from the aircraft GPS records with the HCl concentration ranges of the two plume transects in this period.

Figure 26 converts the data in Figure 25 to Cartesian coordinates centered on SLC-40.

28
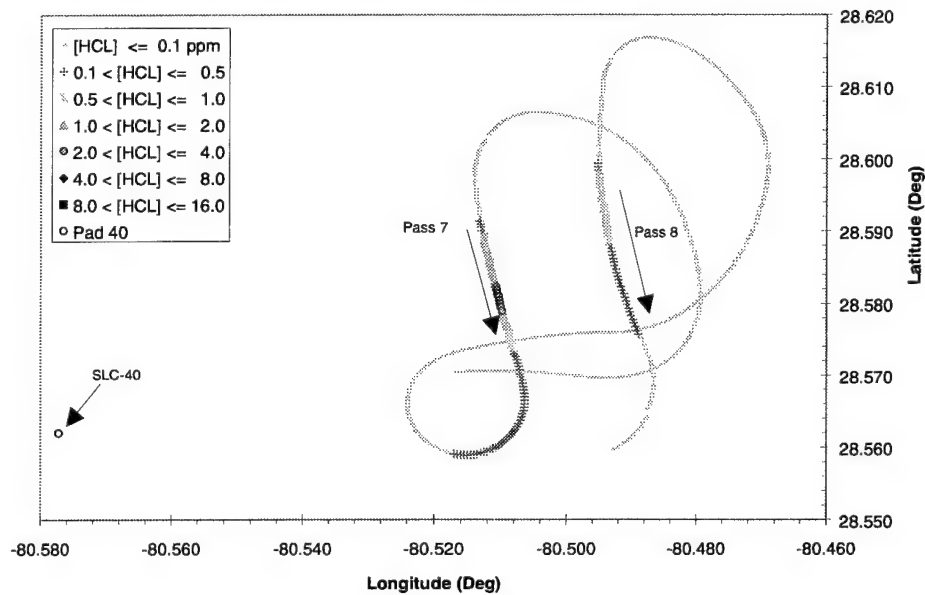
Figure 25. Aircraft GPS Latitude and Longitude: T=14:05–14:15 Zulu.
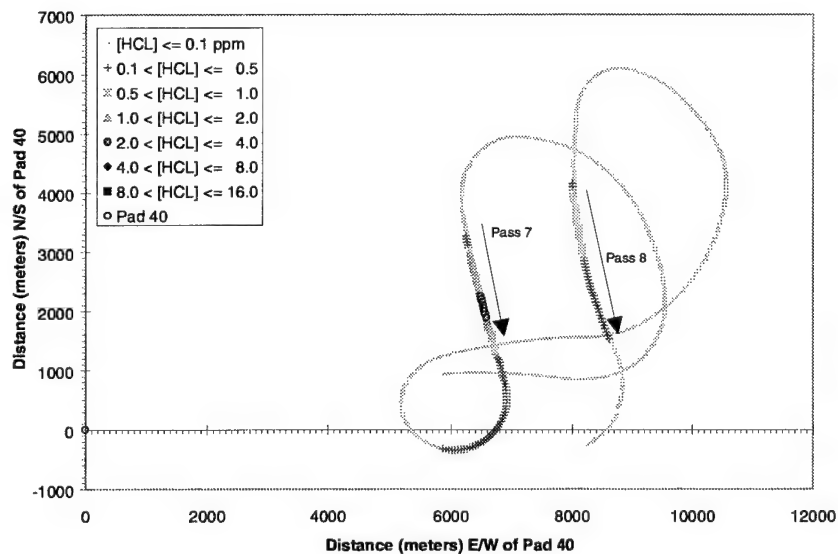
Figure 26. Cartesian Coordinates of the Aircraft Flight Pattern: T=14:05–14:15 Zulu.

29

Figure 27 is a composite of aircraft sampling data (passes 7 and 8) giving HCl concentrations, aircraft altitude, and plume imagery data (for the first 20 min subsequent to launch only) showing the top and the bottom of the observed visible ground cloud. The most salient feature of this plot is that when the two HCl hits are reported, the aircraft is located rather close to the last documented altitude of the bottom of the ground cloud. This could be a major contributing factor to the peak concentration difference (roughly a factor of 3) observed between pass 7 (which was at several hundred meters higher altitude than was pass 8) and pass 8.

Figure 27. HCl Concentration, Visible Ground Cloud Dimensions (0–20 min), and Aircraft Altitude as a Function of Time (T=0–T=30 min).

Figure 28 shows a higher time resolution representation of the data in Figure 27 for the third 10 min of monitoring. The last recorded positions of the top and bottom of the ground cloud as determined by imagery are indicated in the figure.

Figure 28. HCl Concentration and Aircraft Altitude as a Function of Time (T=20–T=30 min).

Figure 29 shows the direction of aircraft flight for the two transects occurring during this third 10 min window. Passes 7 and 8 varied polar angle at constant range from SLC-40 (roughly 7.0 and 8.6 km, respectively). As mentioned above, pass 8 may be quite close to the bottom of the plume (see Figure 30 below), and thus the measurement of its angular spread may not be reliable. Pass 7 is expected to be within the core of the plume, and its angular spread (245°–260°; [HCl] > 0.5 ppm) should be more meaningful.

Figure 30 provides supporting data to Figure 29, showing that the altitude of each of the two transects was roughly constant when HCl hits were experienced. As stated previously, pass 8 occurred very close to the last known altitude of the imagery-derived bottom of the plume; however, pass 7 should be within the plume.

31
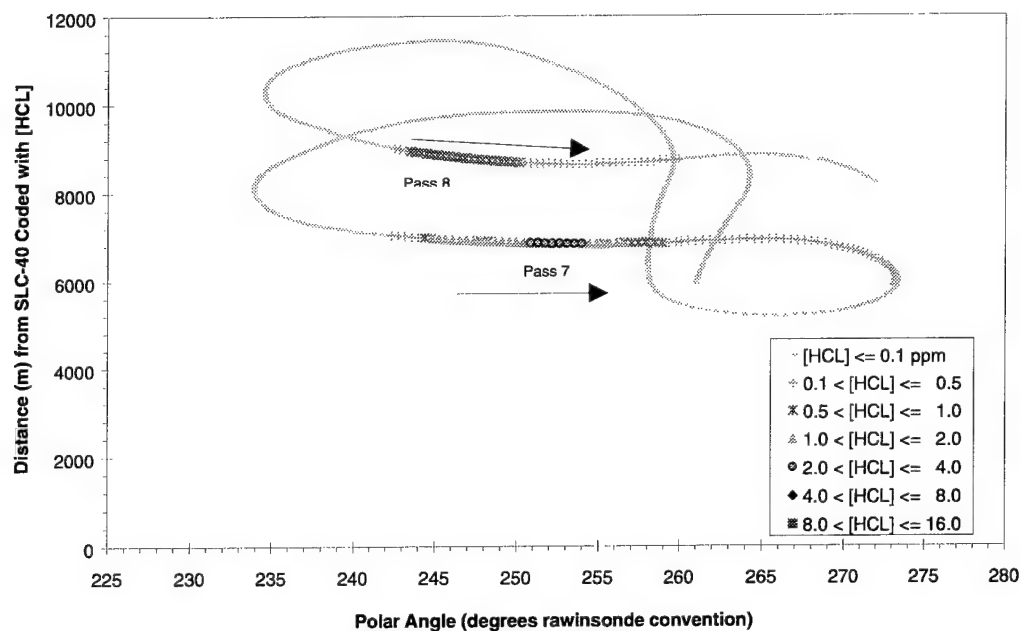
Figure 29. Aircraft Polar Coordinate Position During the T=20–T=30 min Transects.

Figure 30. Aircraft Altitude and Angular Position During the T=20–T=30 min Transects.

3.2.4 Aircraft Sampling from T=30 to T=40 min

Figure 31 shows the raw and baseline-corrected HCl concentration data for the one definable plume transect conducted by the aircraft in this time window. The sharp leading edge of the trace is still quite obvious; the slow decay on the trailing edge of the hit is less obvious at the low signal-to-noise (S/N) ratio involved.
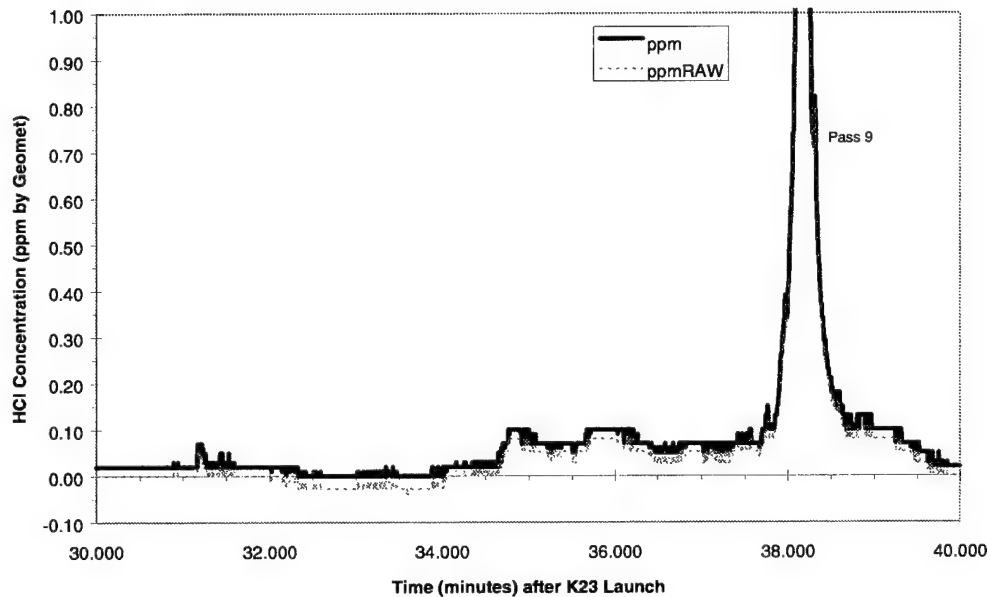
Figure 31. Raw and Baseline-Corrected Geomet Traces: T=14:15–14:25 Zulu.

Figure 32 presents the GPS positional information from the aircraft records, together with the HCl concentration ranges for the one transect in this period that observed an HCl hit.

Figure 33 converts the data in Figure 32 to Cartesian coordinates centered on SLC-40.
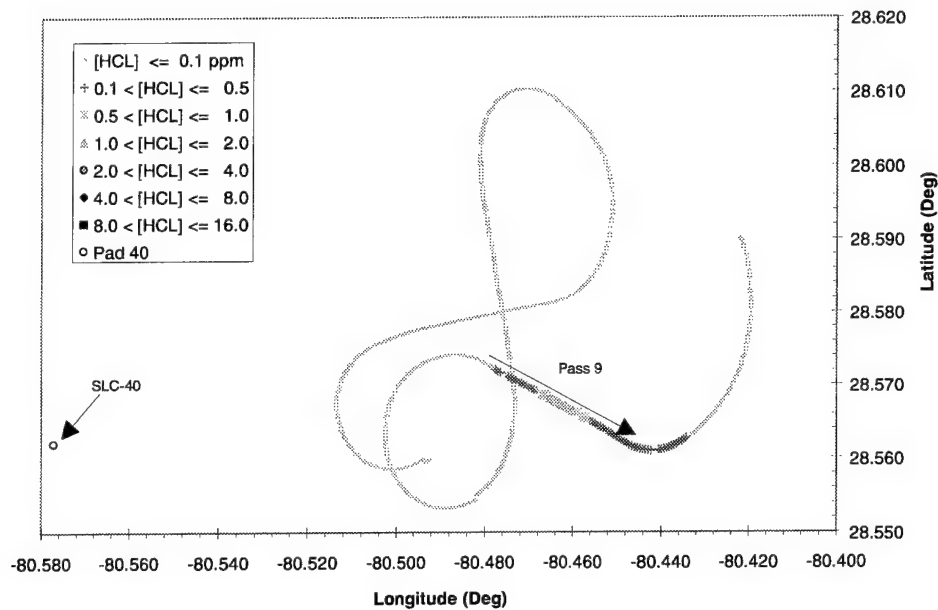
**Figure 32. Aircraft GPS Latitude and Longitude: T=14:15–14:25 Zulu.**

Figure 33. Cartesian Coordinates of the Aircraft Flight Pattern: T= 14:15–14:25 Zulu.

Figure 34 is a composite of aircraft sampling data (pass 9) giving HCl concentrations and aircraft altitude during the period 30–40 min after launch. In addition, plume imagery data taken during the first 20 min following launch show the evolution of the top and the bottom of the observed visible ground cloud. The most salient feature of this plot is that the aircraft altitude appears to be below the bottom of the probable stabilized altitude of the ground cloud until just prior to the hit documented as pass 9.
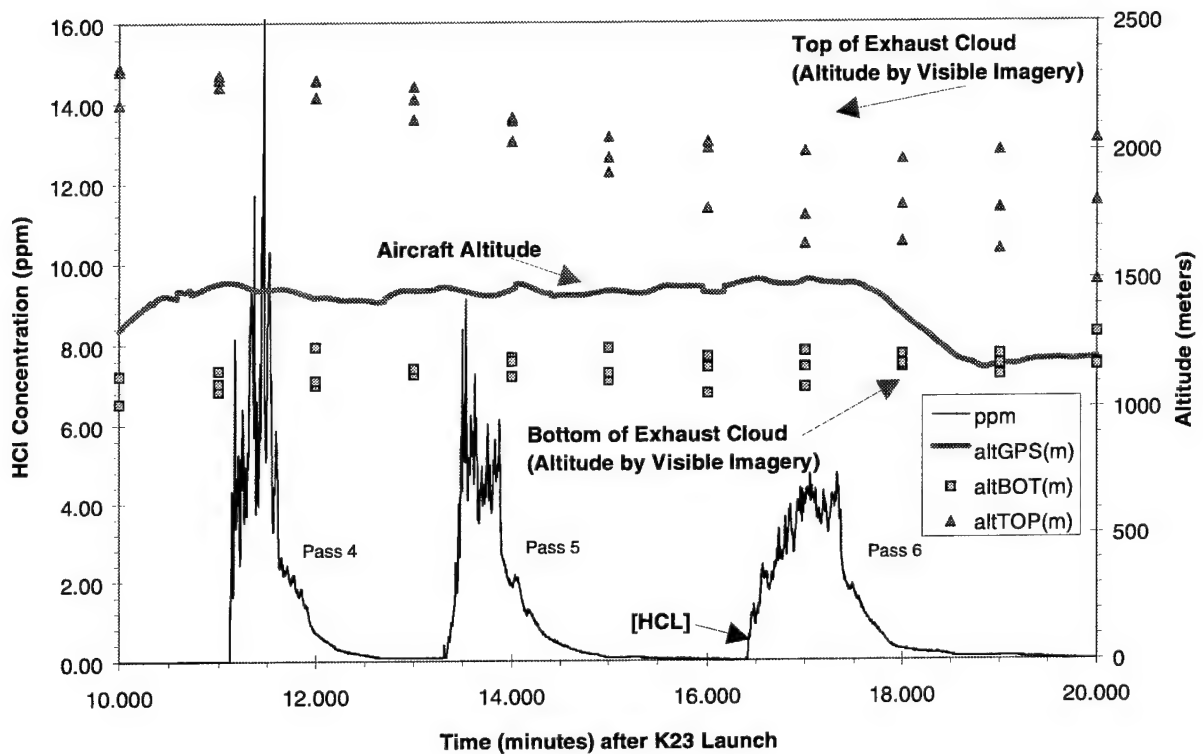

Figure 34. HCl Concentration, Visible Ground Cloud Dimensions (0–20 min), and Aircraft Altitude as a Function of Time (T=0–T=40 min).

Figure 35 shows a higher time resolution representation of the data in Figure 34 for the fourth 10 min segment of monitoring. The last positions of the top and bottom of the ground cloud measured by imagery are roughly 1900 and 1100 m, respectively.

Figure 36 shows the direction of aircraft flight for the pass 9 transect occurring during this fourth 10 min window. Both polar angle and distance to SLC-40 are varying over a relatively narrow angular spread (265°–270°) and range (10-14 km). The HCl hit occurred roughly 38 min after launch. At 5 m/sec wind speed, the center of the plume should be approximately 11.5 km downwind. This agrees well with the center of the hit in pass 9.
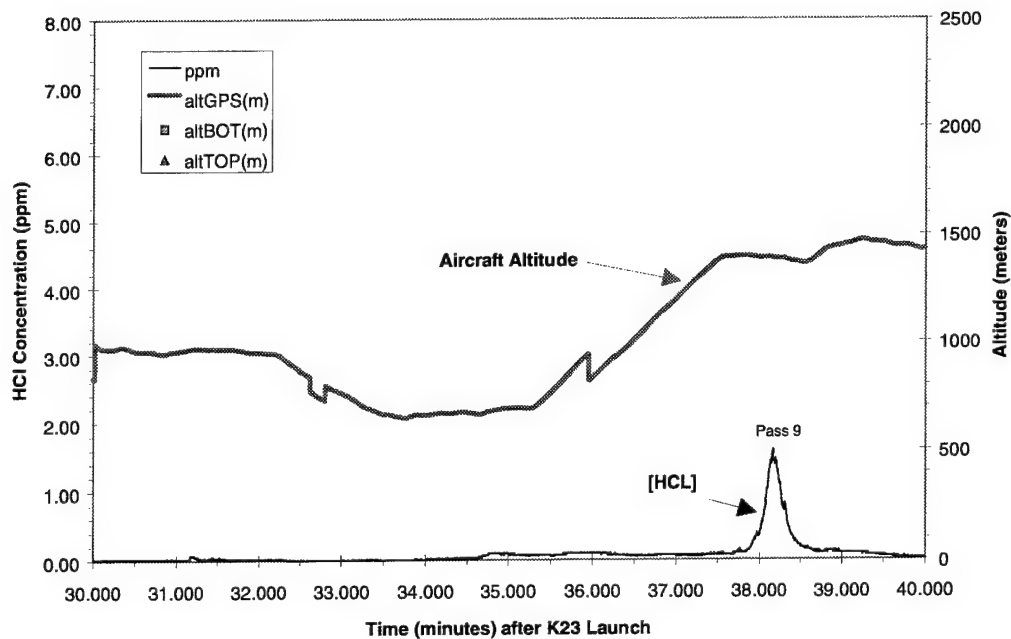
Figure 35. HCl Concentration and Aircraft Altitude as a Function of Time (T=30–T=40 min.
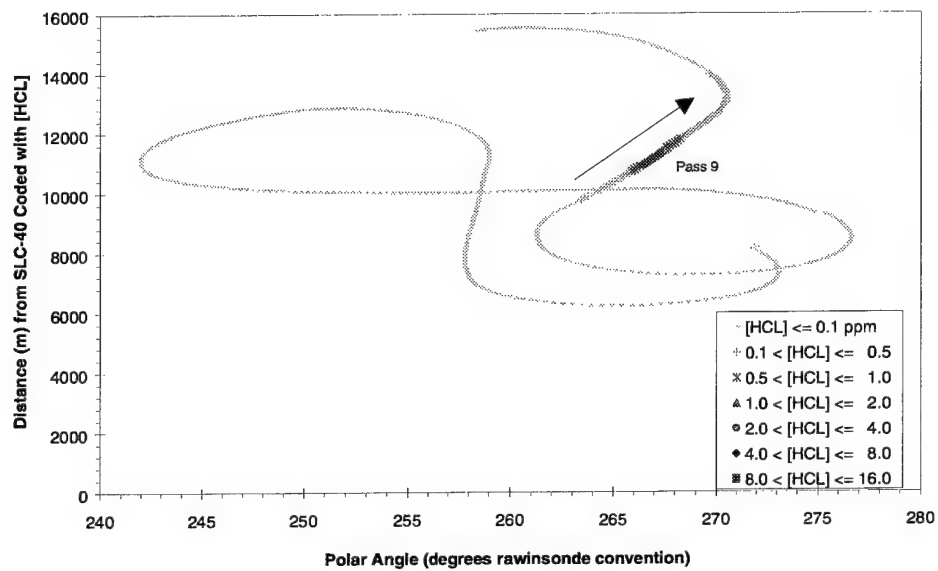
Figure 36. Aircraft Polar Coordinate Position During the T=30–T=40 min Transect.

Figure 37 provides supporting data to Figure 36, showing that the altitude of the pass 9 transect was roughly constant when the HCl hit was experienced. This pass occurred at an altitude close to the center of the stabilized ground cloud, as documented by visible imagery during the first 20 min after launch.

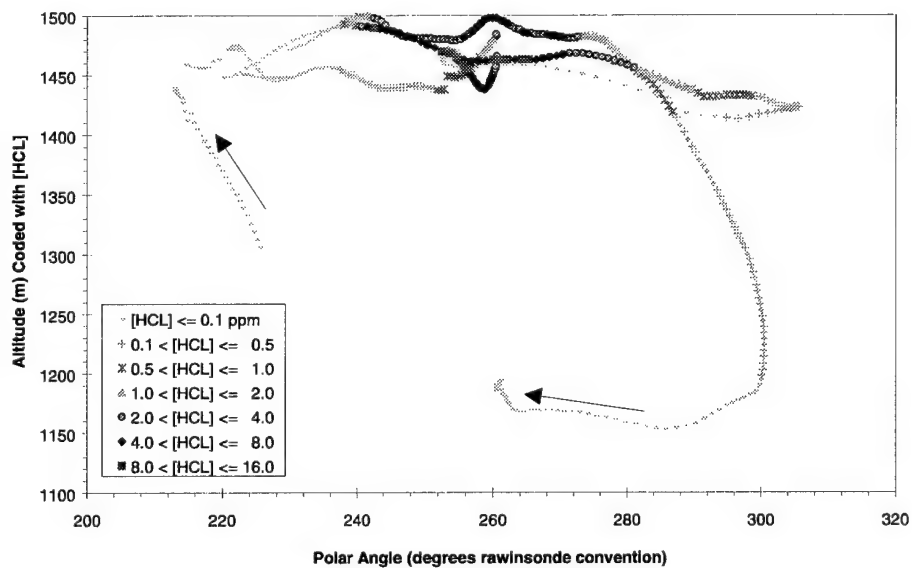**Figure 37. Aircraft Altitude and Angular Position During the T=30–T=40 min Transect.**

3.2.5 Aircraft Sampling from T=40 to T=50 min

Figure 38 shows the raw and baseline-corrected HCl concentration data for the three plume transects observed by the aircraft in this time window. The sharp leading edge and the slow decay on the trailing edge are discussed in Appendix 3 of this report. Signal-to-noise ratio and instrument drift may be complicating factors for these very small signals.
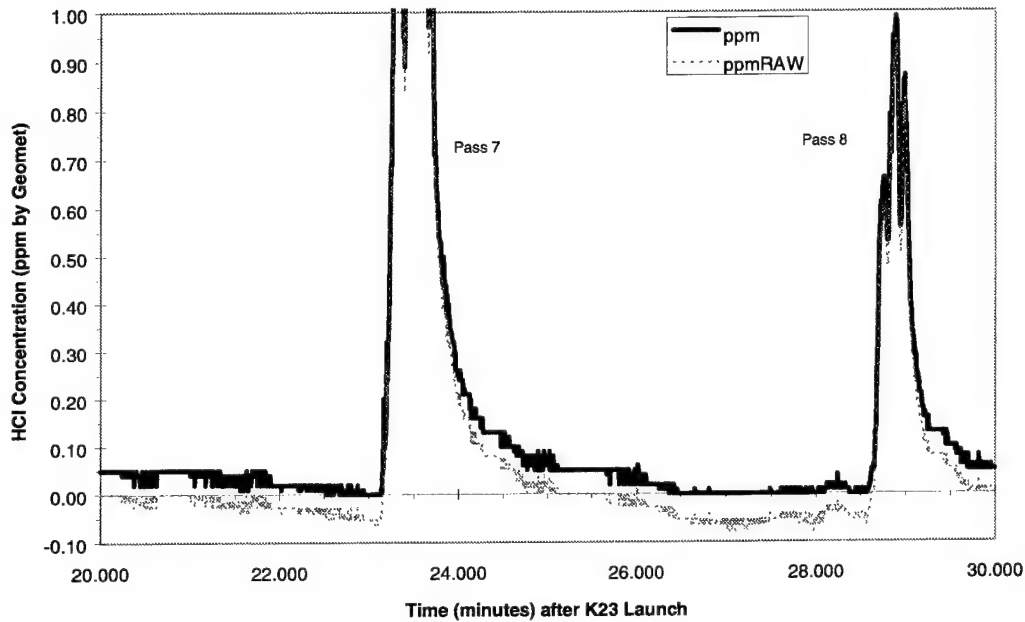
Figure 39 presents the positional information from the aircraft GPS records, together with the HCl concentration ranges of the three plume transects observed during this period.

37

Figure 38. Raw and Baseline-Corrected Geomet Traces: T=14:25–14:35 Zulu.
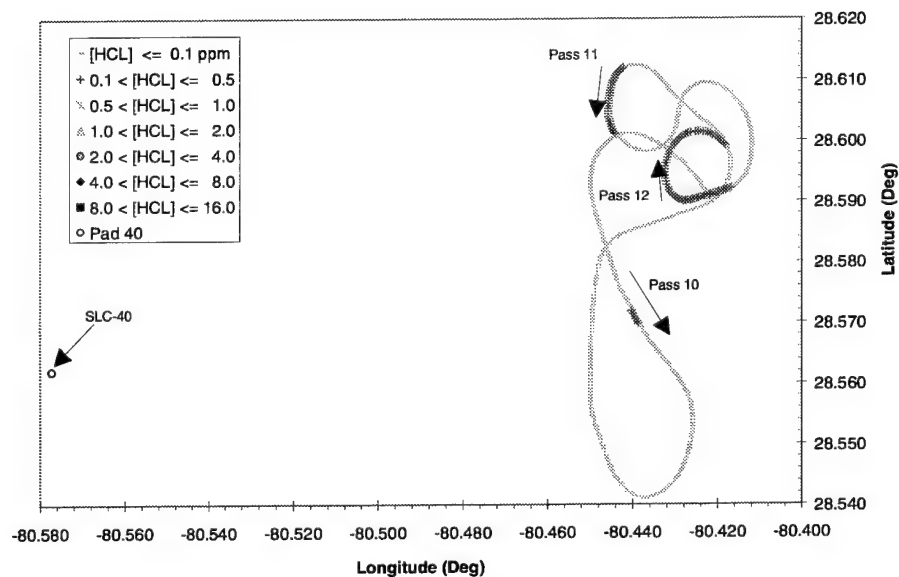
Figure 39. Aircraft GPS Latitude and Longitude: T=14:25–14:35 Zulu.

Figure 40 converts the data in Figure 39 to Cartesian coordinates centered on SLC-40.
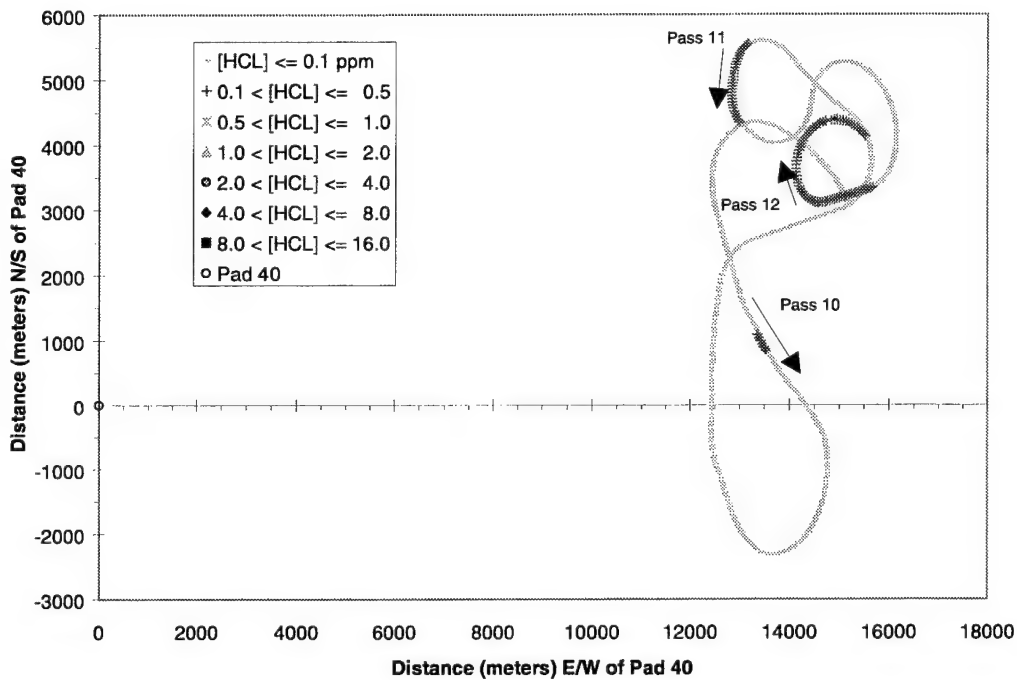
Figure 40. Cartesian Coordinates of the Aircraft Flight Pattern: T=14:25–14:35 Zulu.

Figure 41 is a composite of aircraft sampling data (passes 10–12) giving HCl concentrations and aircraft altitude between T=40 and 50 min. Visible plume imagery data of the last measurements of top and the bottom of the visible ground cloud (T=0–20 min) are also displayed. The most unusual feature of this plot is that pass 10, which is barely detectable, occurs at an altitude near the center of the stabilized ground cloud, while passes 11 and 12 (which are larger hits) occur at or significantly below the bottom of the stabilized ground cloud as last determined by visible imagery. However, as discussed below, pass 10 is significantly farther off the nominal plume centerline than are passes 11 and 12.

Figure 42 shows a higher time resolution representation of the data in Figure 41 for the fifth 10 min period of monitoring.
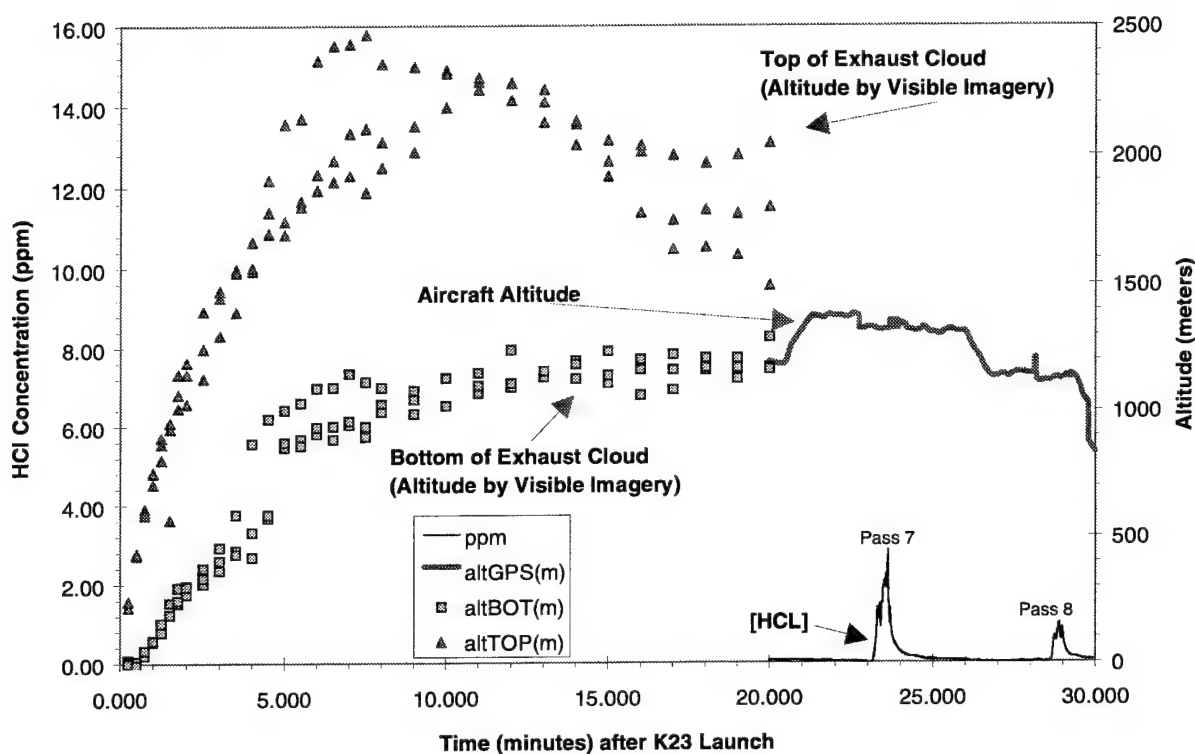
Figure 41. HCl Concentration, Visible Ground Cloud Dimensions (0-20 min), and Aircraft Altitude as a Function of Time (T=0–T=50 min).
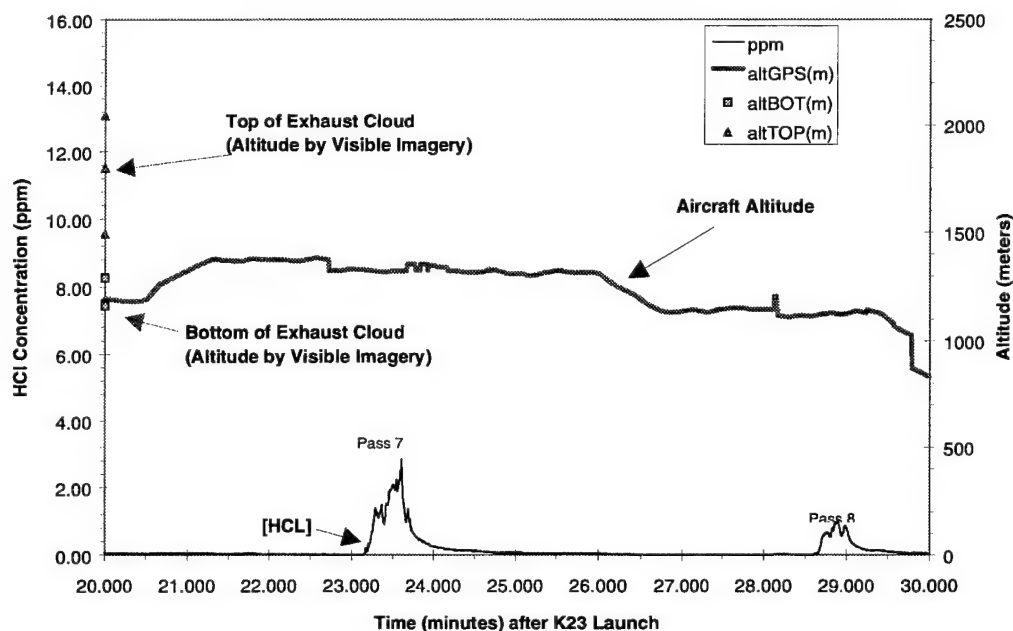

Figure 42. HCl Concentration and Aircraft Altitude as a Function of Time (T=40–T=50 min).

Figure 43 shows the direction of aircraft flight for the three transects occuring during this fifth 10 min window. Pass 10 shows an extremely weak hit, approximately 15° off the nominal plume track, as documented by visible imagery during the first 20 min of the launch. Passes 11 and 12 occur close (247°–257°) to the nominal ground cloud track vector (249°). These passes occur at roughly 48 min after launch, implying that the plume center should be at 14.5 km downwind. This calculation is in good agreement with the pass 11 and 12 data.
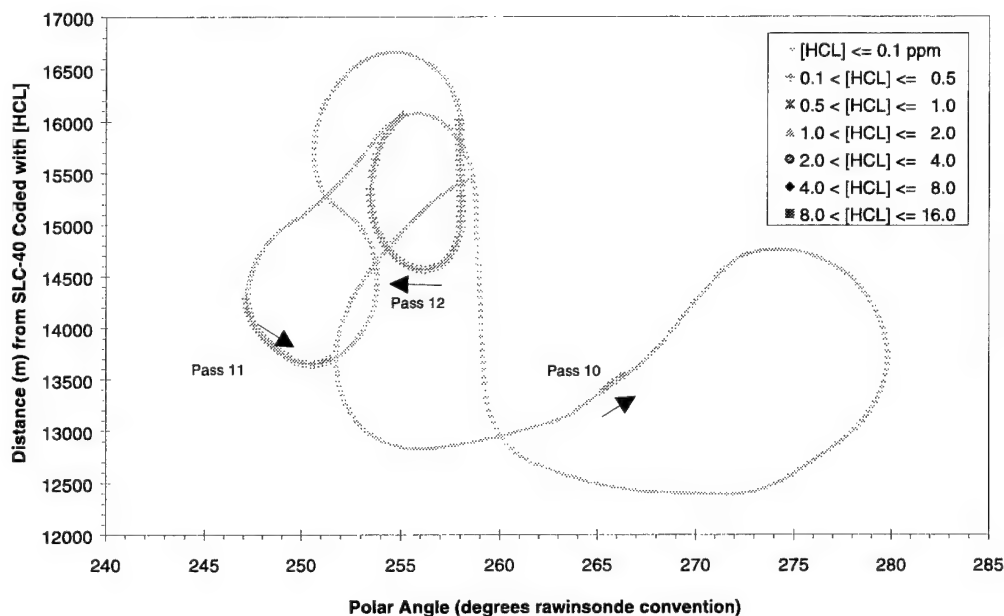
Figure 43. Aircraft Polar Coordinate Position During the T=40–T=50 min Transects.

Figure 44 provides supporting data to Figure 43, showing the altitudes of the three transects. The very weak hit on pass 10 occurs at a constant altitude that should be close to the center of the ground cloud in altitude but is 16° off (265°) the nominal ground track (249°). There is some variation of altitude during passes 11 and 12. The most interesting result is the relatively strong hit for pass 12 between 400 and 600 m altitude, which is substantially lower than the last observed location of the bottom of the visible plume determined 20 min after launch.
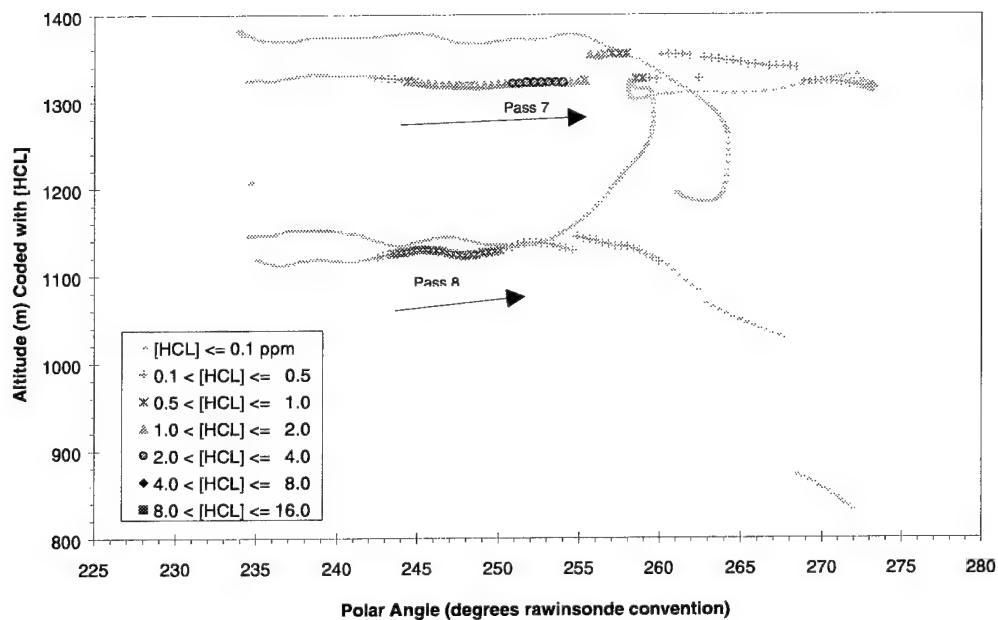
Figure 44. Aircraft Altitude and Angular Position During the T=40–T=50 min Transects.

3.2.6 Aircraft Sampling from T=50 to T=60 min

Figure 45 shows the raw and baseline-corrected HCl concentration data for the single successful plume transect observed by the aircraft in this time window. The sharp leading edge characteristic of the Geomet is clearly demonstrated, but the slow trailing edge is not obvious in this trace.

Figure 46 presents the positional information from the aircraft GPS records labeled with the HCl concentration ranges for the single plume transect in this sampling period.

Figure 45. Raw and Baseline-Corrected Geomet Traces: T=14:35–14:45 Zulu.
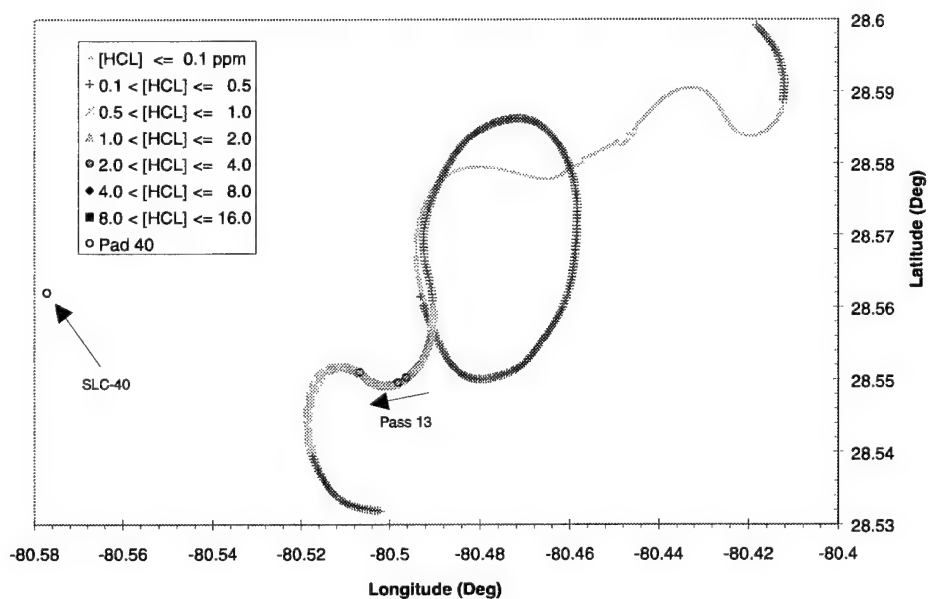
Figure 46. Aircraft GPS Latitude and Longitude: T= 14:35–14:45 Zulu.

43

Figure 47 converts the data in Figure 46 to Cartesian coordinates centered on SLC-40.
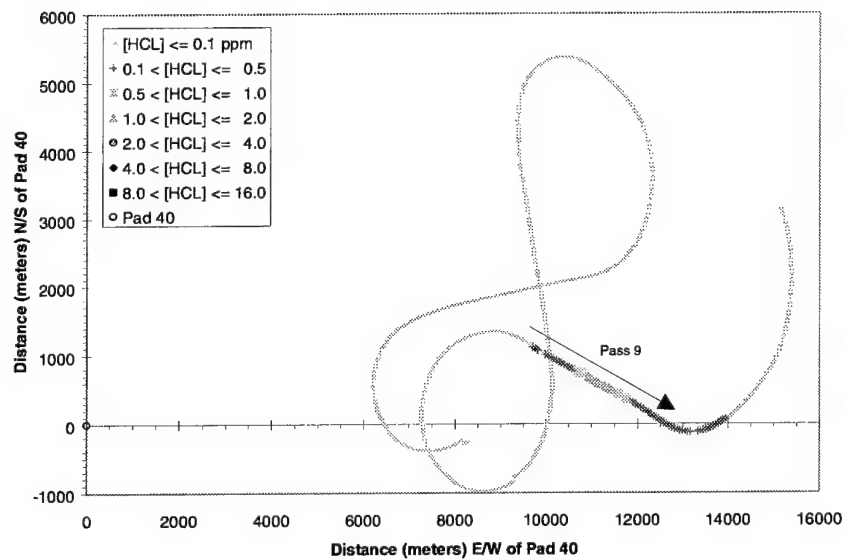

Figure 47. Cartesian Coordinates of the Aircraft Flight Pattern: T= 14:35–14:45 Zulu.

Figure 48 is a composite of aircraft sampling data (pass 13) giving HCl concentrations and aircraft altitude between T=50 and 60 min as well as plume imagery data showing the top and the bottom of the observed visible ground cloud taken between T=0 and 20 min. The most salient feature of this plot is that the aircraft is making a rapid transition (climbing at nearly 10 m/sec) to a flight pattern centered on higher altitudes.

Figure 49 shows a higher time resolution representation of the data in Figure 48 for the sixth 10 min period of monitoring. It can be seen that a rather significant HCl hit occurs at–or in fact above–the altitude of the imagery-determined top of the stabilized ground cloud.
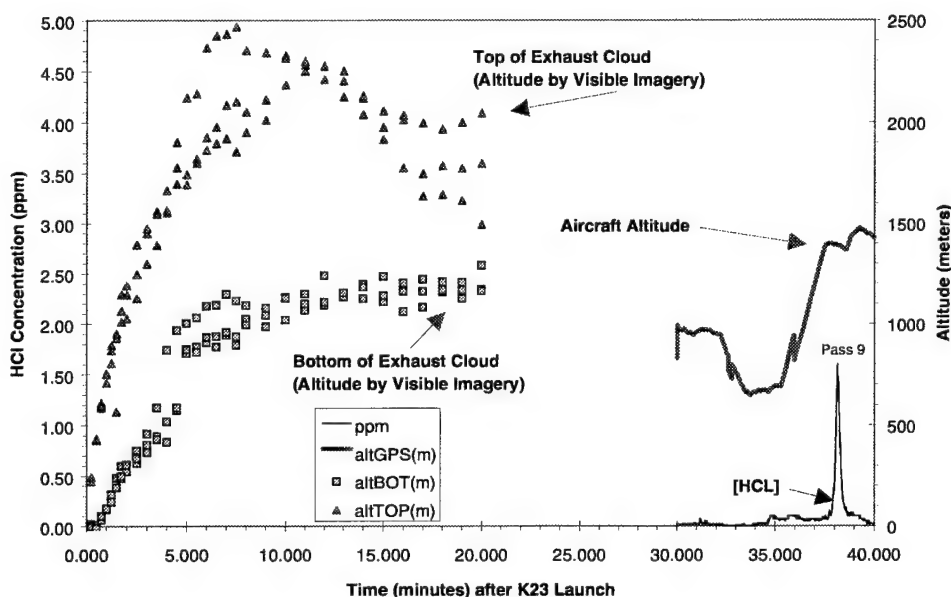
Figure 48. HCl Concentration, Visible Ground Cloud Dimensions (0–20 min), and Aircraft Altitude as a Function of Time (T=0–T=60 min).
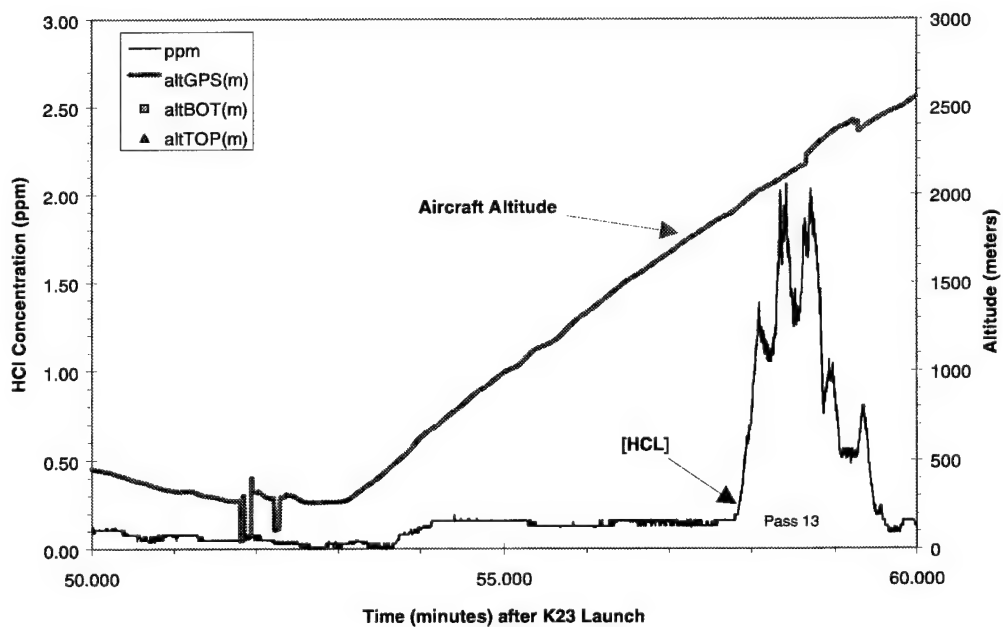
Figure 49. HCl Concentration and Aircraft Altitude as a Function of Time (T=50–T=60 min).

45

Figure 50 shows the direction of aircraft flight for the single successful transect occurring during this sixth 10 min window. In addition to flying at higher altitudes, the aircraft has transitioned to a region significantly closer to the launch complex. The larger HCl hits are seen at a range of 6 to 8 km from SLC-40 and at polar angles significantly south (270°–295°) of the stabilized ground cloud track (249°), as documented by visible imagery during the first 20 min after launch. The visible imagery qualitatively documented a significant plume above and to the south of the stabilized ground cloud. It appears that the aircraft successfully sampled this portion of the higher altitude launch column.

Figure 50. Aircraft Polar Coordinate Position During the T=50–60 min Transect.

Figure 51 provides supporting data to Figure 50, emphasizing that while low levels of HCl are observed over a wide range of altitudes, the significant HCl hit occurs at high altitudes (2000–2500 m) and significantly south of the initial plume track. One should also note that this hit occurs 59 min after the launch. As noted previously, this large hit occurred at 6 to 8 km from the complex. Examination of the T-0.3 hr rawinsonde data (Appendix 1) shows that at altitudes from 2.0 to 2.5 km, the average wind speed varies between 1.0 and 1.5 m/sec. Taking a mean wind speed of 1.25 m/sec in this altitude range, HCl initially deposited at this altitude would have traveled 4.4 km. The Mosquito Lagoon profiler data (Appendix 1) are more consistent with wind speeds of 3.5 m/sec at this altitude, thus predicting a downwind distance of 12.4 km. The wind orientation measurements in this altitude region are 265°–290°, which is quite consistent with the data in Figure 51. We tentatively conclude that the hit reported as pass 13 represents part of the attached launch column deposited in an altitude range (2000–2500 m). This altitude is characterized by low wind speeds and wind directions out of the west-northwest. The apparent low rates of HCl dispersion translate into the relatively high concentrations (2 ppm peak) observed 1 hr after launch.
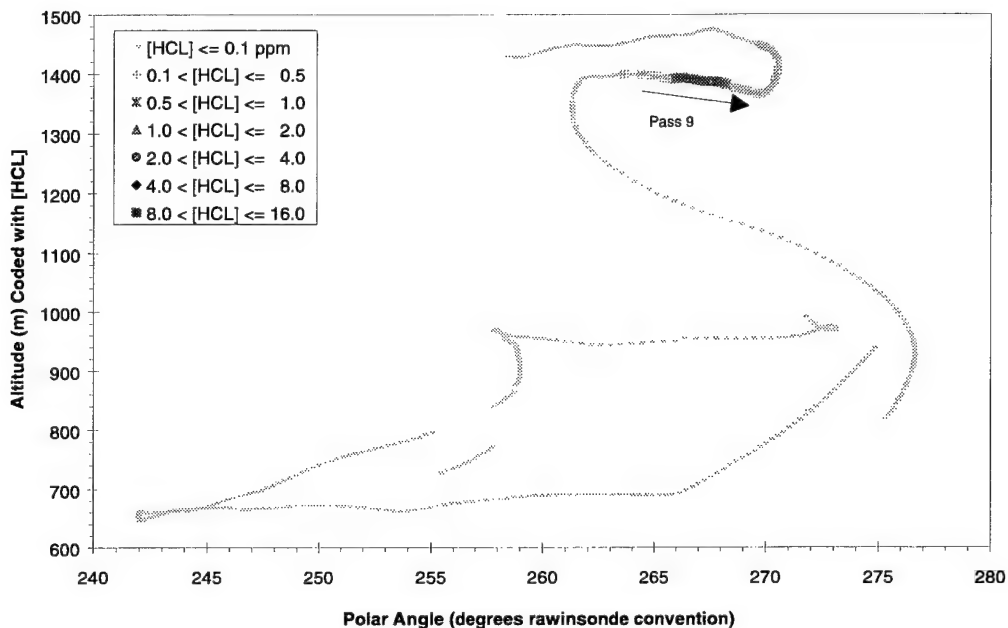

Figure 51. Aircraft Altitude and Angular Position During the T=50–T=60 min Transect.

3.2.7 Aircraft Sampling from T=60 to T=70 min

Figure 52 shows the raw and baseline-corrected HCl concentration data for a broad, low, high altitude hit (unnumbered) and three numbered plume transects conducted by the aircraft in this time window. The sharp leading edge and the slow decay on the trailing edge have been discussed in Appendix 3 of this report.
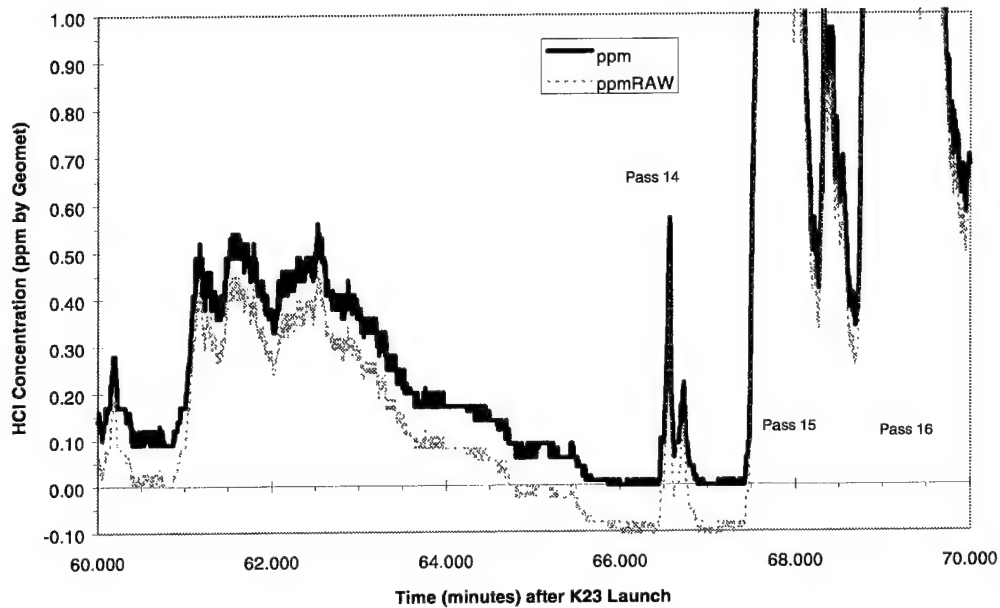
Figure 52. Raw and Baseline-Corrected Geomet Traces: T=14:45–14:55 Zulu.

Figure 53 presents the positional information from the aircraft GPS records labeled with the HCl concentration ranges of the three plume transects (and the broad feature) observed in this period.
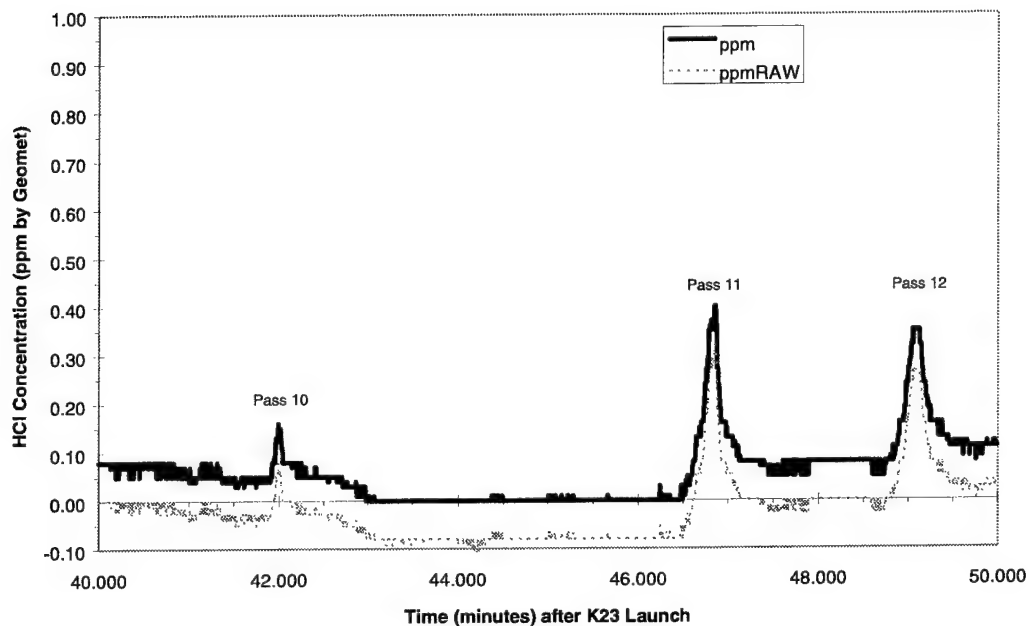
Figure 54 converts the data in Figure 53 to Cartesian coordinates centered on SLC-40.

48
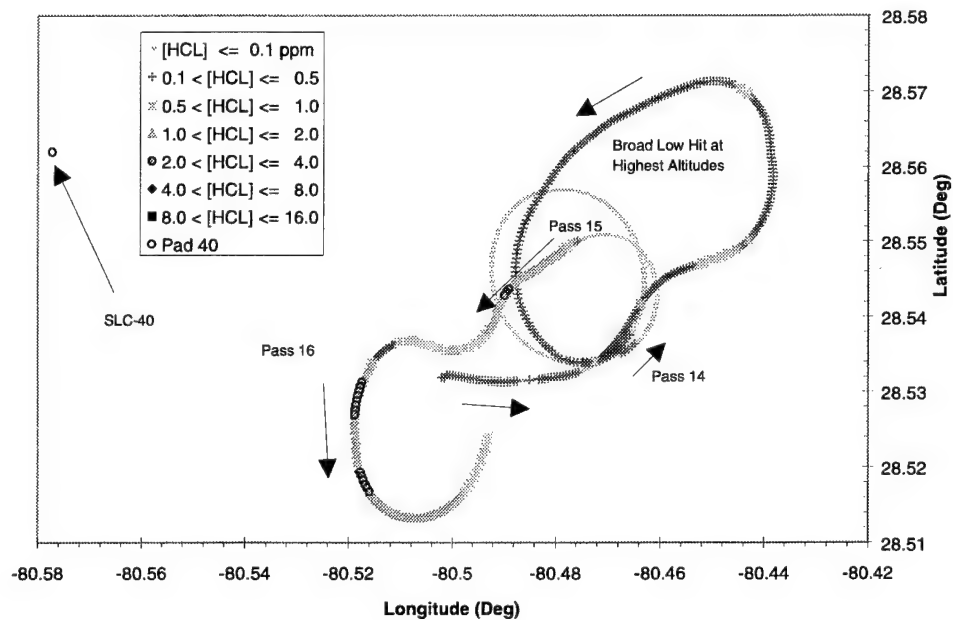
**Figure 53. Aircraft GPS Latitude and Longitude: T=14:45–14:55 Zulu.**
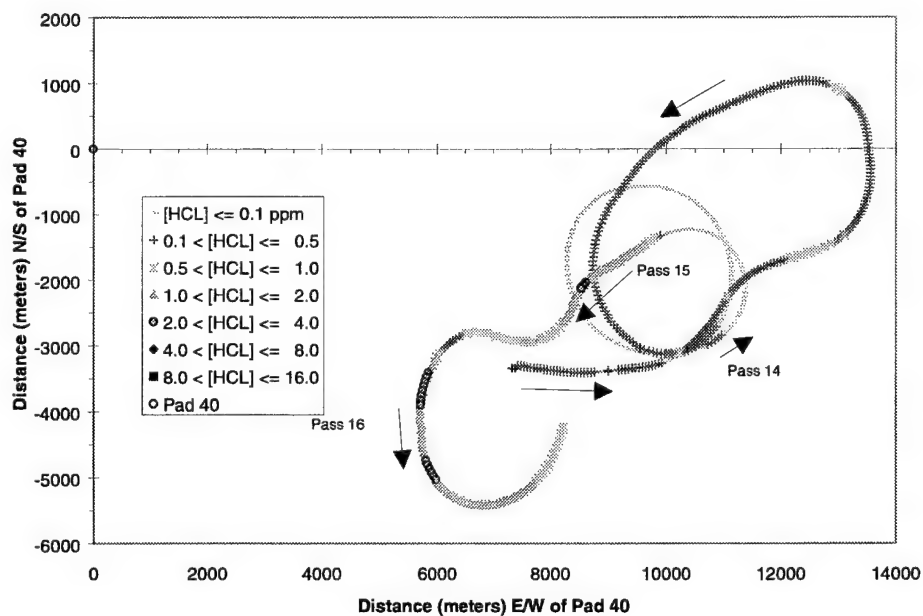
Figure 54. Cartesian Coordinates of the Aircraft Flight Pattern: T=14:45–14:55 Zulu.

49

Figure 55 shows a composite of aircraft sampling data (broad features and passes 14–16), giving HCl concentrations and aircraft altitude between T=60 and 70 min as well as plume imagery data describing the top and the bottom of the visible ground cloud between T=0 and 20 min. The most salient features of this plot are that the broad, low density (0.5 ppm) hit is associated with the highest altitudes flown by the aircraft (2500–3700 m) and the strong HCl hits occur in the 2000–2500 m altitude region described in the previous section as resulting from the attached launch column.
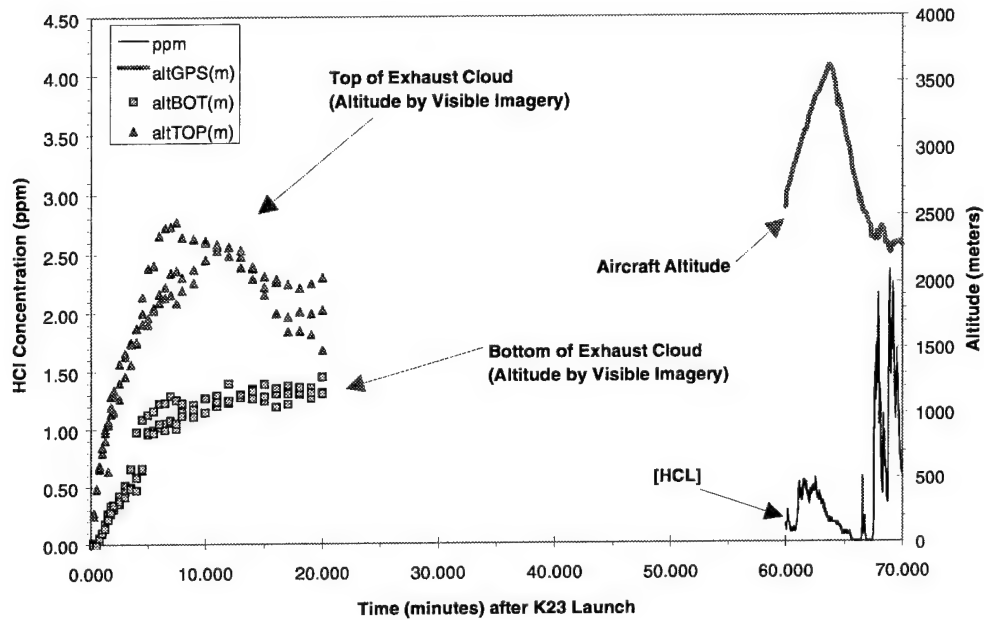
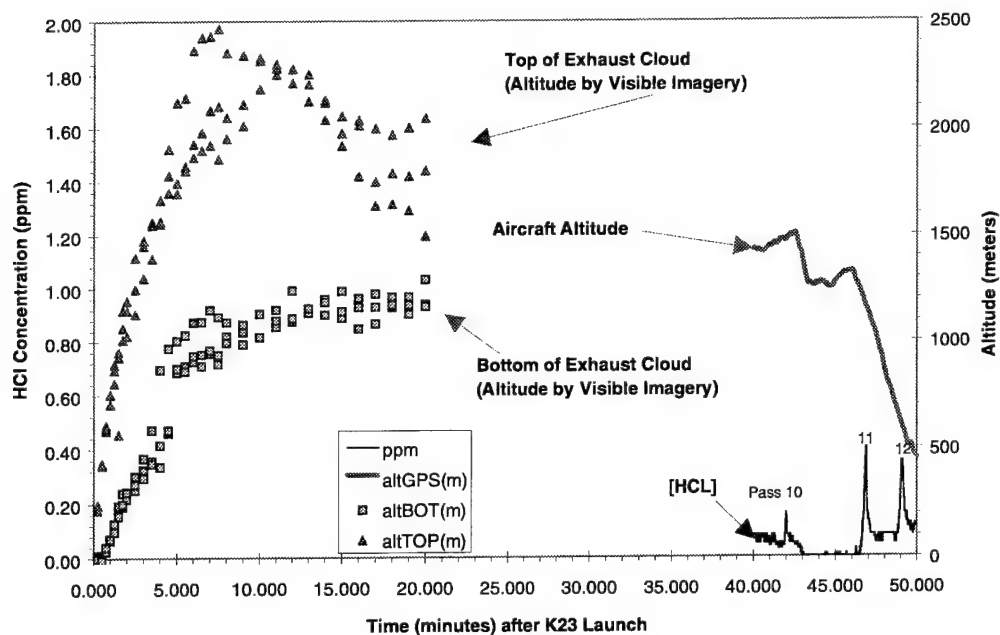**Figure 55.** HCl Concentration, Visible Ground Cloud Dimensions (0-20 min), and Aircraft Altitude as a Function of Time (T=0-T=70 min).

Figure 56 shows a higher time resolution representation of the data in Figure 55 for the seventh 10 min period of monitoring.
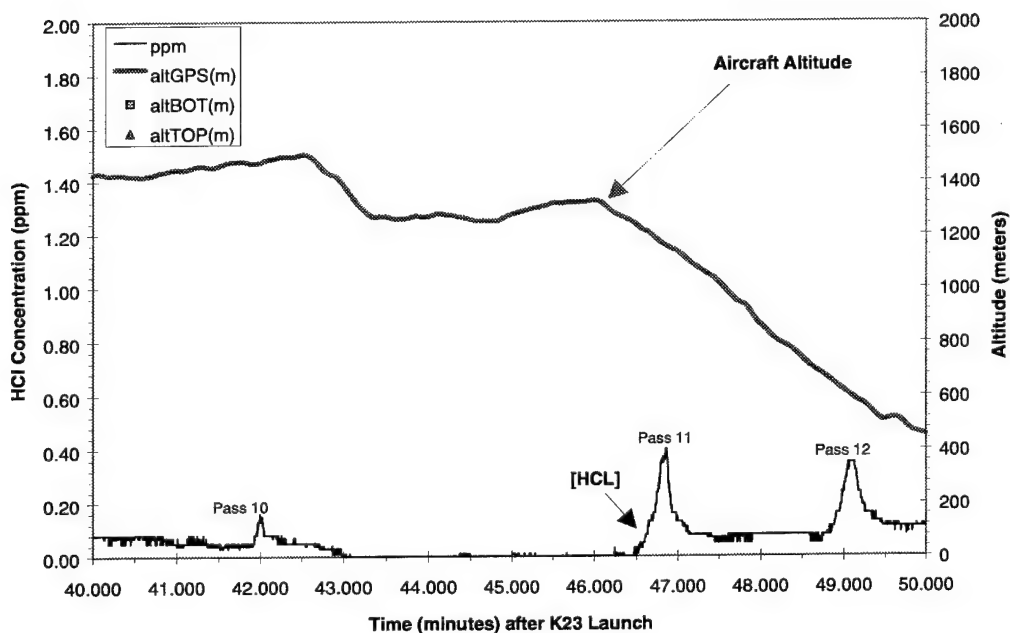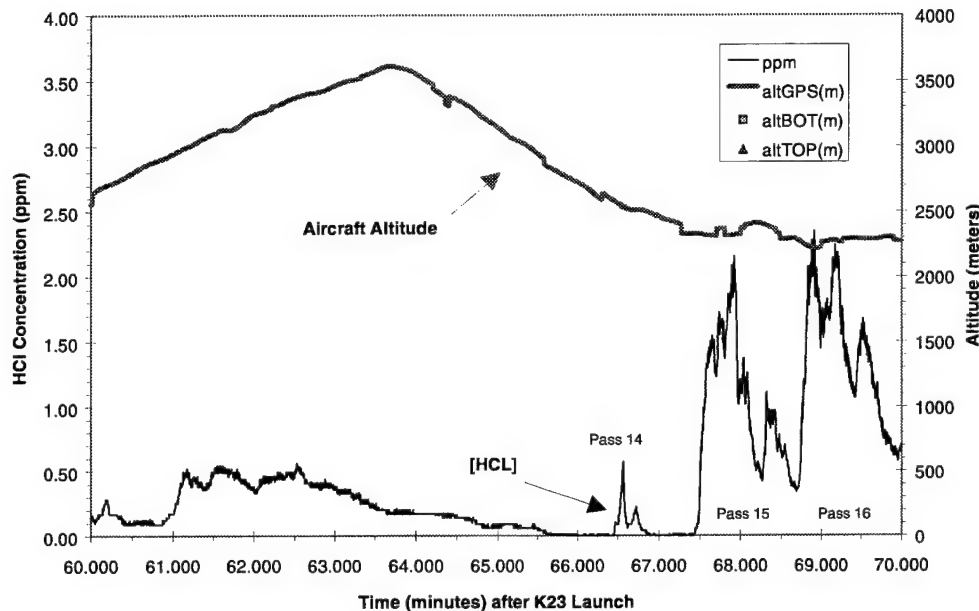

Figure 56. HCl Concentration and Aircraft Altitude as a Function of Time (T=60–T=70 min).

Figure 57 shows the direction of aircraft flight for the broad high altitude HCl hit and the three labeled transects that occurred during the seventh 10 min window.

The broad HCl hit is encountered as the aircraft flies a complex trajectory, first ascending, then descending in altitude, flying away from, and then toward the launch complex. During this time, the aircraft flies away from the locus of the high altitude launch column, toward the locus of the ground cloud, and back again.

Pass 14, although somewhat lower in altitude, is still 10–11 km from the launch complex at 67 min after the launch. Noting the low wind speed (rawinsonde) at this altitude (1–1.5 m/sec) discussed in the previous section, the attached launch column may not have dispersed to this distance from the pad. The higher wind speeds observed by the profiler (3.5 m/sec) would permit transport of some HCl to 11 km. Passes 15 and 16 are closer to the pad, near 2200 m, which appears to be a region of high HCl density, and in the angular range of 275° to 310°, which reflects the higher altitude wind orientation. All the data suggest that this HCl derives from the attached launch column.

Figure 58 provides supporting data to Figure 57, showing that the altitudes of the three transects (passes 14–16) were roughly constant when HCl hits were experienced. The broad low level feature occurs over a very large range of altitudes (2600–3600 m).

51
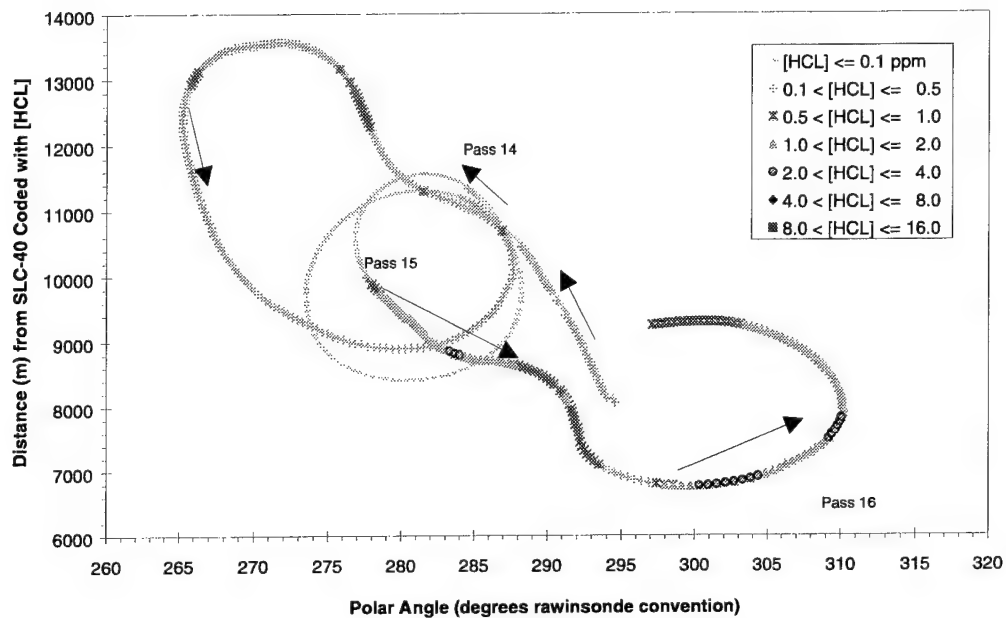
Figure 57. Aircraft Polar Coordinate Position During the T=60–T=70 min Transects.
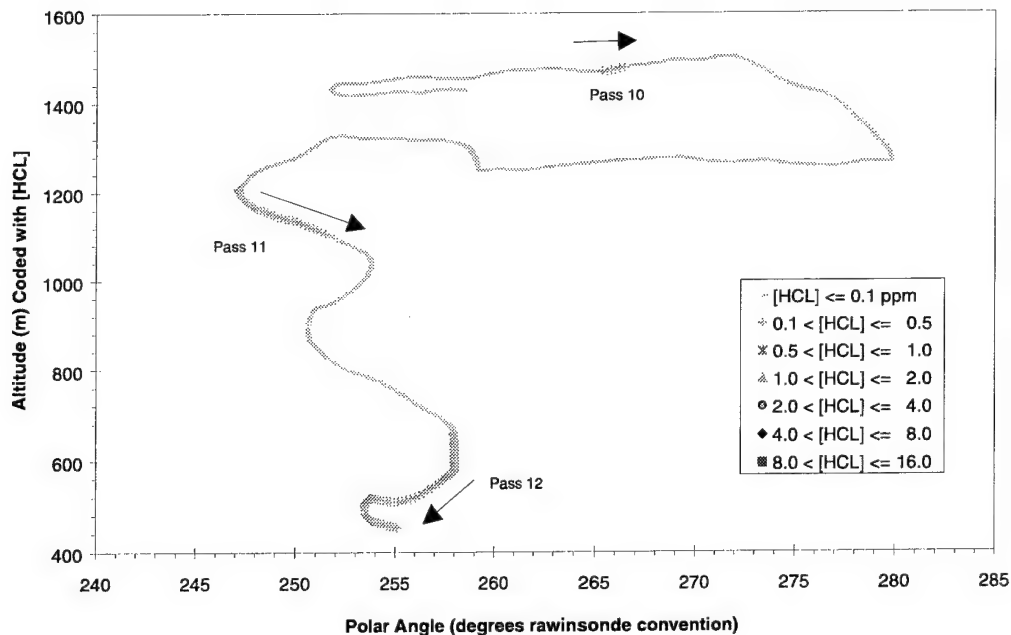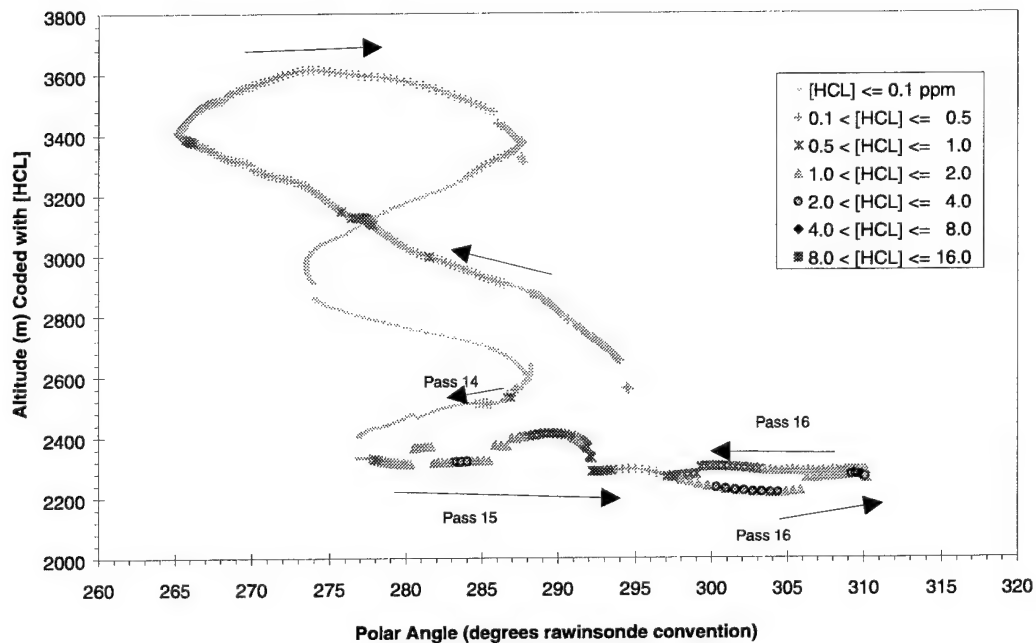

Figure 58. Aircraft Altitude and Angular Position During the T=60–T=70 min Transects.

3.2.8 Aircraft Sampling from T=70 to T=80 min

Figure 59 shows the raw and baseline-corrected HCl concentration data for the transects conducted by the aircraft in this time window. Five HCl hits are labeled (passes 17–21). It is obvious that HCl is beginning to "fill in" a rather broad spatial region at the altitude of 2000 to 2500 m. The sharp leading edge and the slow decay on the trailing edge of the Geomet data are masked by the number of hits experienced.
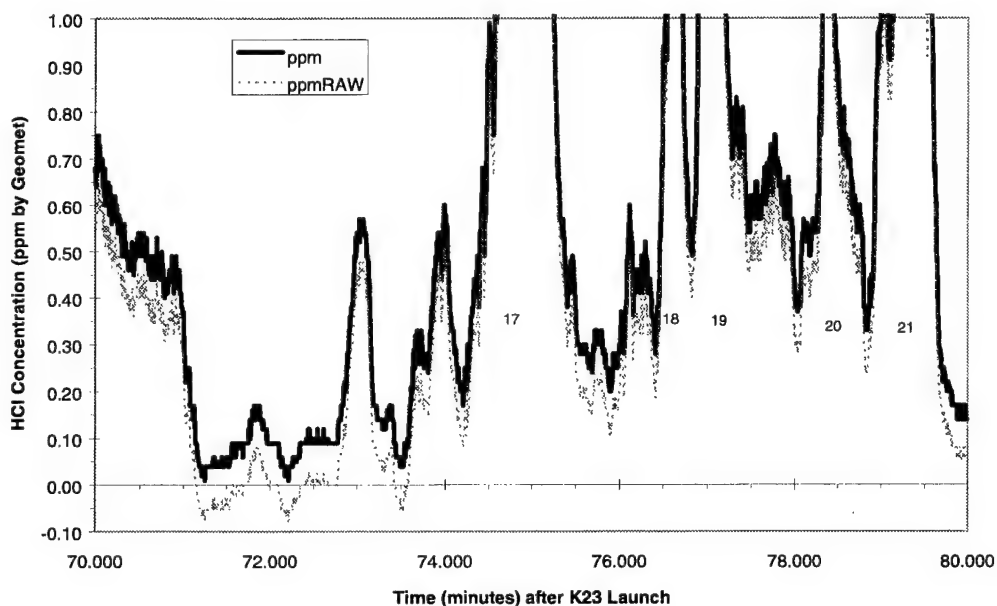
Figure 59. Raw and Baseline-Corrected Geomet Traces: T=14:55–15:05 Zulu.

Figure 60 presents the positional information from the aircraft GPS records labeled with the HCl concentration ranges of the five plume transects identified during this period.
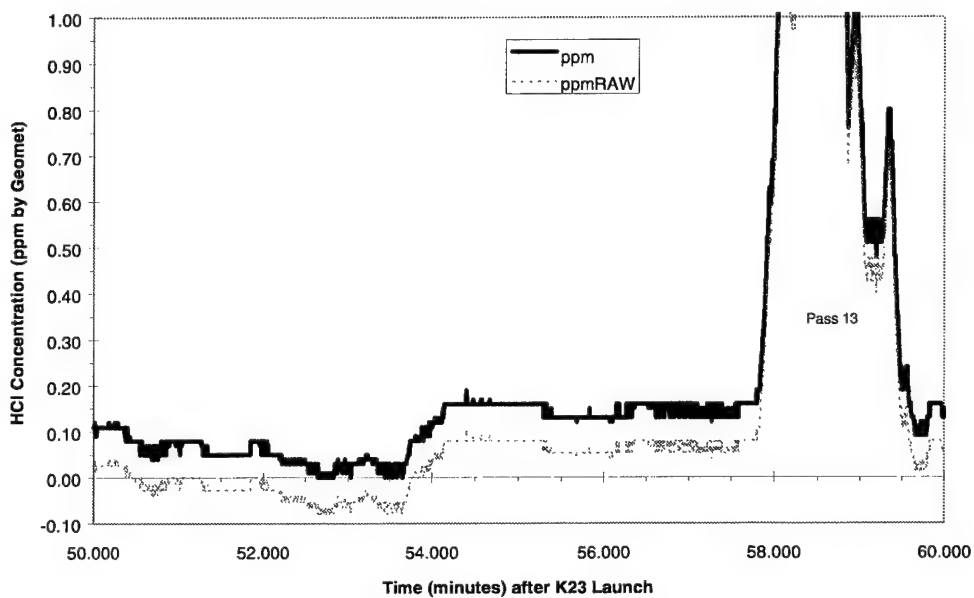
Figure 61 converts the data in Figure 60 to Cartesian coordinates centered on SLC-40.
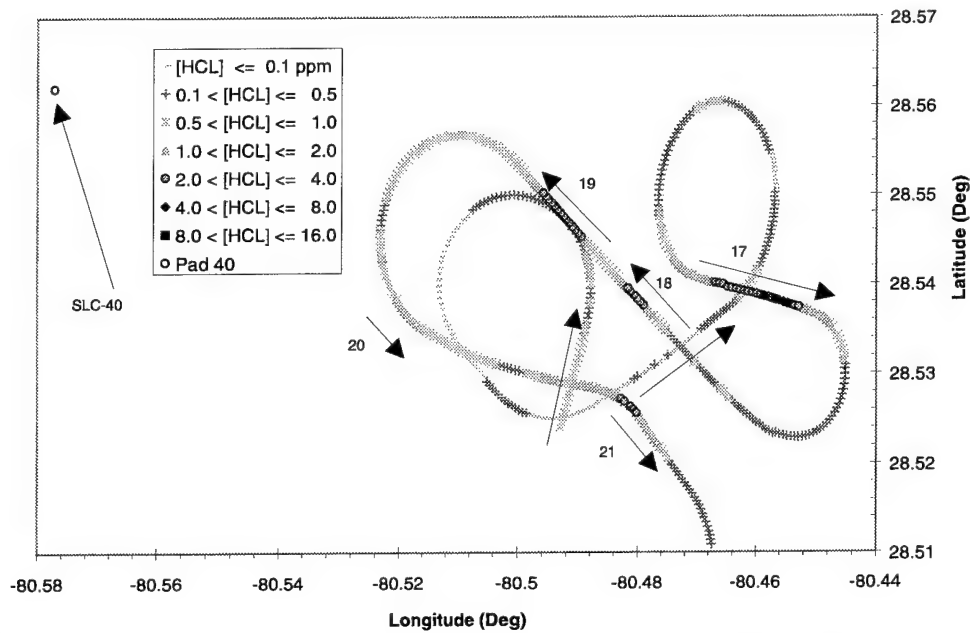
Figure 60. Aircraft GPS Latitude and Longitude: T=14:55–15:05 Zulu.
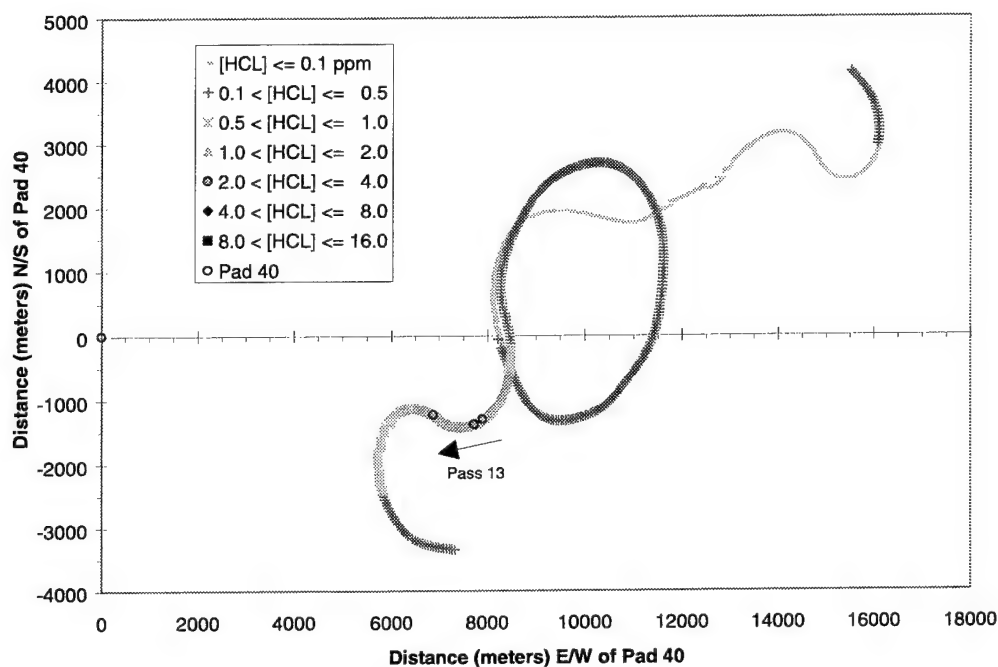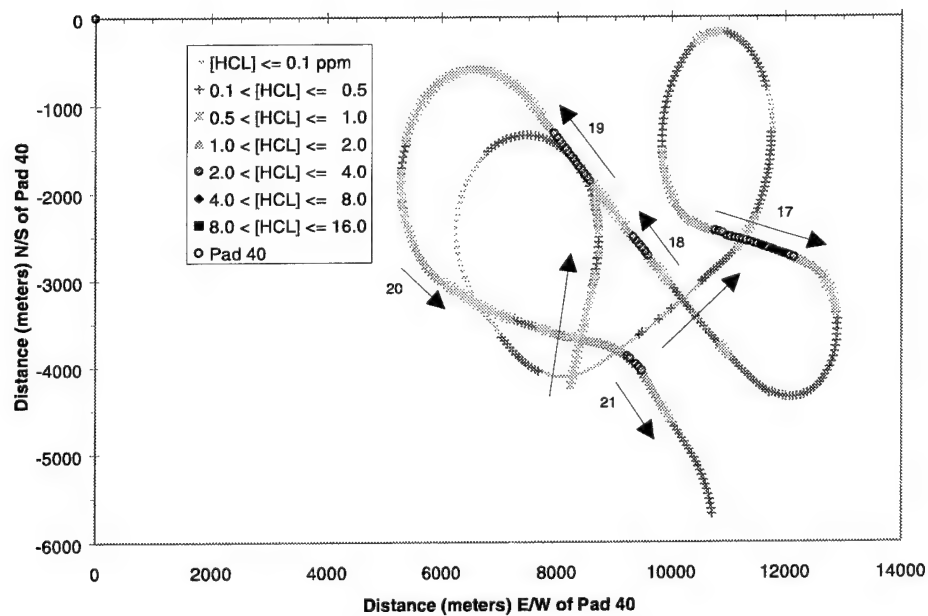

Figure 61. Cartesian Coordinates of the Aircraft Flight Pattern: T= 14:55–15:05.

Figure 62 is a composite of aircraft sampling data (passes 17–21) giving HCl concentrations and aircraft altitude between T=70 and 80 min, as well as the plume imagery data showing the top and the bottom of the visible ground cloud between T=0 and 20 min. The most salient feature of this plot is the large number of relatively strong HCl hits experienced in the altitude range between 2000 and 2500 m.
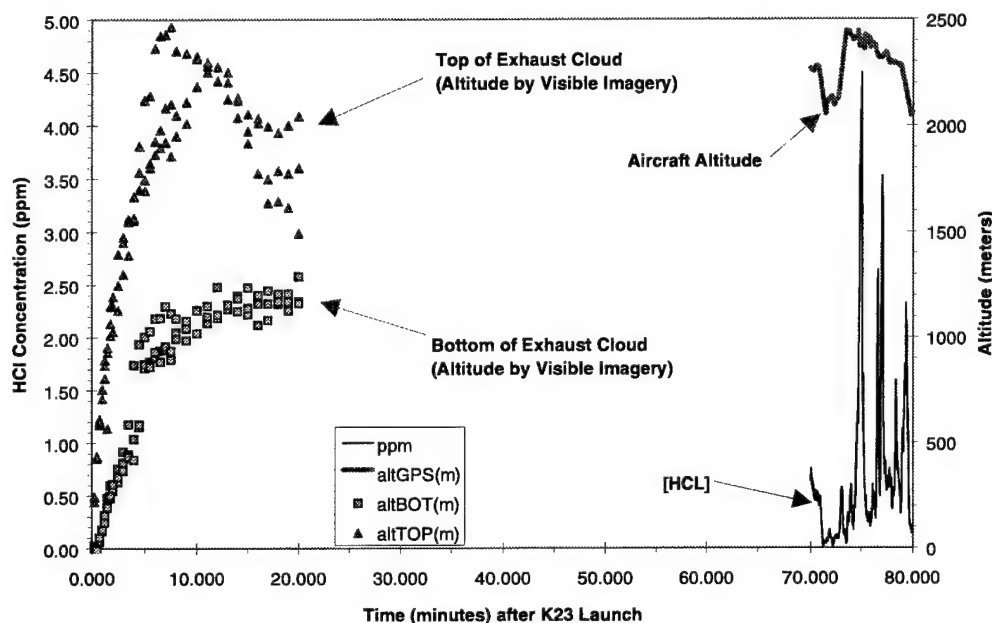
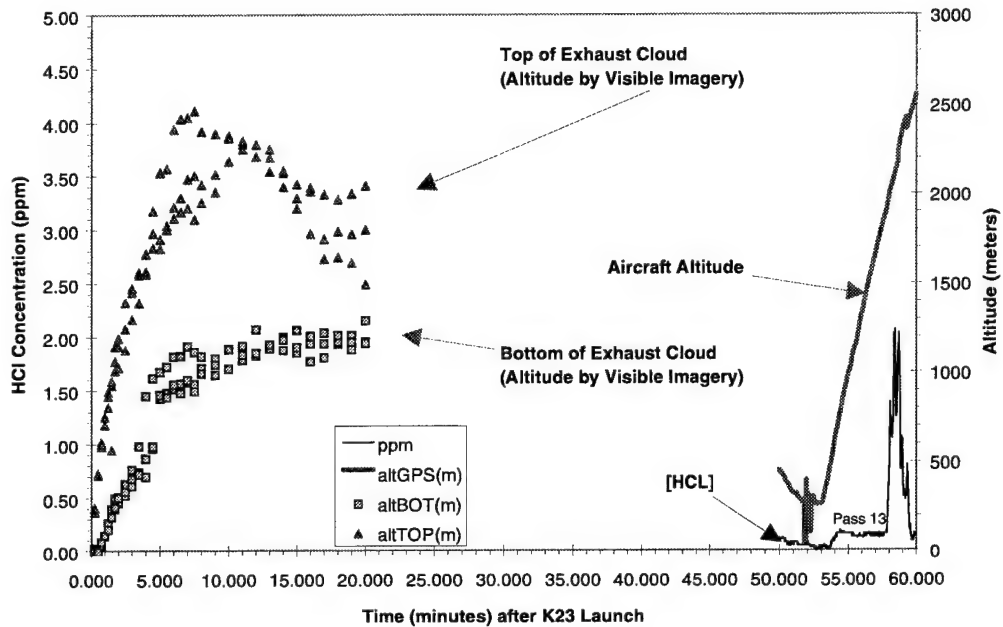**Figure 62. HCl Concentration, Visible Ground Cloud Dimensions (0–20 min), and Aircraft Altitude as a Function of Time (T=0–T=80 min).**

Figure 63 shows a higher time resolution representation of the data in Figure 62 for the eighth 10 min period of monitoring. It is worth noting that pass 17 shows a high peak concentration of HCl (> 4 ppm at 75 min after the launch), albeit at a rather high altitude.

Figure 64 shows the direction of aircraft flight for the five transects occurring during this eighth 10 min window. This time window is of particular interest, because the altitude of the aircraft remained between 2050 and 2450 m over the entire 10 min. Stated somewhat differently, the intersections of flight trajectories presented in this plot go through very nearly the same region of space separated in time by several minutes at most. We observe strong hits (passes 17–19) at angles between 277° and 287°, which is expected, but also moderate hits (passes 20 and 21) around 295°, which is somewhat suprising in this altitude range (although see T+5.5 min wind profiler data in Appendix 1). The strong hits near 283° occur some 83 min after launch at downwind distances of 8 to 13 km. This would imply average wind speeds at this altitude closer to 2–2.5 m/sec rather than the 1–1.5 m/sec that are derived from the T-0.3 hr rawinsonde. The larger values are more consistent with the wind profiler data at T+5.5 min.

55
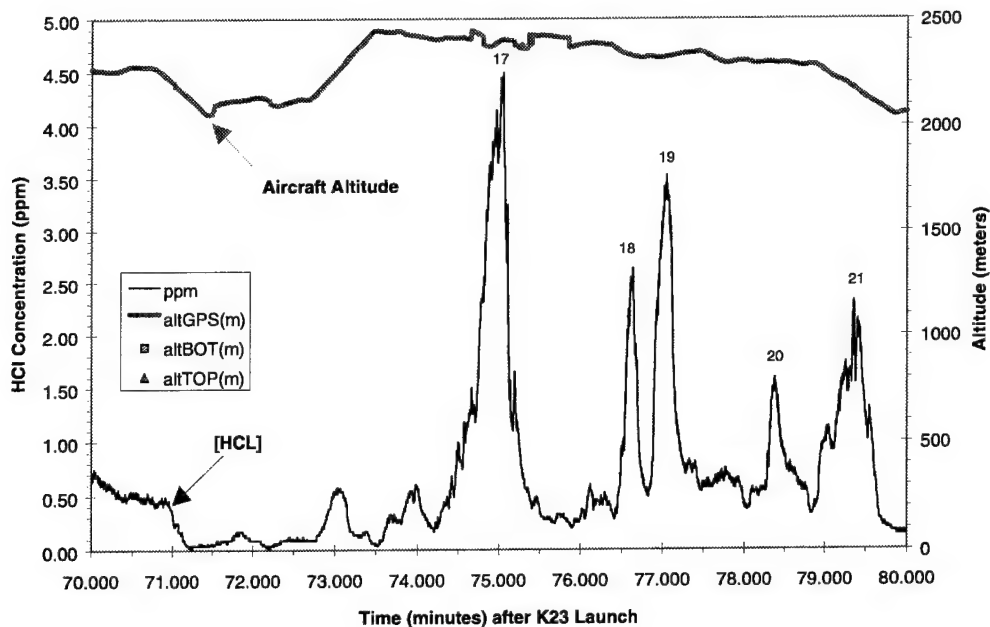
Figure 63. HCl Concentration and Aircraft Altitude as a Function of Time (T=70–T=80 min).
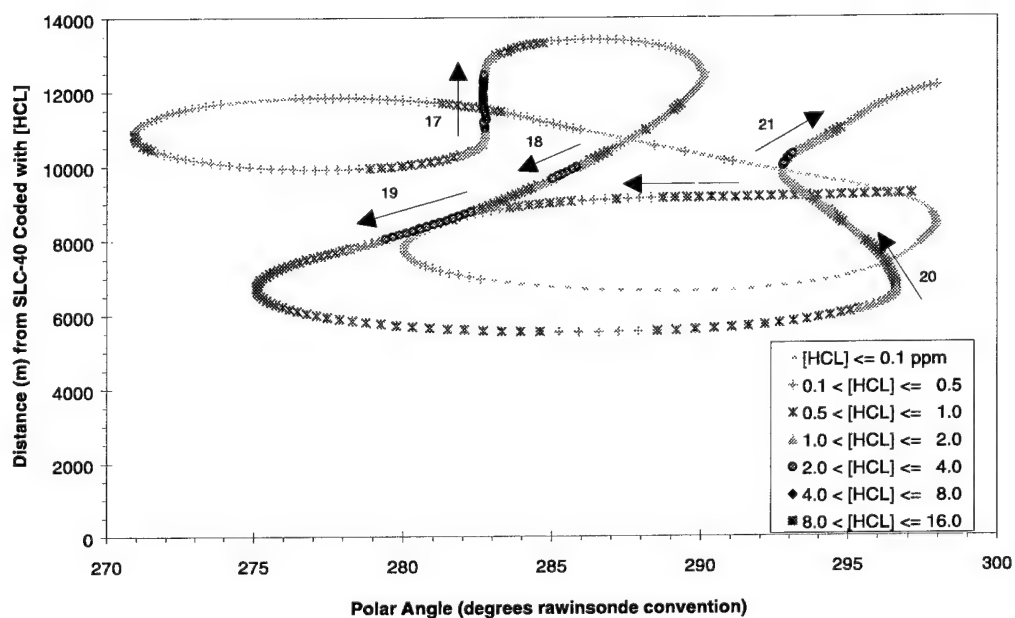
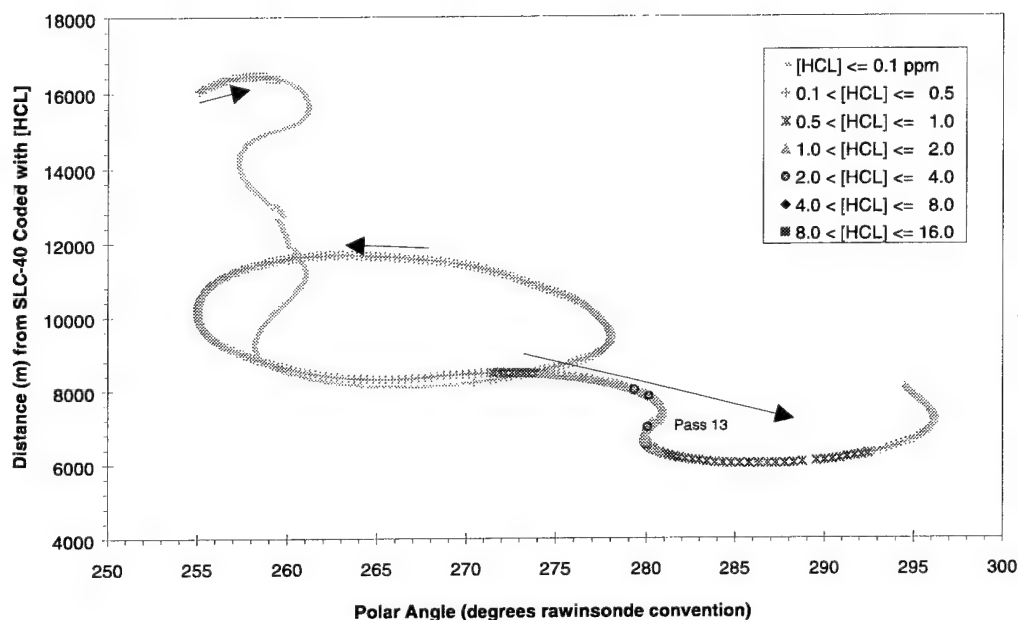**Figure 64. Aircraft Polar Coordinate Position During the T=70–T=80 min Transects.**

Figure 65 provides supporting data to Figure 64, showing the altitudes of the five transects (note that the altitude scale is expanded) when HCl hits were experienced. Passes 18–20 occurred at roughly constant altitude. Passes 17 and 21 were ascending and decending passes, respectively, with distance from SLC-40 increasing in both.
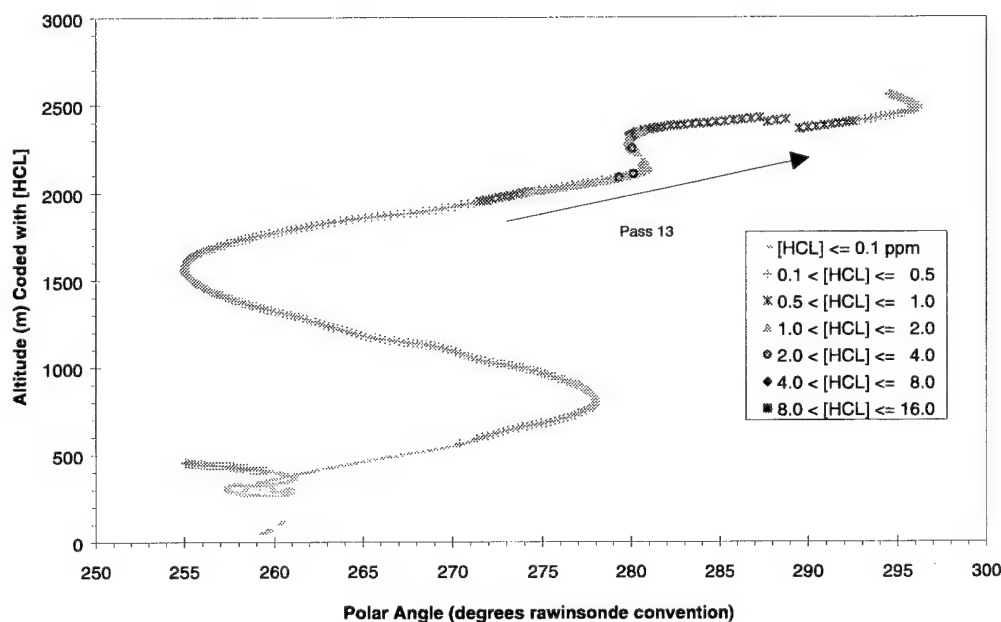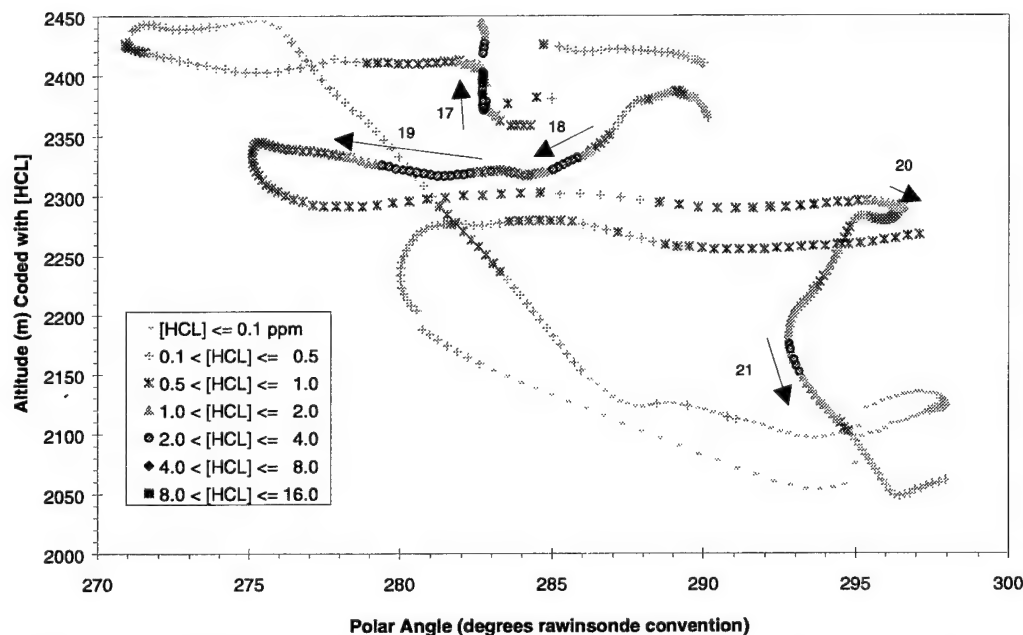

Figure 65. Aircraft Altitude and Angular Position During the T=70–T=80 min Transects.

3.2.9 Aircraft Sampling from T=80 to T=90 min

Figure 66 shows the raw and baseline-corrected HCl concentration data for the two minor plume transects conducted by the aircraft in this time window. As can be seen, virtually no HCl is detected; however, that has significance when the aircraft altitude profiles are examined.

Figure 67 presents the positional information from the aircraft GPS records labeled with the HCl concentration ranges of the two plume transects performed in this period.
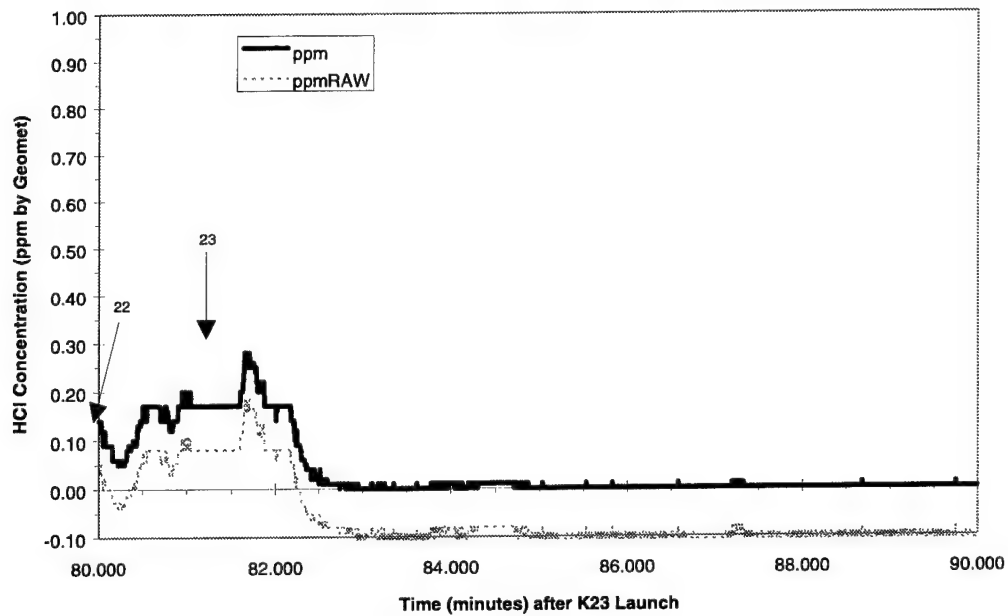
Figure 66. Raw and Baseline-Corrected Geomet Traces: T=15:05–15:15 Zulu.
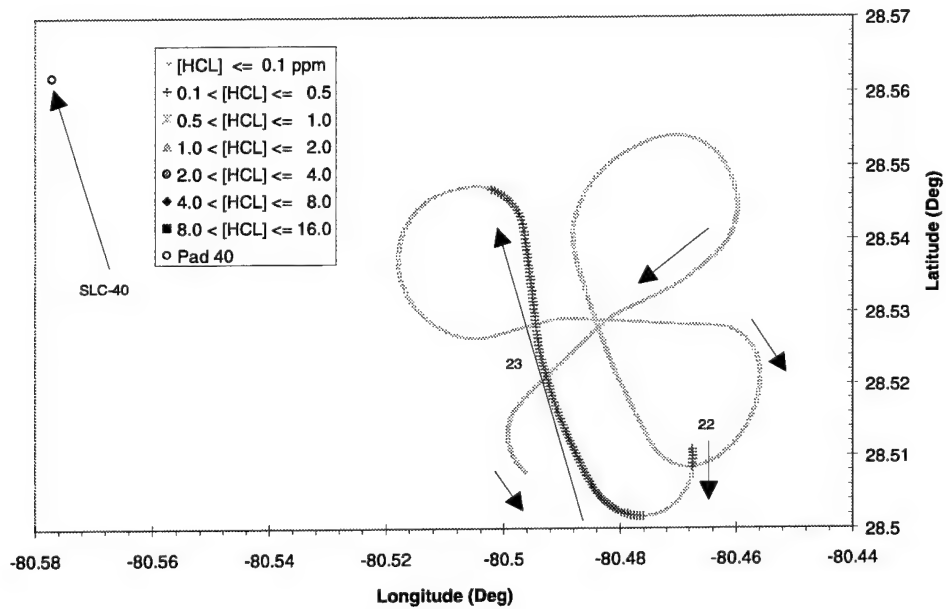
Figure 67. Aircraft GPS Latitude and Longitude: T=15:05–15:15 Zulu.

58

Figure 68 converts the data in Figure 67 to Cartesian coordinates centered on SLC-40.
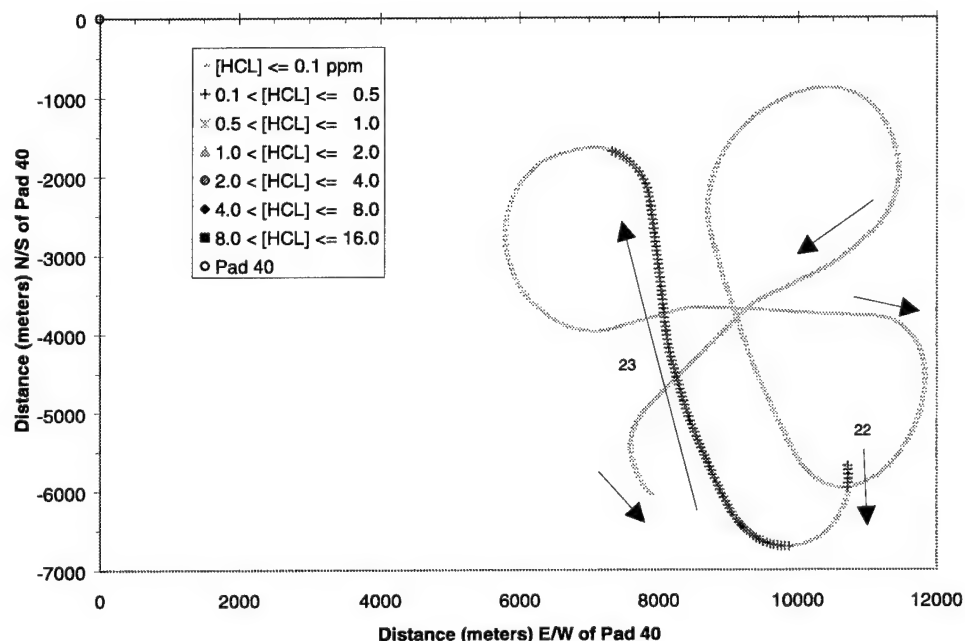
Figure 68. Cartesian Coordinates of the Aircraft Flight Pattern: T=15:05–15:15 Zulu.

Figure 69 is a composite of aircraft sampling data (passes 22–23) giving HCl concentrations and aircraft altitude between T=80 and 90 min as well as plume imagery data showing the top and the bottom of the observed visible ground cloud between T=0 and 20 min. The most salient feature of this plot is that HCl is observed only at the *high* altitudes sampled in this period and not at low altitudes characteristic of the early time stabilized plume.

Figure 70 shows a higher time resolution representation of the data in Figure 69 for the ninth 10 min period of monitoring.
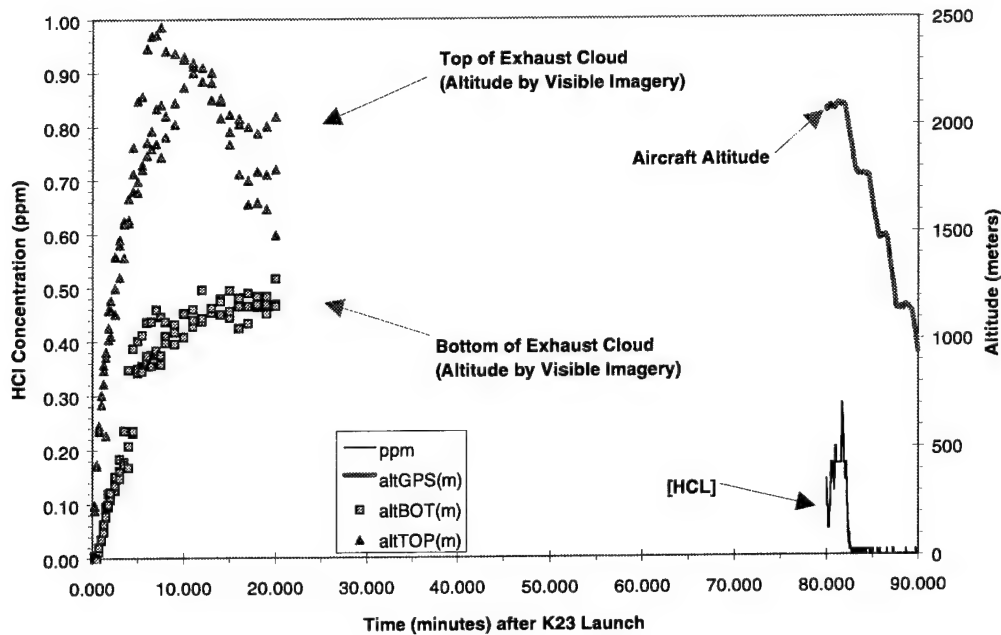
Figure 69. HCl Concentration, Visible Ground Cloud Dimensions (0–20 min), and Aircraft Altitude as a Function of Time (T=0–T=90 min).
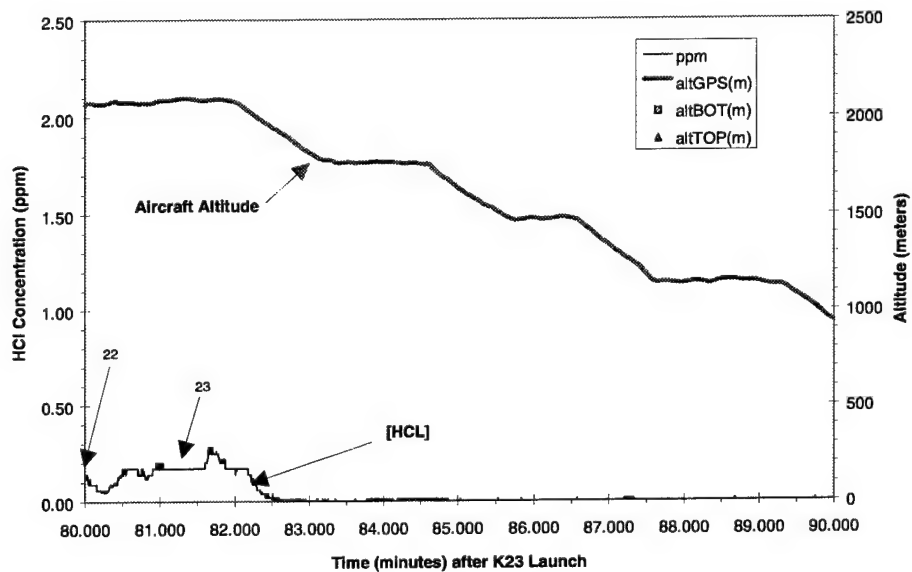
Figure 70. HCl Concentration and Aircraft Altitude as a Function of Time (T=80–T=90 min).

60

Figure 71 shows the direction of aircraft flight for the two transects occurring during this ninth 10 min window. These HCl hits are extremely small and are in the southeast quadrant with respect to the launch complex.
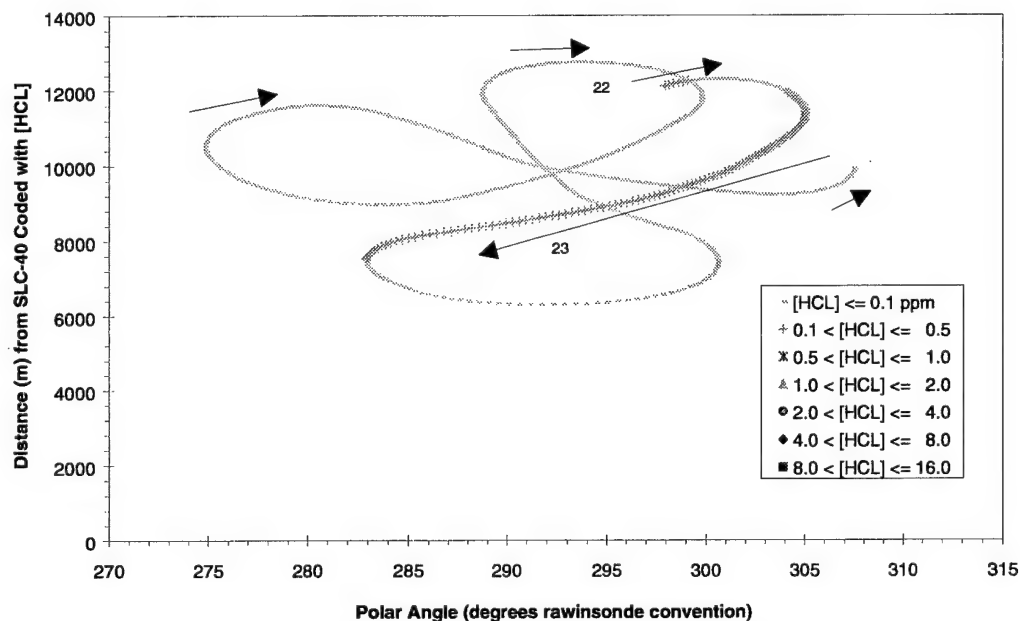
Figure 71. Aircraft Polar Coordinate Position During the T=80–T=90 min Transects.

Figure 72 provides supporting data to Figure 71 showing that *no HCl is detected below an altitude of 2000 m even though broad angular patterns are flown.* Once again, this would seen to confirm that the source of this material was the attached launch column and not the original stabilized ground cloud that moved toward the northeast as documented by visible imagery and aircraft sampling prior to T=50 min.

61
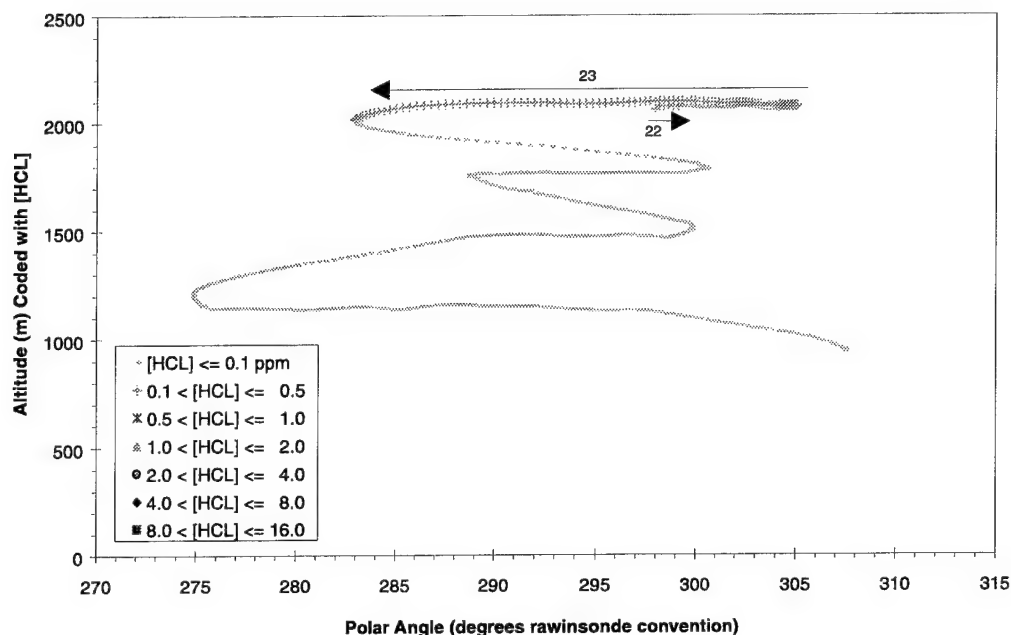
Figure 72. Aircraft Altitude and Angular Position During the T=80–T=90 min Transects.

3.2.10 Aircraft Sampling from T=90 to T=100 min

Figure 73 shows the raw and baseline-corrected HCl concentration data for the trajectory flown by the aircraft in this time window. No HCl was detected.

Figure 74 presents the positional information from the aircraft GPS records for this period.

Figure 75 converts the data in Figure 74 to Cartesian coordinates centered on SLC-40.

Figure 76 is a composite of aircraft sampling data giving HCl concentrations and aircraft altitude between T=90 and 100 min as well as plume imagery data showing the top and the bottom of the observed visible ground cloud between T=0 and 20 min. The aircraft was descending from an altitude of 1000 m during this period, and no measurable HCl was observed.
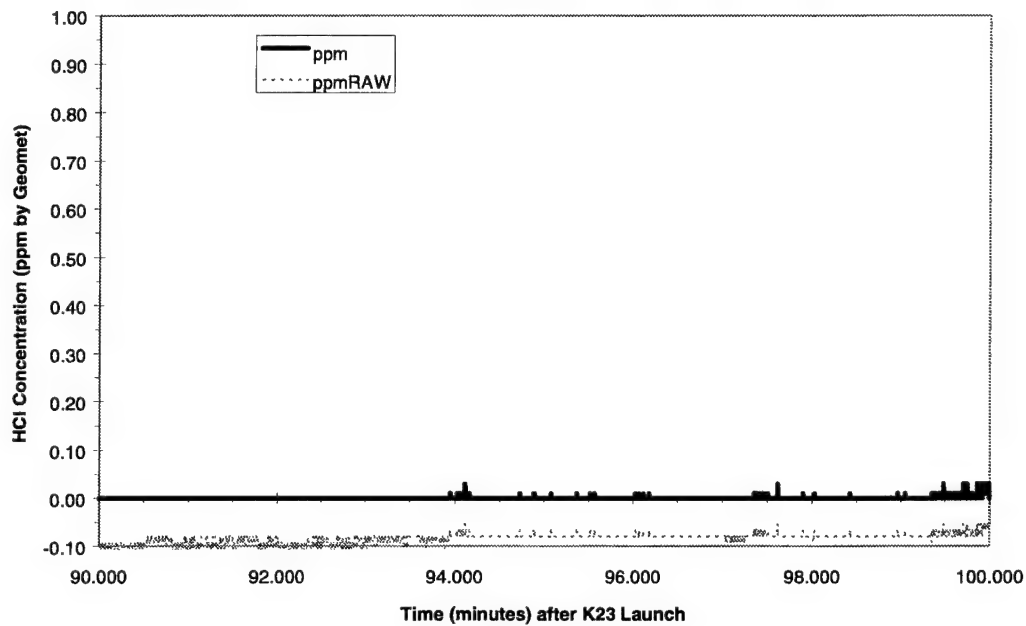
Figure 73. Raw and Baseline-Corrected Geomet Traces: T=15:15—15:25 Zulu.
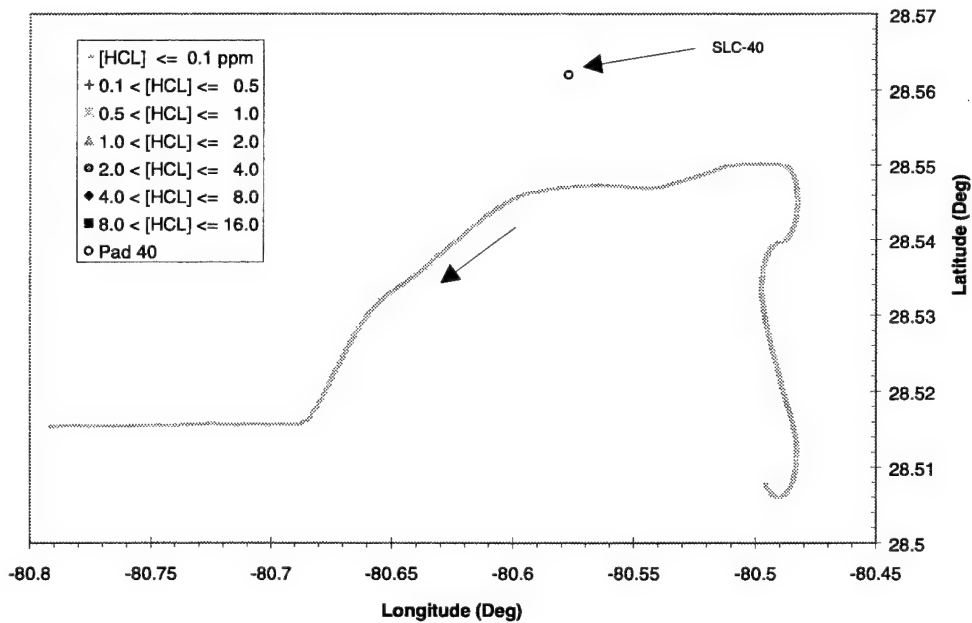
Figure 74. Aircraft GPS Latitude and Longitude : T=15:15—15:25 Zulu.

63

Titan K23 Launch Cloud Sampling and Imagery (14 May 1995)

Legend:
- ⁓ [HCL] <= 0.1 ppm
- + 0.1 < [HCL] <= 0.5
- ✕ 0.5 < [HCL] <= 1.0
- △ 1.0 < [HCL] <= 2.0
- ⊚ 2.0 < [HCL] <= 4.0
- ◆ 4.0 < [HCL] <= 8.0
- ■ 8.0 < [HCL] <= 16.0
- ○ Pad 40

Y-axis: Distance (meters) N/S of Pad 40 (0 to -7000)
X-axis: Distance (meters) E/W of Pad 40 (-25000 to 10000)
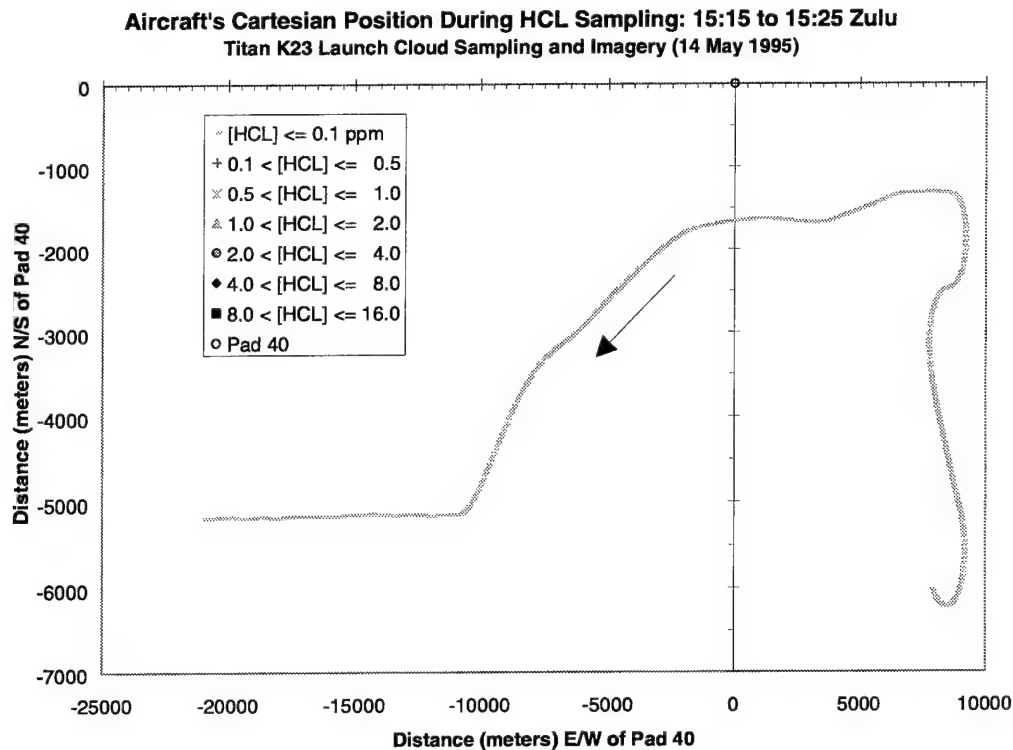
Figure 75. Cartesian Coordinates of the Aircraft Flight Pattern: T=15:15–15:25 Zulu.

Y-axis left: HCl Concentration (ppm) (0.00 to 1.00)
Y-axis right: Altitude (meters) (0 to 2500)
X-axis: Time (minutes) after K23 Launch (0.000 to 100.000)

Top of Exhaust Cloud
(Altitude by Visible Imagery)

Bottom of Exhaust Cloud
(Altitude by Visible Imagery)

Aircraft Altitude

[HCL]

Legend:
- —— ppm
- —— altGPS(m)
- ⊡ altBOT(m)
- ▲ altTOP(m)
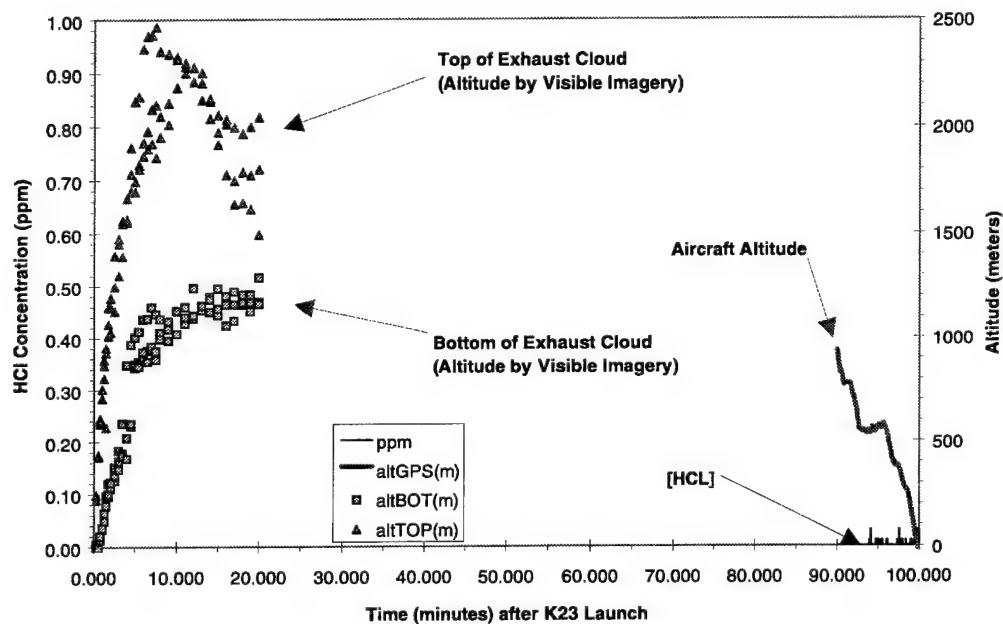
Figure 76. HCl Concentration, Ground Cloud Dimensions (0–20 min), and Aircraft Altitude as a Function of Time (T=0–T=100 min).

64

Figure 77 shows a higher time resolution representation of the data in Figure 76 for the tenth 10 min period of monitoring.
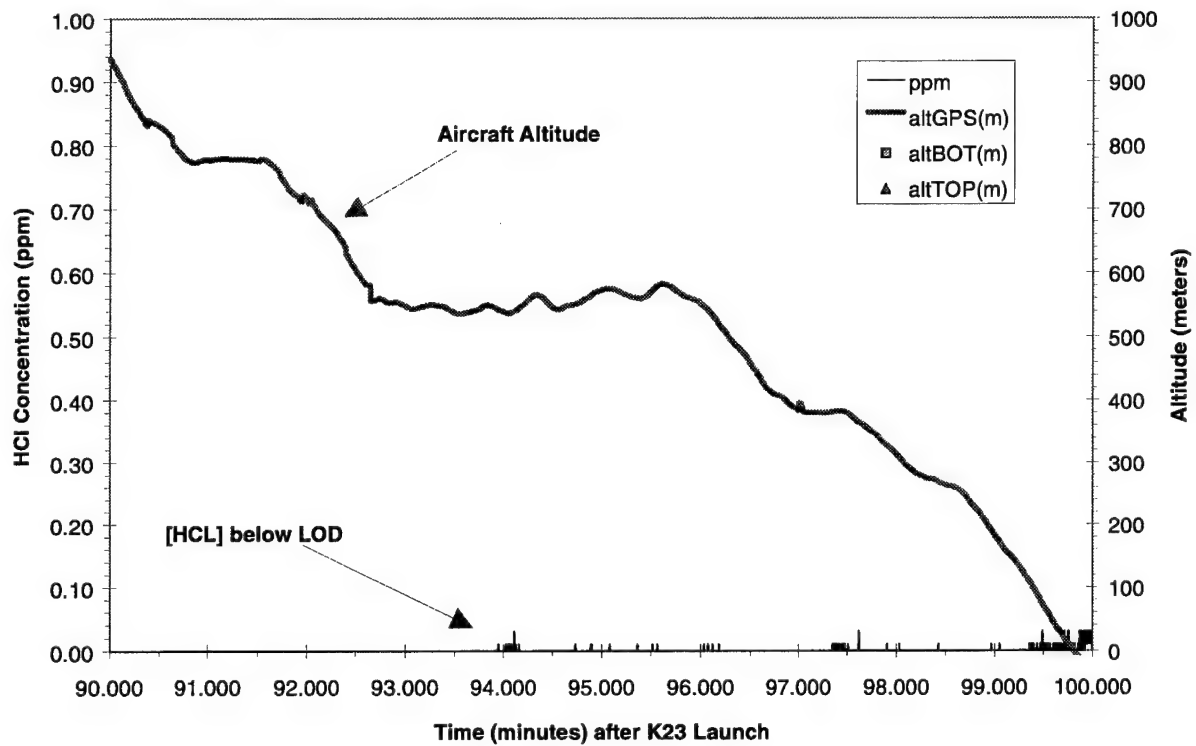
Figure 77. HCl Concentration and Aircraft Altitude as a Function of Time (T=90–T=100 min).

Figure 78 depicts the flight path of the aircraft toward its landing strip. Figure 79 provides supporting data to Figure 78, showing the aircraft decending from 1000 m to its landing strip.
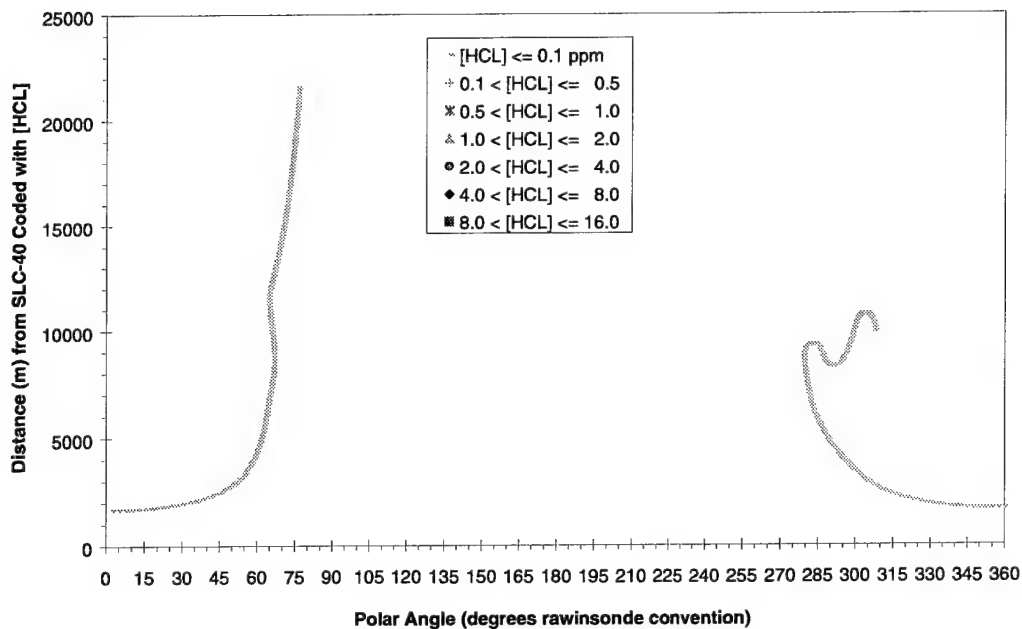
Figure 78. Aircraft Polar Coordinate Position During the T=90–T=100 min Transects.
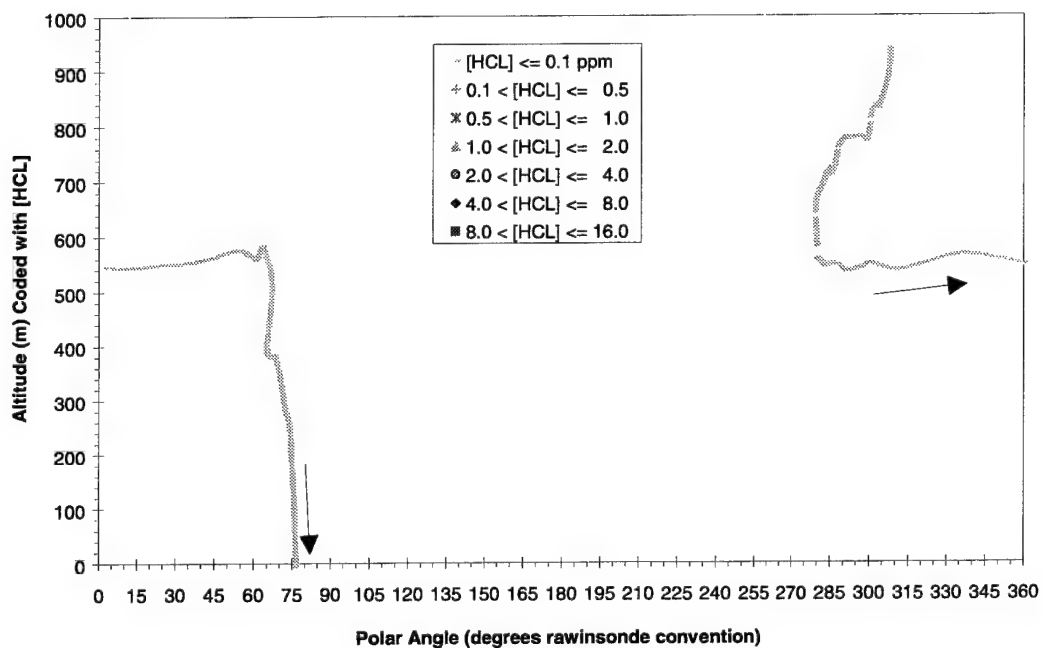
Figure 79. Aircraft Altitude and Angular Position During the T=90–T=100 min Transects.

66

4. Discussion

The representation of Titan ground clouds by the REEDM dispersion modeling code is highly simplified. REEDM pictures the heated exhaust plume as an expanding sphere whose diameter grows linearly with height as it rises, entrains ambient air, cools, and ultimately stabilizes at a height where it becomes neutrally buoyant with respect to the surrounding atmosphere.

Because real launch-vehicle effluent plumes are more complex in their spatial structure, they are more difficult to model and they present serious model validation challenges. The REEDM code derives from the NASA/Marshall Space Flight Center's (MSFC's) Multilayer Diffusion Model.[10] Because of the complexities alluded to above, the MSFC code was developed in parallel with aircraft sampling studies conducted by the NASA LaRC Atmospheric Sciences Division for both Titan III and STS launches. Aircraft data for at least 15 Titan III launches and 3 STS launches at CCAS were acquired during the 1970s and 1980s.[4,6]

The NASA/LaRC aircraft campaign had a number of ambitious goals, including discrimination between HCl in the gas phase and in acidic water aerosols.[3,4] This discrimination was accomplished by flying both a Geomet[9] (measuring total HCl) and a nondispersive IR instrument (measuring gas phase HCl only). Since the K-23 sampling aircraft used a Geomet detector only, this report limits its discussion to total HCl profiles and time dependencies.

For both Titan III and STS launches, the extensive NASA/LaRC campaign showed that the peak density of HCl decays according to a simple power law dependence

$$C = C_0 t^a \qquad\qquad (2)$$

where C_0 is the intercept at a nondimensionalized t=1 and "a" is a nondimensional constant, which is predicted by theory to be between -1.0 and -1.5. In other words, if the first concentration measurement, C_0, is made at a time of 2 min (defined as t = 1) following the launch, the concentration, C, measured at 20 min (t = 10) would be 0.1 C_0 for a = -1.0. Empirical fits of data from 8 Titan III flights [4,10] support reasonably linear fits of log C versus log t; however, the slopes of those lines vary considerably more than is predicted by results of the NASA/MSFC Multilayer Diffusion Model run for the applicable stability class at the time of launch.

In order to connect the current Titan IV monitoring campaign to the earlier Titan III campaign, data from the 20 August 1977 Titan III launch[11] are reproduced in Figure 80. Superimposed are the data for passes 1–12 of the K-23 campaign, which satisfied the following criteria: (1) the aircraft passes relatively close to the center of the plume in the vertical axis (passes 1–3 are in fact close to the bottom of the plume); and (2) the peak concentration was found at a polar angle relative to SLC-40 that confirmed the hit was indeed part of the ground cloud.

67

In actuality, the Titan III and IV data are not directly comparable. The source terms are somewhat different, as are the measured stabilization heights: Titan III (20 August 1977) = 1.2–1.3 km; Titan IV (14 May 1995) = 1.7 km. Nevertheless, the K-23 data are well within the range of both peak HCl concentration and "a" coefficient encountered during the Titan III campaigns. In addition, the peak HCl predicted by REEDM for the stabilized K-23 cloud is plotted in Figure 80.

Airborne Effluent Measurements
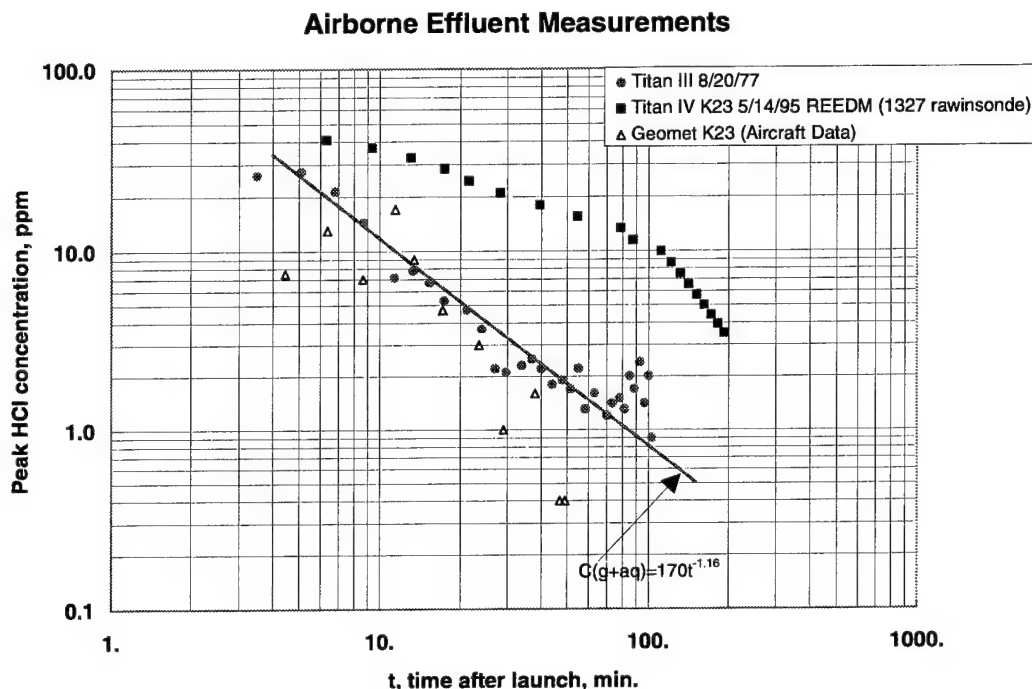
Figure 80. Comparison of Peak HCl Concentration Falloff of the 20 August 1977 Titan III Launch (closed circles) and the 14 May 1995 Titan IV Launch (open triangles) at CCAS. The closed squares represent the REEDM calculated elevated maximum centerline concentration at the computed stabilization height of 787.6 m. REEDM calculates the arrival and departure times of the cloud at a series of down-range distances. The mean of those two times was used to plot the REEDM data in this figure.

Table 2 summarizes the data on HCl "hits" detected by the aircraft in Sections 3.2.1 through 3.2.10. Data taken in the ground cloud are represented by passes 1–12; data taken in the attached launch column are represented by passes 13–21.

68

Table 2. Summary of Aircraft Sampling Data Derived from Titan IV K-23

No.	Time of Pass	Peak HCl	Sampling Altitude	Type of Pass	Aircraft Location w.r.t. SLC-40		Plume to Pad	Plume Parameter ΔD	$\Delta\theta$
	(min)	(ppm)	(meters)		D(m)	$\theta(°)$	(m)	(m)	(°)
				Grd Cloud					
1	4.45	7.5	660 +/- 10	Downwind	1300	268	1418	600	5
2	6.37	13	1000 +/- 40	Crosswind	1750	255	2007	50	29
3	8.65	7	1100 +/- 20	Downwind	2600	245	2683	1450	4
4	11.45	17	1480 +/- 10	Crosswind	3150	260	3463	450	55
5	13.5	9	1450 +/- 30	Downwind	4300	258	4139	3500	9
6	17.2	4.7	1500 +/- 20	Crosswind	5000	260	5169	500	50
7	23.5	3	1320 +/- 10	Crosswind	7000	253	7022*	400	14
8	29	1	1120 +/- 10	Crosswind	8800	247	8640*	400	7
9	38	1.6	1390 +/- 20	Cross/Down	11000	267	11361*	1100	3
10	42	0.2	1480 +/- 10	Cross/Down	13500	266	12464*	200	2
11	47	0.4	1150 +/- 50	Crosswind	13800	249	13935*	700	4
12	49	0.4	560 +/- 100	Crosswind	14500	256	14415*	1500	5
				Column					
13	58.5	2.0	2250 +/-250	Cross/Up	8000	280	n/a	2300	21
14	66.5	0.5	2520 +/- 20	Cross/Down	10600	287	n/a	200	2
15	68	2.0	2350 +/- 50	Cross/Up	8600	284	n/a	2600	16
16	69.5	2.25	2250 +/- 50	Cross/Down	6700	303	n/a	2900	13
17	75	4.5	2400 +/- 50	Downwind	12000	283	n/a	3600	3
18	76.5	2.5	2325 +/- 30	Up/Cross	9800	285	n/a	2000	4
19	77	3.5	2320 +/- 20	Up/Cross	8200	281	n/a	2000	7
20	78.5	1.5	2300 +/- 20	Downwind	6400	296	n/a	2000	4
21	79.5	2.25	2160 +/- 60	Downwind	10000	293	n/a	2400	3

Notes

[1] The time of pass is reported as the time corresponding to the observed peak in the HCl concentration.

[2] The sampling altitude is reported at $[HCl]_{max}$; the uncertainty represents the maximum and minimum altitude excursions during the pass.

[3] The plume-to-pad distance for the first six passes was calculated using the imagery-derived wind speed; that speed was also assumed to apply to the next six entries along the ground cloud track (passes 6–12).

[4] The aircraft location is reported in polar coordinates when it encounters $[HCl]_{max}$. A transformation has been made such that the rawinsonde wind angle (θ) is reported.

[5] The "type of pass" compares the rawinsonde wind vector with the aircraft velocity vector when $[HCl]_{max}$ is encountered.

[6] The "plume parameters" report the dimensions of the plume encountered *by the aircraft* during a pass using the same polar coordinate system adopted for aircraft location. Crosswind passes ideally have $\Delta D=0$; down- or up-wind passes ideally have $\Delta\theta=0$.

5. Summary and Conclusions

An instrumented sampling aircraft incorporating a Geomet total HCl detector was deployed to monitor the Titan IV K-23 launch effluent cloud. This aircraft campaign obtained a large quantity of HCl concentration data as a function of time following launch while logging the altitude and horizontal coordinates of the aircraft using GPS. The first 20 min of the aircraft sampling data have been correlated with 3-D visible imaging of the ground cloud in both the present and in previous reports.[7,8]

For favorable aircraft transects, plume concentration profiles could be isolated against a single variable (e. g., spread in polar angle, extent of along-wind spatial dimension). The aircraft HCl hits fell into two groups. The first group of hits was clearly due to the stabilized ground cloud at altitudes below about 2000 m and centered along a heading of roughly 250°. The second group of hits occurred at higher altitudes (2000–2500 m) and was centered roughly around a heading of 285° although that heading neared 300° for some time windows. Evidence was presented suggesting that these higher altitude HCl hits resulted from the transport of the attached launch column. This portion of the exhaust plume was initially deposited at relatively high altitudes, where low wind speed and wind orientations from the west-northwest pushed it into the southeast quadrant with respect to SLC-40.

Although the sampling data have been presented as [HCl] in units of ppm referenced to laboratory temperature and pressure conditions, several factors influence the reliability of the ppm values as reported. Most important is the fact that the Geomet detector has a complex, relatively slow response time. Moreover, that response time is a function of the [HCl]. A second influence on the data has been examined associated with aerodynamics effects on the aircraft's sampling inlet. These factors are discussed in Appendix 3.

Finally, it can be said that the data are consistent with more extensive measurement campaigns conducted in the 1970s and 1980s by NASA LaRC for both Titan III and STS launches. Peak [HCl] of 20 ppm near stabilization is typical of these earlier launches as well as the K-23 Titan IV launch. The data presented provide the opportunity to test predictions made by REEDM and other plume dispersion modeling codes.

Appendix 1a

Meteorological Rawinsonde Data (T-0.3 hr)

Input to the REEDM Code

```
1**************************************************************************
                ROCKET EXHAUST EFFLUENT DIFFUSION MODEL REEDM        PAGE    3
                         VERSION 7.05 AT  KSC
                         1109 EST 14 FEB 1996
                  launch time:  0945 EDT 14 MAY 1995
     RAWINSONDE ASCENT NUMBER      0, 1327   Z 14 MAY    95   T  -0.3 HR
**************************************************************************

                  ----- METEOROLOGICAL RAWINSONDE DATA -----


         RAWINSONDE MSS/MSS
         TIME- 1327   Z    DATE- 14 MAY    95
         ASCENT NUMBER       0


                     ----- T  -0.3 HR SOUNDING -----
```

MET. LEV. NO.	ALTITUDE MSL (FT)	ALTITUDE GND (FT)	GND (M)	WIND DIR (DEG)	WIND SPEED (M/S)	WIND SPEED (KTS)	AIR TEMP	AIR PTEMP (DEG C)	AIR DPTEMP	AIR PRESS (MB)	AIR RH (%)	H M	INT-ERP
1	16	0.0	0.0	270	3.1	6.0	29.5	31.4	23.9	1016.7	72.0		
2	67	51.3	15.6	275	3.5	6.7	28.8	30.7	23.5	1014.9	73.1		**
3	119	102.5	31.2	280	3.9	7.5	28.0	30.1	23.0	1013.1	74.3		**
4	170	153.8	46.9	284	4.2	8.2	27.3	29.4	22.5	1011.4	75.5		**
5	221	205.0	62.5	289	4.6	9.0	26.5	28.7	22.1	1009.6	77.0		
6	314	297.7	90.7	284	4.6	9.0	26.3	28.9	22.4	1006.4	79.2		**
7	406	390.3	119.0	279	4.6	9.0	26.2	29.1	22.8	1003.2	81.6		**
8	499	483.0	147.2	274	4.6	9.0	26.0	29.2	23.1	1000.0	84.0		
9	603	587.0	178.9	269	4.6	9.0	25.9	29.5	23.5	996.4	86.9		**
10	707	691.0	210.6	263	4.6	9.0	25.7	29.8	23.9	992.9	90.0	*	
11	854	837.5	255.3	260	4.6	8.9	25.9	30.3	23.2	987.9	85.1		**
12	1000	984.0	299.9	256	4.5	8.8	26.1	30.8	22.5	983.0	81.0		
13	1253	1237.0	377.0	251	4.6	9.0	26.4	31.6	21.2	974.4	73.0		
14	1524	1508.0	459.6	246	4.6	9.0	26.0	32.1	20.9	965.4	73.2		**
15	1795	1779.0	542.2	241	4.6	9.0	25.7	32.5	20.5	956.4	73.0		
16	2000	1984.0	604.7	239	4.9	9.5	25.2	32.5	20.1	949.7	73.0		
17	2349	2333.0	711.1	234	5.1	10.0	24.4	32.7	19.4	938.3	74.0		
18	3000	2984.0	909.5	231	4.8	9.3	22.8	32.9	18.2	917.4	75.0		
19	3542	3526.0	1074.7	234	4.6	9.0	21.3	33.0	17.6	900.0	80.0		
20	3921	3905.0	1190.2	236	4.1	8.0	20.4	33.2	17.3	888.3	83.0		
21	4000	3984.0	1214.3	237	4.0	7.8	20.2	33.2	17.2	885.8	83.0		
22	4462	4446.0	1355.1	243	3.6	7.0	19.2	33.5	16.7	871.6	85.0		
23	5000	4984.0	1519.1	253	2.7	5.2	18.3	34.0	14.8	855.2	80.0		
24	5163	5147.0	1568.8	256	2.6	5.0	18.2	34.4	14.2	850.0	78.0		
25	5582	5565.5	1696.4	266	2.0	3.9	17.6	35.0	13.0	837.6	74.6		**
26	6000	5984.0	1823.9	276	1.4	2.8	17.1	35.6	11.8	825.4	71.0		
27	6863	6847.0	2087.0	284	1.0	2.0	15.7	36.2	4.9	800.0	50.0		
28	7000	6984.0	2128.7	283	1.0	2.0	15.5	36.2	3.2	796.4	45.0		
29	7259	7243.0	2207.7	281	1.0	2.0	15.0	36.2	-0.5	789.1	35.0		
30	7839	7823.0	2384.5	267	1.5	3.0	13.4	36.8	5.1	772.8	57.0		
31	8000	7984.0	2433.5	266	1.4	2.7	13.2	37.0	4.2	768.3	54.0		
32	8650	8634.0	2631.6	269	1.5	3.0	12.1	37.9	2.3	750.0	51.0		
33	9272	9255.5	2821.1	294	1.4	2.8	11.0	38.7	2.7	733.6	57.5		**
34	9772	9755.5	2973.5	323	1.7	3.2	10.4	39.4	-1.0	720.4	46.5		**

```
  *  - INDICATES THE CALCULATED TOP OF THE SURFACE MIXING LAYER
  ** - INDICATES THAT DATA IS LINEARLY INTERPOLATED FROM INPUT METEOROLOGY
```

Appendix 1b

Meteorological Wind Profiler Data (T-9.5 min)

Determined from the Mosquito Lagoon Site

Mosquito Lagoon
  Latitude/Longitude 28.60   80.59   3
  Date 95 05 14 Time (hrs., min., secs.) 13 35 29   0
    9
  8 7 8   5 5 5   2.0 2.0 2.0
  188 188 42 42 700 700 43 43
  10.1 10.1 1 1700 1700 32 32 700 700
  130 67   220 67   0.117   5.0 326   -1.77   -0.44   0.13   8 7 8
25
  20   24

Height (km)	Wind Speed (m/sec)	Wind Dir. (deg.)	Oblique Velocities (m/sec)		Vertical Velocity (m/sec)	# of samples (8 max.)			Signal to Noise Ratio		
0.214	5.1	319	-1.87	-0.21	0.12	8	7	8	28	26	31
0.311	5.7	331	-1.92	-0.65	0.18	8	7	8	26	20	24
0.407	5.4	321	-1.95	-0.29	0.12	8	7	8	23	21	26
0.504	4.9	294	-1.97	0.40	-0.15	8	6	8	13	21	13
0.601	4.4	270	-1.43	1.02	-0.11	8	7	8	11	13	8
0.697	4.6	265	-1.24	1.28	0.03	8	7	8	4	2	-0
0.794	4.0	242	-0.63	1.37	-0.07	8	7	8	3	-0	-2
0.891	4.1	242	-0.60	1.50	0.01	8	7	8	-4	3	-6
0.987	4.1	237	-0.47	1.51	-0.02	8	7	8	-1	-2	-3
1.084	4.3	238	-0.51	1.62	0.03	8	7	8	3	-2	-2
1.181	4.7	234	-0.54	1.69	-0.09	8	7	8	2	-1	-3
1.277	5.1	229	-0.43	1.82	-0.15	8	7	8	-1	-4	1
1.374	4.8	241	-0.79	1.64	-0.14	8	7	8	-7	-7	-6
1.471	4.7	257	-1.12	1.46	-0.00	8	7	8	-7	-6	-11
1.567	4.9	259	-1.39	1.28	-0.22	8	6	7	-8	-7	-4
1.664	4.6	267	-1.43	1.11	-0.12	8	7	8	-5	-11	-6
1.760	4.1	275	-1.29	0.95	0.04	8	7	8	-8	-7	1
1.857	3.6	280	-1.14	0.78	0.08	8	7	8	1	-2	7
1.954	3.2	286	-1.10	0.57	0.07	8	7	8	7	6	-2
2.050	3.4	288	-1.21	0.53	0.03	8	7	8	6	7	-10
2.147	3.4	290	-1.21	0.48	0.03	8	7	8	-1	0	-10
2.244	2.4	284	-0.84	0.44	0.02	8	7	8	-6	-9	-5
2.340	1.3	280	-0.40	0.32	0.06	8	7	8	-2	-4	-5
2.437	1.5	267	-0.36	0.46	0.07	8	7	8	1	-0	-3
2.534	2.0	258	-0.42	0.69	0.07	8	7	8	-1	-0	1
2.630	2.7	256	-0.57	0.90	0.05	8	7	8	-3	-1	-6
2.727	3.1	278	-0.79	0.90	0.27	8	7	6	-2	-2	-12
2.824	3.1	266	-0.87	0.83	-0.00	8	7	5	-3	-3	-16
2.920	2.9	266	-0.83	0.80	-5.30	8	7	3	-6	-7	-18
3.017	2.2	260	-0.56	0.67	-5.56	8	7	2	-10	-14	-19
3.114	9999.0	9999	-0.48	-0.27	-3.50	8	3	2	-13	-18	-19

Appendix 1c

Meteorological Wind Profiler Data (T+5.5 min)

Determined from the Mosquito Lagoon Site

Mosquito Lagoon
  Latitude/Longitude 28.60   80.59   3
  Date 95 05 14 Time (hrs., min., secs.) 13 50 26   0
   9
  8 7 8   5 5 5   2.0 2.0 2.0
  188 188 42 42 700 700 43 43
  10.1 10.1 1   1700 1700 32 32 700 700
  130 67   220 67

Height	Wind Speed	Wind Dir.	Oblique Velocities		Vertical Velocity	# of samples			Signal to Noise Ratio		
(km)	(m/sec)	(deg.)	(m/sec)		(m/sec)	(8 max.)					
0.117	5.6	322	-2.13	-0.46	0.01	7	7	8	22	21	27
0.214	5.5	327	-2.00	-0.58	0.04	7	7	8	27	24	27
0.311	5.8	323	-2.26	-0.56	-0.04	8	7	8	25	23	29
0.407	5.7	326	-2.27	-0.73	-0.13	7	7	8	24	21	27
0.504	5.5	326	-2.19	-0.70	-0.13	8	7	8	18	12	19
0.601	4.5	311	-2.07	-0.36	-0.35	8	7	8	10	12	8
0.697	4.2	289	-1.38	0.73	0.16	8	7	8	9	7	2
0.794	3.8	279	-1.19	0.84	0.08	8	7	7	2	3	7
0.891	3.6	255	-0.62	1.35	0.20	7	6	8	2	-0	6
0.987	4.0	245	-0.52	1.58	0.16	8	7	8	1	-0	-3
1.084	4.1	242	-0.52	1.58	0.08	8	7	8	-8	-2	-4
1.181	4.6	249	-0.83	1.63	0.06	8	7	8	-9	-6	-4
1.277	4.9	246	-0.81	1.77	0.05	8	7	8	-6	-4	-3
1.374	5.2	243	-0.82	1.82	-0.03	8	7	8	-3	-2	-3
1.471	5.1	254	-1.12	1.65	0.01	8	7	8	-5	-5	-4
1.567	4.9	268	-1.40	1.28	0.02	8	7	8	-3	-4	-13
1.664	4.3	281	-1.41	0.89	0.08	8	7	8	-8	-8	-12
1.760	3.6	280	-1.16	0.77	0.07	8	7	8	-5	-9	·0
1.857	3.4	284	-1.16	0.62	0.04	8	7	8	-2	-3	8
1.954	3.5	291	-1.25	0.48	0.05	8	7	8	8	6	2
2.050	3.8	297	-1.38	0.40	0.06	8	7	8	10	7	-8
2.147	4.0	299	-1.49	0.34	0.05	8	7	8	4	1	-10
2.244	3.2	300	-1.23	0.23	0.02	8	7	8	-4	-8	-8
2.340	1.9	289	-0.68	0.29	0.02	8	7	8	-4	-2	-7
2.437	1.8	271	-0.57	0.40	-0.04	8	7	8	-1	-0	-6
2.534	2.4	257	-0.64	0.68	-0.08	8	7	8	-1	-1	-2
2.630	2.9	253	-0.72	0.87	-0.10	8	7	8	-4	-4	-3
2.727	3.1	268	-0.97	0.72	-0.09	8	7	8	-3	-1	-14
2.824	3.5	276	-1.12	0.75	1.50	8	7	4	-1	-1	-19
2.920	3.5	275	-1.11	0.79	1.97	8	7	3	-5	-5	-19
3.017	2.9	269	-0.87	0.75	-2.49	8	7	3	-11	-12	-17
3.114	9999.0	9999	-0.59	9.29	-8.60	7	2	2	-14	-20	-20

83

Appendix 2

Summary of K-23 Plume Parameters Derived from REEDM

Modeling, Imagery, and Meteorology Data

Table A2.1 contains a variety of measured and computed information regarding the stabilization and transport of the K-23 ground cloud. The initial table entries give the stabilization height, direction, and speed of the ground cloud as calculated by the REEDM code. REEDM #1 is based on T-1.4 hr rawinsonde data (see Reference 7). REEDM #2 is based on T-0.3 hr rawinsonde data (see Appendix 1a). Table A2.1 shows the reported rawinsonde and wind profiler data for the altitudes closest to the computed stabilization height of the ground cloud. Although the measured wind directions and wind speeds are in relatively good agreement with the calculation, the imagery data indicates that the REEDM calculation for stabilization height is in error by roughly a factor of 2.

If we examine the rawinsonde and wind profiler wind orientations and speeds at the ground cloud stabilization heights (bottom, middle, and top) measured by imagery, we find a significant difference in the ranges of orientations and speeds at the higher plume altitude determined by imagery. It should be remembered that the rawinsondes and the profiler sample different spatial regions from each other and from the plume. The meteorological data presented in Table A2.1 are also taken at somewhat different times, ranging from about T-18 min to T+5.5 min.

Table A2.1: Summary of Selected Dispersion Modeling , Imaging, and Meteorological Information for the K-23 Ground Cloud.

Modeling Data	REEDM Plume Output			T-0.3 hr Rawinsonde			T-9.5/T+5.5 min Profiler		
	Height	Angle	Speed	Height	Angle	Speed	Height	Angle	Speed
	(m)	(°)	(m/s)	(m)	(°)	(m/s)	(m)	(°)	(m/s)
REEDM #1	737.3	233.7	5.2	711.1	234	5.1	697	265/289	4.6/4.2
REEDM #2	787.6	250.0	5.2	909.5	231	4.8	794	242/279	4.1/3.8
Imagery Data	Plume Imagery Output			T-0.3 hr Rawinsonde			T-9.5/T+5.5 min Profiler		
	Height	Angle	Speed	Height	Angle	Speed	Height	Angle	Speed
	(m)	(°)	(m/s)	(m)	(°)	(m/s)	(m)	(°)	(m/s)
Plume Bottom	1152+/-50	n/a	n/a	1190.2	236	4.1	1181	234/249	4.7/4.6
Plume Middle	1640+/-74	249	5.1	1696.4	266	2.0	1664	267/281	4.6/4.3
Plume Top	2211+/-118	n/a	n/a	2207.7	281	1.0	2244	284/300	2.4/3.2

Appendix 3

Response Characteristics of the Geomet HCl Detector

The chemiluminescent method employed by the Geomet HCl detector was patented and commercialized in the early 1970s.[9,12] The most comprehensive data on Geomet characteristics was published in 1977 by G. L. Gregory of NASA LaRC and R. H. Moyer of Geomet, Inc.[9] Since the mid-70s, these detectors have been used in a variety of harsh field environments from static and mobile platforms (air, sea, and land).

From the standpoint of launch cloud characterization, a number of attributes are highly advantageous. The Geomet HCl detector has shown a lower detection limit of $< 5 \times 10^{-3}$ ppm by volume, whereas 0.2 ppm would be sufficient for launch cloud monitoring. Although there are some problems with molecular specificity, none of the potential exhaust products from solid rocket motors is significant with respect to the amount of HCl present. It has been demonstrated (see Reference 9, Table II) that the detector is equally sensitive to an equivalent weight of HCl whether present as a gas or as a liquid aerosol. Its response accuracy (linearity) is estimated to be +/- 10% from 0.1 to 50 ppm (see Reference 9, Figure 3). The calibration versus an HCl standard is extremely stable, as long as the inlet tube has been properly coated with the aqueous bromate/bromide solution. Gregory and Moyer report that the useful life of a coating for the *standard* inlet tube length of 45 cm is 9×10^{3} ppm-sec. This far exceeds the integrated exposure to HCl encountered during the K-23 mission.

For the purposes of airborne HCl sampling of launch plumes, the only intrinsically limiting attribute of the Geomet is its response time. This is illustrated in Figure A3.1.
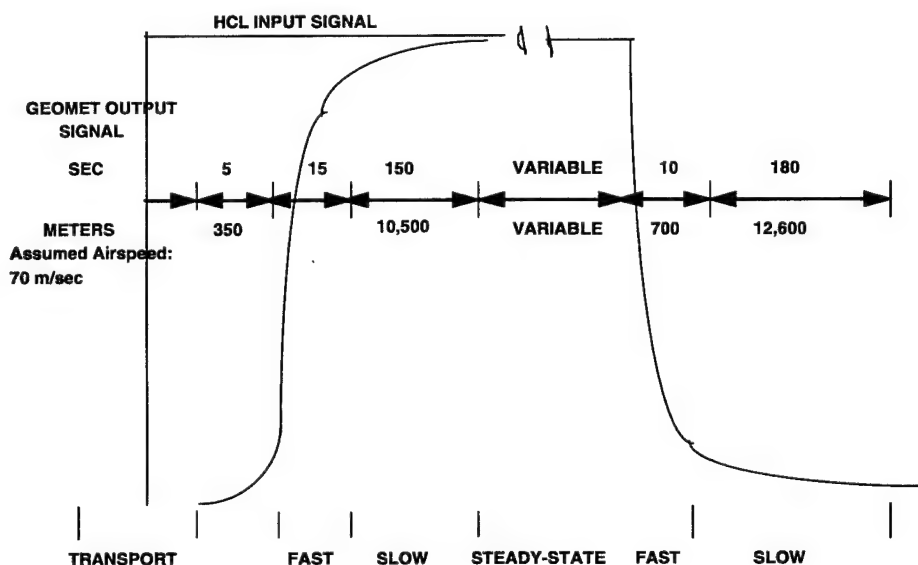

Figure A3.1. Schematic Response of the Geomet Detector to a Rectangular Pulse of HCl. Noted on the figure is the spatial discrimination possible at an aircraft flight speed of 70 m/sec.

Reference 9 (Figure 2) presents an actual plot for the initial response of a Geomet to a 1 ppm HCl mixture. In Table I of that reference, data are presented that show the response time (to 90% of peak) to be inversely proportional to [HCl] over the concentration range of 1 to 50 ppm. For example, the response time is 0.5 sec for 50 ppm, but is 10 sec for 1 ppm. Referring to Figure A3.1 above, the aircraft travels 700 m in 10 sec, which is comparable to the size of the K-23 ground cloud.

Although no quantitative data are presented in Reference 9, it is stated that the response time decreases as the inlet tube is shortened and the sampling rate (in liters per minute) is increased. A "standard" sampling rate of 2.2 l/min was used on the K-23 campaign; however, a significantly *longer* inlet tube (122 cm) was used instead of the standard tube (45 cm). Presumably, the response time during K-23 was slower than the data in Reference 9 indicate.

Figure A3.2 shows the actual calibration curve recorded by I-NET prior to the K-23 launch. A series of 5.0 min exposures to 1.1 ppm of HCl was used. Figure A3.2 quanitatively illustrates that the Geomet has two response times on both the leading *and* trailing edge of exposure to HCl. Unfortunately, no data exist for the dependence of the slow time constant on concentration. In addition, no data have been published on the dependence of the fast *recovery* time of the instrument following exposure to various fixed HCl concentrations.
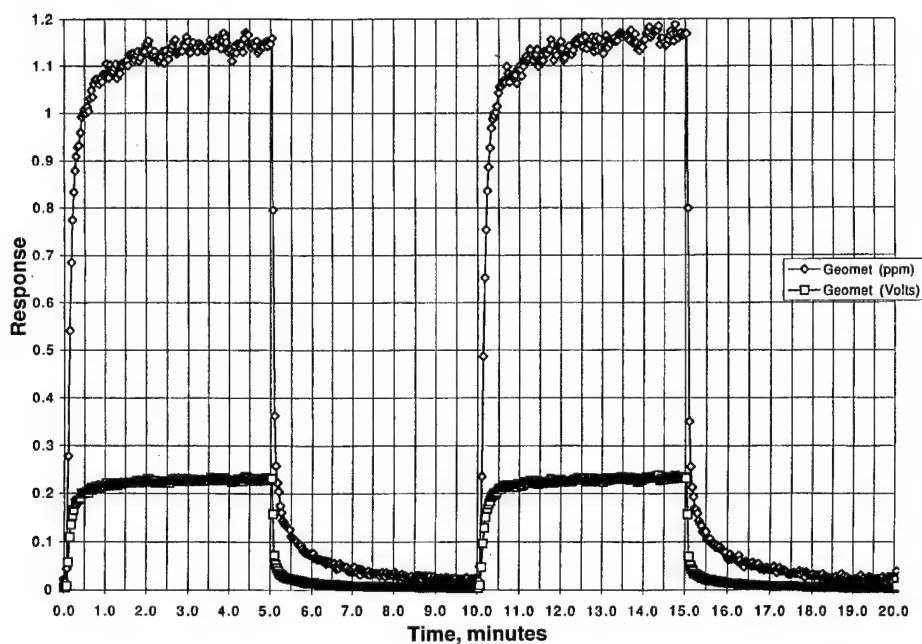

Figure A3.2. Actual Calibration Curve recorded by I-NET Prior to the K-23 Launch.

These response time attributes of the Geomet make edge detection for an elevated exhaust cloud very complex. The Geomet is slow to respond to low concentrations at the leading edge. In addition, it is slow to recover to the baseline at the trailing edge of the cloud. The line-integrated HCl (along the flight path) is expected to be accurate. The ambiguity resides in accurate determination of the concentration *profile* (including peak concentration) of HCl within the cloud.

In addition, I-NET has expressed concern that errors may also arise from aerodynamic effects associated with the aircraft platform. In particular, the concern is that the hydrodynamic pressure generated at the sample tube inlet may be different from the ambient pressure. That would cause a change in the mass flow rate (proportional to p^2) since the Geomet is actually a mass flow detector, i. e., the detected chemiluminescence is proportional to the mass of HCl sampled per second. Of course, the pressure in the atmosphere also changes with altitude. Refering to the T-0.3 hr rawinsonde data (Appendix 1), the pressure at the surface is 1016.7 mbar, while the pressure at 2087 m is 800.0 mbar. The pressure at the sampling inlet compared to the free stream pressure can be calculated from Bernoulli's equation if the geometry of the sampling system, and the aircraft velocity, are specified. To estimate the magnitude of the effect in this case, one can imagine a pitot tube that is being used to measure the airspeed of the aircraft according to the equation

$$P_1 = P_2 + 1/2 \; \rho v^2$$

where P_1 is pressure at the probe inlet, P_2 is the pressure perpendicular to the flight velocity vector, v is the air speed, and ρ is the density of air. For air speeds of 70 m/sec, P_1 and P_2 differ by only 2%. It would therefore appear that correcting for the ambient atmospheric pressure would be a much more significant effect than any aerodynamic correction.

References

1. J. R. Bjorklund, *User's Manual for the REEDM Version 7 (Rocket Exhaust Effluent Diffusion Model) Computer Program, Vol. I*, TR-90-157-01, AF Systems Command, Patrick AFB, FL (April 1990).

2. R. L. Nyman, *REEDM Version 7.07: Prototype Software Description*, TR 95-314/69-02, ACTA Inc., Torrance, CA, AFSPC 45th Space Wing, Patrick AFB, FL, and 30th Space Wing, Vandenberg AFB, CA (September 1995).

3. D. I. Sebacher, R. J. Bendura, and D. E. Wornom, "Hydrochloric Acid Aerosol and Gaseous Hydrogen Chloride Partitioning in a Cloud Contaminated by Solid Rocket Exhaust," *Atmospheric Environment* **14**, 543-547 (1980).

4. G. L. Pellett, D. I. Sebacher, R. J. Bendura, and D. E. Wornom, "HCl in Rocket Exhaust Clouds: Atmospheric Dispersion, Acid Aerosol Characteristics, and Acid Rain Deposition," *APCA Journal* **33**, 304-311 (1983).

5. D. I. Sebacher, W. R. Cofer III, D. C. Woods and G. L. Maddrea, Jr., "Hydrogen Chloride and Aerosol Ground Cloud Characteristics Resulting from Space Shuttle Launches," *Atmospheric Environment* **18**, 763-770 (1984).

6. W. R. Cofer III, R. J. Bendura, D. I. Sebacher, G. L. Pellett, G. L. Gregory, and G. L. Maddrea, Jr., "Airborne Measurements of Space Shuttle Exhaust Constituents," *AIAA Journal* **23**, 283-287 (1985).

7. Environmental Systems Directorate, *Ground Cloud Dispersion Measurements During the Titan IV Mission #K-23 (14 May 1995) at Cape Canaveral Air Station. Volume 1 - Test Overview and Data Summary*, TR-96(1410)-1, The Aerospace Corporation, El Segundo, CA (27 February 1996).

8. R. N. Abernathy, R. F. Heidner III, B. P. Kasper, and J. T. Knudtson, *Visible and Infrared Imagery of the Launch of Titan IV K-23 from Cape Canaveral Air Force Station on 14 May 1995*, TOR-96(1410)-1, The Aerospace Corporation, El Segundo, CA (15 November 1995).

9. G. L. Gregory and R. H. Moyer, "Evaluation of a Hydrogen Chloride Detector for Environmental Monitoring." *Rev. Sci. Instrum.* **48**, 1464-1468 (1978).

10. G. L. Pellett and W. L. Staton, Application of a Gaussian Multilayer Diffusion Model to Characterize Dispersion of Vertical HCl Column Density in Rocket Exhaust Clouds, NASA Technical Paper 1956 (1981), National Aeronautics and Space Administration, and references therein.

11. D. C. Woods, R. J. Bendura, and D. E. Wornom, *Launch Vehicle Effluent Measurements during the August 20, 1977, Titan III Launch at Air Force Eastern Test Range*, TM-78778, National Aeronautics and Space Administration (1979).

12. *Hydrogen Chloride Detection, Measurement and Monitoring*, CPIA Publication No. 272, D. S. Gaarder and A. V. Jensen (eds.), The Johns Hopkins University Applied Physics Laboratory (December 1975).

TECHNOLOGY OPERATIONS

The Aerospace Corporation functions as an "architect-engineer" for national security programs, specializing in advanced military space systems. The Corporation's Technology Operations supports the effective and timely development and operation of national security systems through scientific research and the application of advanced technology. Vital to the success of the Corporation is the technical staff's wide-ranging expertise and its ability to stay abreast of new technological developments and program support issues associated with rapidly evolving space systems. Contributing capabilities are provided by these individual Technology Centers:

Electronics Technology Center: Microelectronics, VLSI reliability, failure analysis, solid-state device physics, compound semiconductors, radiation effects, infrared and CCD detector devices, Micro-Electro-Mechanical Systems (MEMS), and data storage and display technologies; lasers and electro-optics, solid state laser design, micro-optics, optical communications, and fiber optic sensors; atomic frequency standards, applied laser spectroscopy, laser chemistry, atmospheric propagation and beam control, LIDAR/LADAR remote sensing; solar cell and array testing and evaluation, battery electrochemistry, battery testing and evaluation.

Mechanics and Materials Technology Center: Evaluation and characterization of new materials: metals, alloys, ceramics, polymers and composites; development and analysis of advanced materials processing and deposition techniques; nondestructive evaluation, component failure analysis and reliability; fracture mechanics and stress corrosion; analysis and evaluation of materials at cryogenic and elevated temperatures; launch vehicle fluid mechanics, heat transfer and flight dynamics; aerothermodynamics; chemical and electric propulsion; environmental chemistry; combustion processes; spacecraft structural mechanics, space environment effects on materials, hardening and vulnerability assessment; contamination, thermal and structural control; lubrication and surface phenomena; microengineering technology and microinstrument development.

Space and Environment Technology Center: Magnetospheric, auroral and cosmic ray physics, wave-particle interactions, magnetospheric plasma waves; atmospheric and ionospheric physics, density and composition of the upper atmosphere, remote sensing using atmospheric radiation; solar physics, infrared astronomy, infrared signature analysis; effects of solar activity, magnetic storms and nuclear explosions on the earth's atmosphere, ionosphere and magnetosphere; effects of electromagnetic and particulate radiations on space systems; space instrumentation; propellant chemistry, chemical dynamics, environmental chemistry, trace detection; atmospheric chemical reactions, atmospheric optics, light scattering, state-specific chemical reactions and radiative signatures of missile plumes, and sensor out-of-field-of-view rejection.